ADVANCED INFRASTRUCTURE TECHNOLOGIES

Calculations Package

for

Wanzer Road Bridge No. 48 BRO 1448(38)

Fairfield, Franklin County, Vermont

April 7, 2014

Complied By:

Jonathan Kenerson, EI

Table of Contents

Bridge Loads

Description of Analysis 1

Arch Analysis Inputs and Element Plot 4

FEA 2D Soil Structure Interaction Load Effects Matrix 6

FEA 2D Soil Structure Interaction Design Envelopes 7

Scaling of Load Effects Due to Skew Effects 10

Arch Design

Arch Capacity Analysis 11

Arch Concrete Fill Inputs and Hollow Tube Capacity Analysis 20

Arch Rebar Cage Analysis 23

ATLAS Deck Design

Deck Profile and Section Properties 25

Deck Bend Test Data 26

Deck Pressure Analysis 27

Deck Pin Bearing Strength Test Data 30

Deck Pin Bearing Analysis 34

Abutment Service Reactions 35

Headwall Design

Headwall Elevations 36

Headwall Panel Data Sheets 38

Waler Data Sheet 46

Geogrid Data Sheet 48

Geogrid Analysis 51

Panel Analysis 62

Connection Bolt and Washer Plate Analysis 73

Waler Analysis 75

Base Angle Analysis 77

Appendix: UMaine Report - "Simplified Modeling to Assess Soil-Structure Interaction Effects" 78

Description of the Buried Arch Analysis

Arch loading:

The buried arch structure is loaded incrementally as follows:

1 – Superstructure Dead Load (DC)

Self weight of arches, concrete fill, and deck panels are applied as gravity loads.

For construction loading, a load factor of 1.0 is used for DC per AASHTO Section 12.5.4. For all other cases, load factors are as specified in AASHTO Table 3.4.1-1 & 3.4.1-2.

2 – Earth Load (EV & EH)

Horizontal and vertical earth loads are applied in incremental lifts based on the maximum backfill lift height allowed in the construction specifications. Earth pressures are calculated as follows:

$\sigma_v = \rho_s * h$	$\sigma_h = \rho_s * h * K$

where ρ_s is the soil unit weight, h is the depth of backfill at any given point for the current loading stage, and K is the earth pressure coefficient, which varies between K_a, K_o, and K_p depending on the deflection of the arch and decking at each point for the current loading stage. Loads are calculated based on the soil pressure at each arch or deck node and the respective vertical and horizontal tributary areas.

Backfill lifts are applied to the finish road grade, and load effects are tracked throughout the backfilling process.

For construction loading, a load factor of 1.0 is used for EV and EH per AASHTO Section 12.5.4. The total locked in loading due to the backfill process is factored as specified in AASHTO Table 3.4.1-1 & 3.4.1-2 for all other design cases and load combinations.

3 – Wearing Surface (DW)

Wearing surface load is applied as a uniform distributed load at the road surface and is factored as specified in AASHTO Table 3.4.1-1 & 3.4.1-2.

4 – Live Load (LL)

AASHTO HL-93 live loading is used as the design vehicle.

Lane load is applied either over half of the span or the entire span to produce the worst case load effects. Lane load is distributed through the soil and applied uniformly to the arch surface.

The design vehicle is positioned at one end of the bridge and advanced along the span to generate envelopes of design load effects. Wheel loads are distributed through the soil based on a Boussinesq distribution (Holtz & Kovacs, 1981), and applied to the arches based on the soil pressure and tributary area of each node.

One and two lanes of live load are considered with their respective multiple presence factors, the dynamic load allowance is included as specified in AASHTO Section 3.6.2.2-1 for buried structures, and all loads are factored as per AASHTO Table 3.4.1-1 and the related sections of Section 3.

Structural Behavior:

A nonlinear finite element model is used to analyze the buried arch bridge superstructure. The model accounts for the nonlinear behavior of the concrete-filled FRP tube arches, load sharing between the arches and deck, and the interaction of the composite/concrete arch bridge superstructure with the surrounding soil in terms of the ability of the soil to resist deformation of the arch under load. The buried arch structure is modeled using frame elements with constitutive relationships defined as follows:

Concrete-Filled FRP Tube Arches	Nonlinear moment-curvature relationship [Burgueno, 1999] in combined flexure/compression
Corrugated FRP Deck Panels	Linear elastic
Envelope Soil	Multi-linear compression-only springs with stiffness based on variation of lateral earth pressure coefficient varying between K_a, K_o, and K_p

A detailed description of the soil-structure interaction analysis is given is available in Clapp & Davids [2011].

SAP FEA Skew Analysis:

Arch bridges constructed on a skew angle introduce out-of-plane horizontal loads to the structural system. These forces are resisted primarily in shear by the FRP deck which acts as a structural diaphragm. The shear forces in the deck are transmitted to the arches through stainless steel fasteners. These fasteners are designed to resist these shear loads. The introduction of the out-of-plane loads into the arches typically increases the critical design moments. Arches are designed to resist the increased moments due to these forces.

AIT arch bridges are analyzed by a 2-dimensional FEA analysis that incorporates nonlinear soil springs to capture the effect of soil-structure interaction. This 2-dimensional analysis on its own does not account for skew effects. For this reason, a 3-dimensional FEA model was developed using SAP2000 (Computers and Structures Inc.) to determine the effect of skew on the structural response of the arches and the shear loads introduced to the deck and the fasteners due to diaphragm action.

The SAP2000 analysis is based on at-rest soil conditions rather than nonlinear soil springs to conservatively model the effects of soil structure interaction. The SAP2000 model has two main purposes.

1. To calibrate the 2-D FEA model for the effect of skew on the critical design moments of the arches. This is accomplished by comparing two models in SAP2000. The first model incorporates the skew geometry and the second model is the equivalent bridge modeled with no skew angle. The results of these two models are compared and a multiplication factor is derived from the ratio of the internal moments of the skew bridge to the internal moments of the square bridge. This "skew factor" is then

multiplied with the predicted internal moments from the 2-D FEA analysis that incorporates the soil structure interaction.

2. To obtain deck and fastener shear values from soil dead loads assuming at-rest conditions. This task is accomplished by directly calculating the fastener shears from the SAP2000 skewed arch model.

Advanced Infrastructure Technologies
20 Godfrey Drive, Orono, ME 04473
Telephone: 207-866-6526
Fax: 207-866-6501

Inputs:

12018 - Fairfield, VT

Buried Arch Analysis Inputs:

Input	Value		Reference
Tube Diameter:	12.0	in	AIT Shop Drawings
Arch Rise (TOF to CL Arch @ Crown):	7.53	ft	Project drawings
Arch Span (CL-CL Arch at TOF):	36.18	ft	Project drawings
Cover Depth (Finish Grade to CL Arch @ Crown):	77.76	in	Project drawings
Wearing Surface Thickness:	3.0	in	Project drawings
Maximum spacing of Arches:	67.84	in	Project drawings
Backfill Lift Height:	8	in	Project Special Provisions
Passive Earth Pressure Coefficient, Kp:	4.0		Arch Analysis Report
At-Rest Earth Pressure Coefficient, Ko:	0.45		Arch Analysis Report
Active Earth Pressure Coefficient, Ka:	0.25		Arch Analysis Report
Arch Concrete Compressive Strength:	6.0	ksi	Project Special Provisions
Backfill soil unit weight:	125	pcf	Typical
Asphalt unit weight:	140	pcf	Typical
Concrete unit weight (unreinforced):	145	pcf	Typical
Vehicle Analysis Increment:	36	in	Typical
Arch Boundary Conditions:	Fixed-Fixed		Arch Analysis Report
Number of Arch Elements:	60		Arch Analysis Report
Number of Transverse Deck Elements:	10		Arch Analysis Report

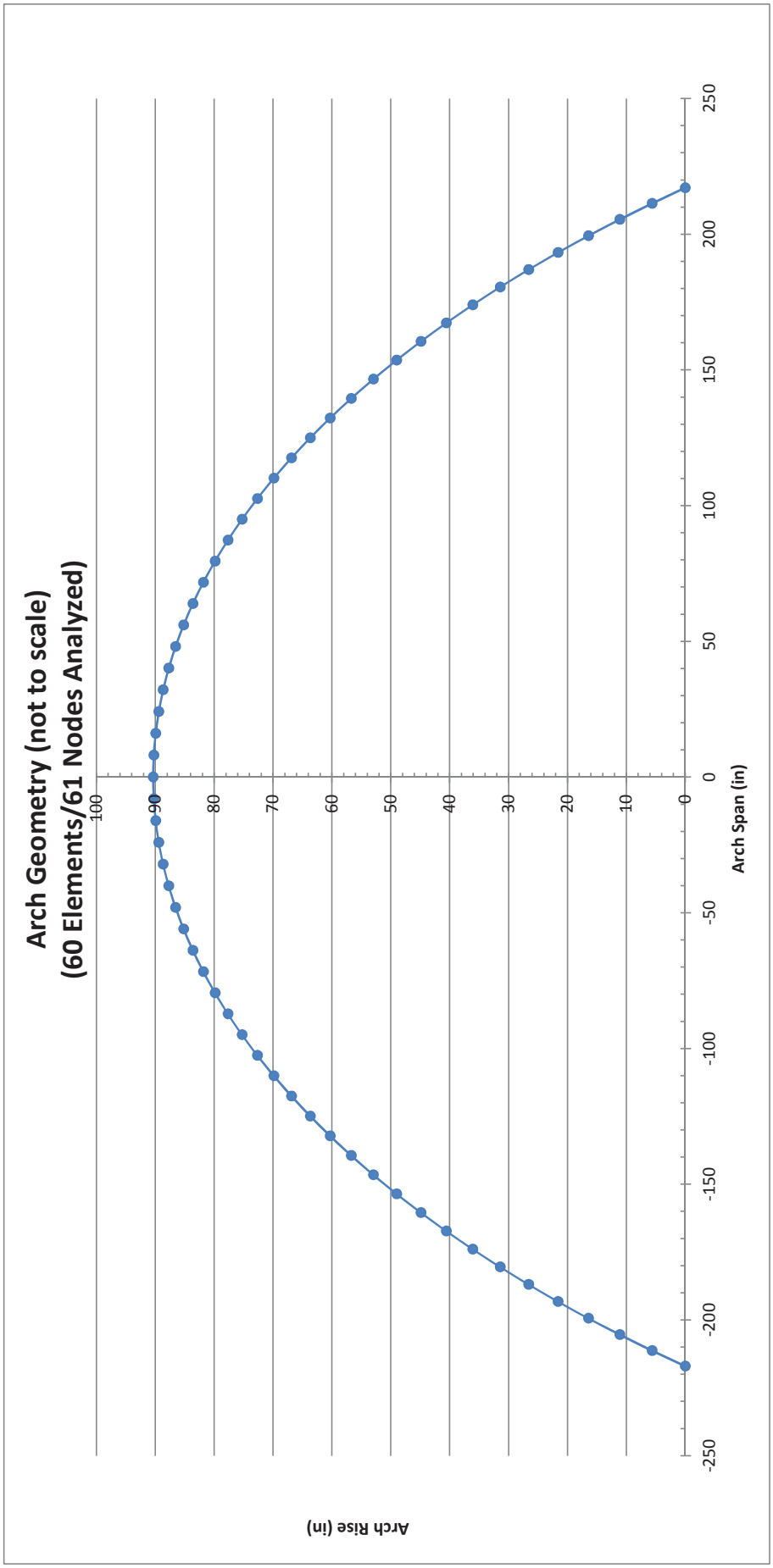
Arch Geometry (not to scale)
(60 Elements/61 Nodes Analyzed)
Arch Rise (in)
Arch Span (in)
100
90
80
70
60
50
40
30
20
10
0
-250
-200
-150
-100
-50
0
50
100
150
200
250

FEA 2D SSI Load Effects

Capacity Matrix Strength

	Max Int. Mom. (in*kip)	Max End Mom. (in*kip)	Max Int. Shear (in*kip)	Max End Shear (in*kip)
MU	463.6	818.7	137.0	818.7
Min A	111.4	130.3	118.8	130.3
Max A	236.2	265.4	247.9	265.4
VU	5.7	21.5	12.6	21.5
MS	339.2	595.3	88.6	595.3
AS	128.8	149.1	136.6	149.1

Capacity Matrix Construction

	Max Int. Mom. (in*kip)	Max End Mom. (in*kip)	Max Int. Shear (in*kip)	Max End Shear (in*kip)
MU	207.2	515.3	90.3	515.3
Min A	13.0	24.6	16.4	24.6
Max A	13.0	24.6	16.4	24.6
VU	0.6	15.8	5.0	15.8
MS	207.2	515.3	90.3	515.3
AS	13.0	24.6	16.4	24.6

Deck Design Values

	Mmin (in*kip/in)	Mmax (in*kip/in)	Vmin (kip/in)	Vmax (kip/in)
Str	-4.92	2.52	-0.41	0.41
Str DL	-4.29	2.20	-0.35	0.35
Str LL	-0.64	0.32	-0.06	0.06

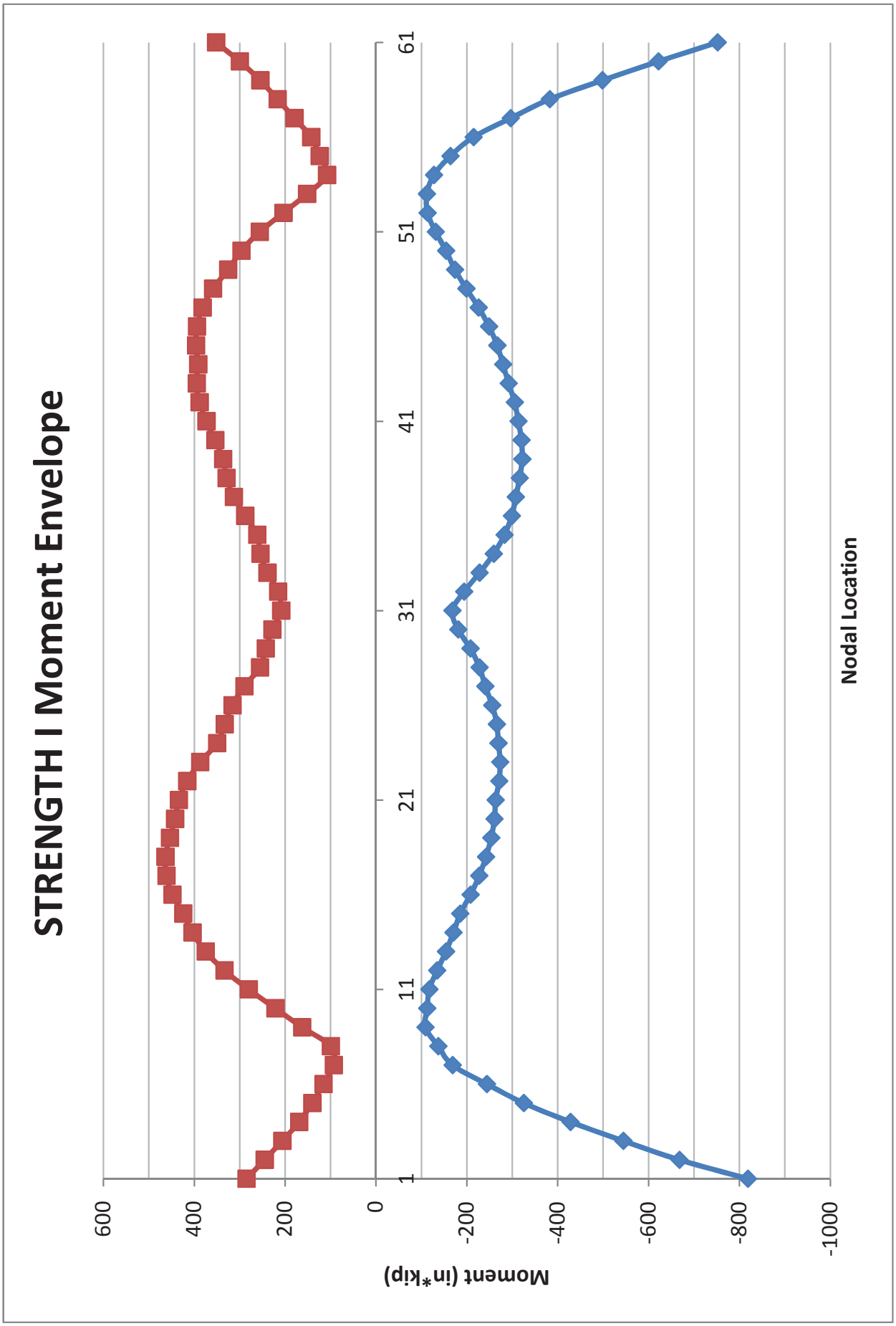
STRENGTH I Moment Envelope
600
400
200
0
-200
-400
-600
-800
-1000
Moment (in*kip)
1
11
21
31
41
51
61
Nodal Location

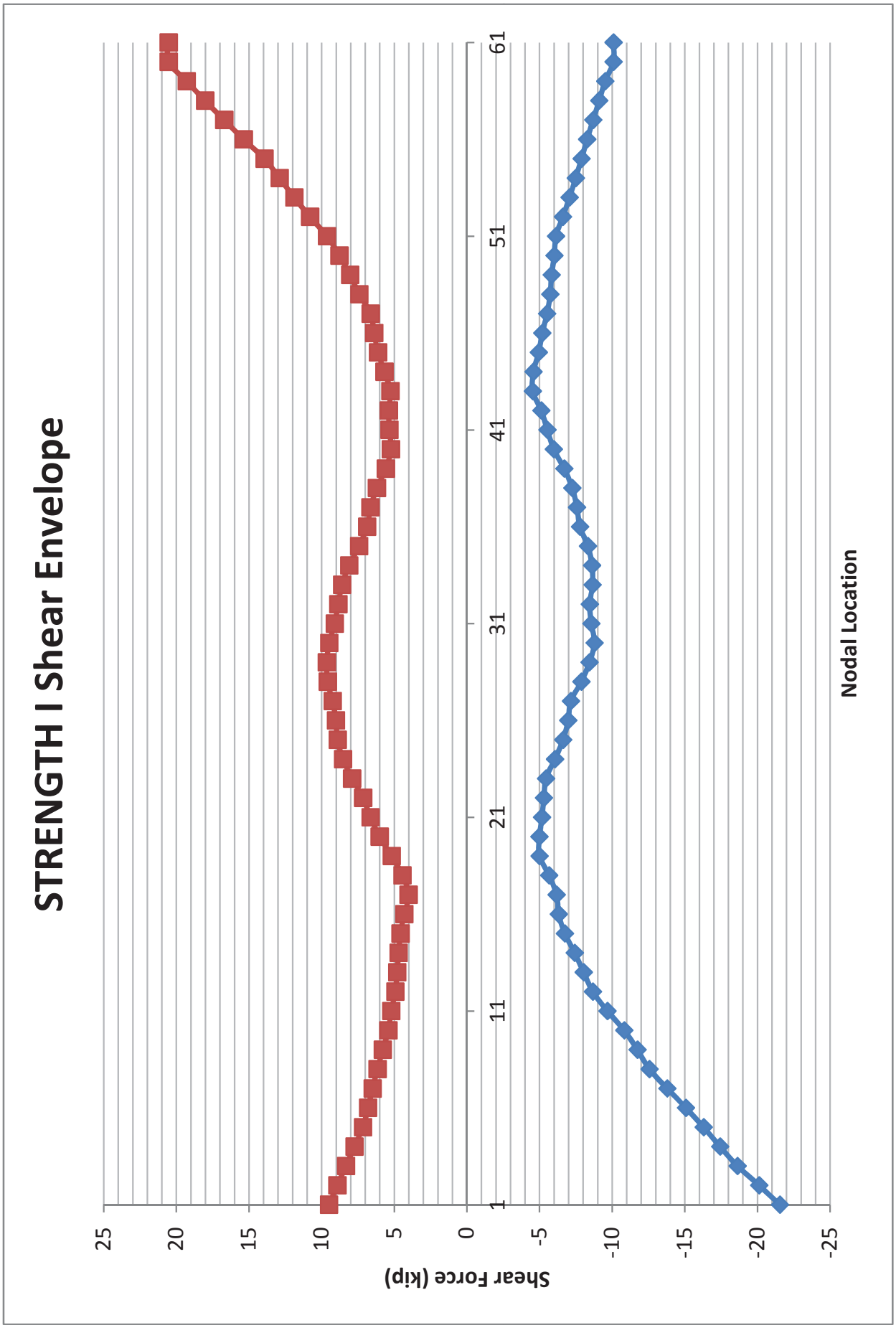
STRENGTH I Shear Envelope
Shear Force (kip)
25
20
15
10
5
0
-5
-10
-15
-20
-25
1
11
21
31
41
51
61
Nodal Location

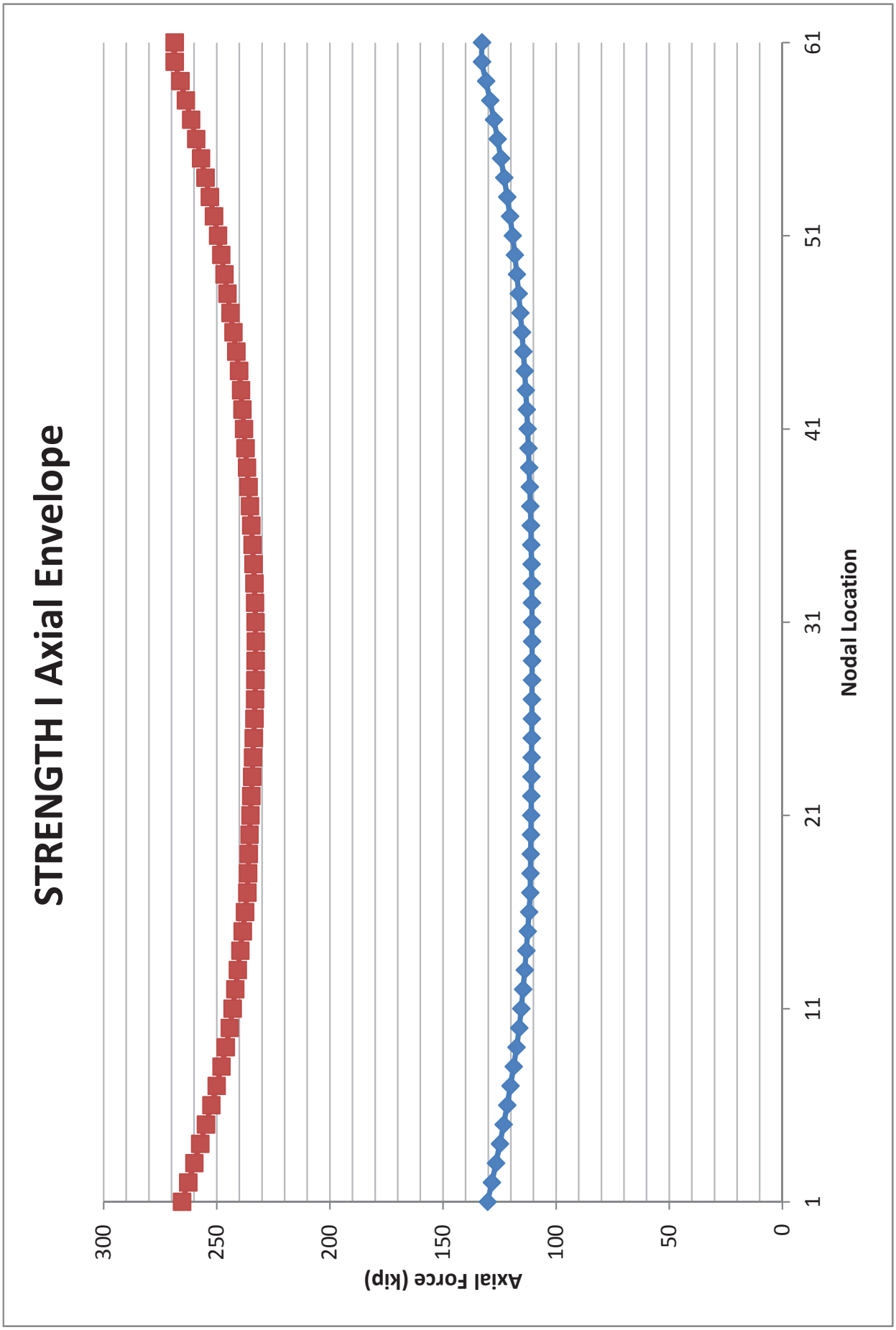
STRENGTH I Axial Envelope
Axial Force (kip)
300
250
200
150
100
50
0
1
11
21
31
41
51
61
Nodal Location

Scaling of Load Effects Due to Skew

	Max Internal Region Moment (in*kip)	Max End Region Moment (in*kip)	Max Connection Shear (kip/model link)
2D SSI Square Analysis Results	463.6	818.7	
3D Square Analysis Results	504.9	174.0	
3D Skew Analysis Results	520.9	177.4	2.08
Skew Factors equal the resulting 3D Skew model Result divided by the 3D Square Model Results	1.03	1.02	
Calculated 2D SSI Skew Effects	478	835	

Advanced Infrastructure Technologies
20 Godfrey Drive, Orono, ME 04473
Telephone: 207-866-6526
Fax: 207-866-6501

Project Name:	Wanzer Road BRO 1448(38)	Name:	JEK
Project Number:	12018	Date:	4/2/2014
Location:	Fairfield, VT	Checked By:	ZU
Client:		Date:	4/2/2014

Geometry, Material Properties, and Reinforcement:

Geometry

Tube diameter	12.07	in
FRP thickness	0.2340	in

Concrete

Concrete Strength	6.00	ksi

Steel Inputs

Number of Bars	6	6, 8, 10, or 12
Steel Grade	60	ksi
Steel modulus	29000	ksi
Concrete cover	1.9	in
Bar size	#6	

FRP

Longitudinal Modulus	4109	ksi
Hoop Modulus	2000.0	ksi
Hoop Strength	13.0	ksi
Ultimate Tensile Strain (Long)	0.01150	
Ultimate Comp. Strain (Long)	0.00379	
Poisson's Ratio	0.370	

Spreadsheet Controls

Diagram of typical steel layout at footings

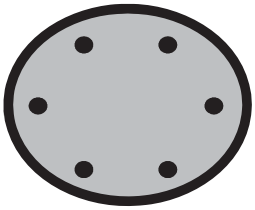

See steel schedule at right for bar sizes, areas, and locations

Steel Schedule:

y (from top), in	Number	Size	Area (in^2)
1.90	1	#6	0.44
3.97	2	#6	0.88
8.10	2	#6	0.88
10.17	1	#6	0.44

Design Load Effects:

	Case 1 - Max. M, Middle Region	Case 2 - Max M, End Region	Case 3 - Max. V, Middle Region	Case 4 - Max. V, End Region
Controlling Load Case	***Design Truck 2 Lanes***	***Design Truck 2 Lanes***	***Design Truck 1 Lane***	***Design Truck 1 Lane***
Ultimate moment, Mu, in*kip	478.0	835.0	137.0	818.7
Envelope ultimate axial force, Pu (min), kip	111.4	130.3	118.8	130.3
Envelope ultimate axial force, Pu (max), kip	238.9	268.8	247.9	265.4
Ultimate shear, Vu, kip	5.7	21.9	12.6	21.5
Service moment, Ms, in*kip	346.8	606.5	88.6	595.3
Envelope service axial force, Ps (min), kip	129.0	149.1	136.6	149.1

Balanced Thickness Calculations:

Ec:	4098.6	ksi
n:	3.20	
eps'c:	0.0021	
alpha:	0.616	
beta:	1.087	
theta:	1.092	

Balanced tube thickness:	0.1503	in
Actual Tube thickness:	0.2340	in

Resistance Factor in Flexure for CFFT with No Steel Reinforcement:

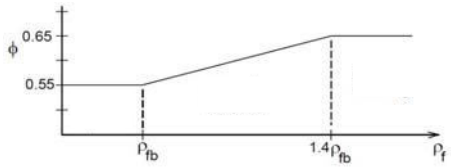

Balanced reinforcement ratio:	5.08%
Actual reinforcement ratio:	7.91%
Resistance Factor for Flexure:	**0.55**

Advanced Infrastructure Technologies
20 Godfrey Drive, Orono, ME 04473
Telephone: 207-866-6526
Fax: 207-866-6501

Reinforced Section - Combined Bending/Compression Capacity:

Design Case:	1	1 or 3
Controlling Load Case	Design Truck 2 Lanes	
Ultimate moment, Mu	478.0	in*kip
Envelope ultimate axial force, Pu (min)	111.4	kip
Envelope ultimate axial force, Pu (max)	238.9	kip
Ultimate shear, Vu	5.7	kip
Service moment, Ms	346.8	in*kip
Envelope service axial force, Ps (min)	129.0	kip

Determine Allowable Concrete Axial Strain:

Concrete Strength, f'c:	6.00	ksi
Elastic modulus of concrete:	4098.6	ksi
Ultimate hoop tensile strain of shell:	0.0065	
Effective hoop strain of shell, εfe:	0.00358	
Ultimate Shear at section of interest:	5.7	kip

Calculate Vc at Section of Interest:

Tension Strain (1)	0.000283	
NA Depth	9.3	in

Click Button to Solve for NA, iterate on Tension Strain (1, above) until error (2, below) goes to 0.

Moment	**347**	in*kip
Target Moment	**347**	in*kip
Error (2)	-0.1%	
Error in Equilibrium	0.000	

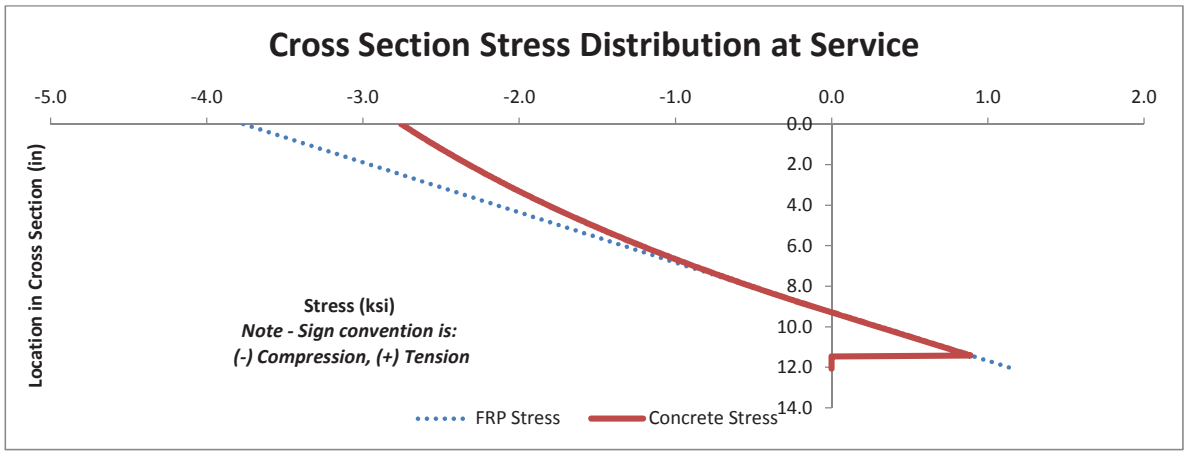

Area of uncracked concrete, Ac	104.59	in^2
Shear contribution of concrete, Vc	**40.5**	kip
Strength reduction factor for shear, ϕ	0.75	
Limit for requirement of shear reinforcement, 0.5*ϕ*Vc	15.2	kip

No Shear Reinforcement Required!

Determine Hoop Strain due to shear:

dv at section of interest:	9.65	in
Hoop strain due to shear, εfv	0.000	
Allowable hoop strain if shell used as shear reinforcement:	0.004	
Effective hoop strain of shell reduced for shear, εfe:	0.00358	
Maximum confining stress in shell:	0.289	ksi
Strain at max stress for unconfined concrete:	0.00213	
Maximum allowable compression strain in core:	**0.00475**	

Set Analysis Case:

Controlling Limit	Compression
Axial Load Case	Maximum

Check that limit state is appropriate based on extreme fiber strains:

	Tension	Compression
Actual	0.0037	0.0047
Limit	0.0115	0.0047
	OK	**OK**

Solve for Equilibrium of Section by iterating on NA Depth:

Total Force due to FRP	-16.2	kip
Total Force due to Concrete	-223.0	kip
Axial Force	238.9	kip
Sum of forces	-0.25	kip
Percent Error	-0.06%	
NA Depth	6.756	in

Solve for NA (Bending)

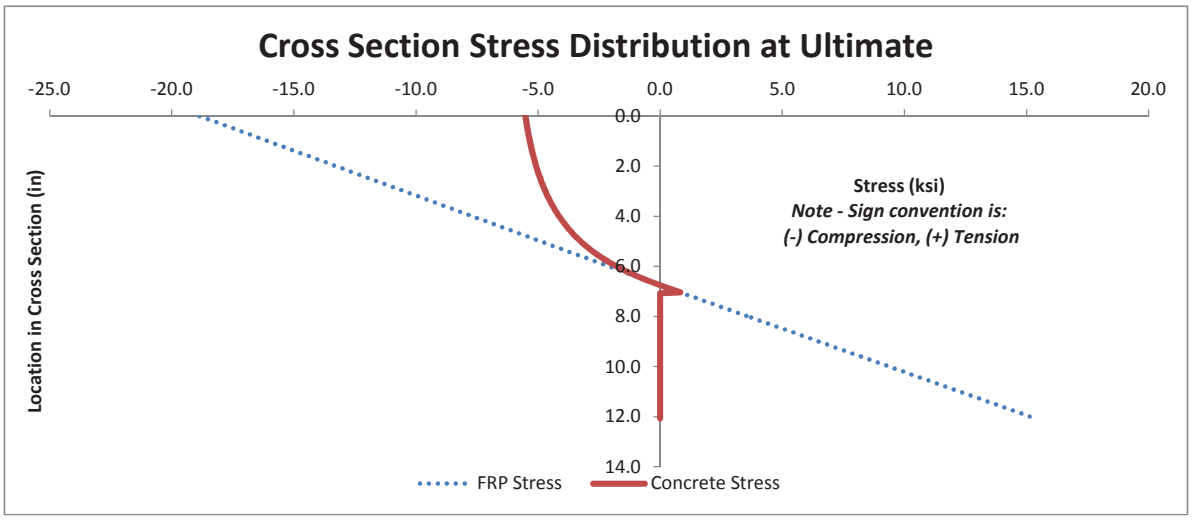

Determine Moment in Section:

Moment due to FRP	440.1	in*kip
Moment due to Concrete	772.2	in*kip
Moment due to axial load	-172.4	in*kip
Nominal Flexural Capacity, Mn	1039.9	in*kip
Strength Reduction Factor, ϕ	0.55	
Reduced Nominal Flexural Capacity, ϕMn	**572.0**	in*kip
Ultimate Factored Moment, Mu	**478.0**	in*kip
Strength Ratio	**1.20**	

Reinforced Section - Shear Capacity:

Calculate concrete contribution to shear capacity, Vc

Shear contribution of concrete, Vc	**40.5**	kip

Calculate FRP contribution to shear capacity, Vf

Hoop tensile strength of tube, ffe	8.00	ksi
Minimum tube thickness, tfmin	0.018	in
	OK	
Effective depth for FRP capacity, dv	9.65	in
Shear contribution of FRP, Vf	**36.1**	kip
Nominal Shear Capacity, Vn	**76.6**	kip
Strength reduction factor, ϕ	0.75	
Reduced Nominal Shear Capacity, ϕVn	**57.5**	
Ultimate Factored Shear, Vu for section of interest	5.7	
Strength Ratio	**10.08**	

Advanced Infrastructure Technologies
20 Godfrey Drive, Orono, ME 04473
Telephone: 207-866-6526
Fax: 207-866-6501

Unreinforced Section - Combined Bending/Compression Capacity:

Design Case:	2	2 or 4
Controlling Load Case	Design Truck 2 Lanes	
Ultimate moment, Mu	835.0	in*kip
Envelope ultimate axial force, Pu (min)	130.3	kip
Envelope ultimate axial force, Pu (max)	268.8	kip
Ultimate shear, Vu	21.9	kip
Service moment, Ms	606.5	in*kip
Envelope service axial force, Ps (min)	149.1	kip

Determine Allowable Concrete Axial Strain:

Concrete Strength, f'c:	6.00	ksi
Elastic modulus of concrete:	4098.6	ksi
Ultimate hoop tensile strain of shell:	0.0065	
Effective hoop strain of shell, εfe:	0.00358	
Ultimate Shear at section of interest:	21.9	kip

Calculate Vc at Section of Interest:

Tension Strain (1)	0.00096	
NA Depth	7.3	in

Click Button to Solve for NA, iterate on Tension Strain (1, above) until error (2, below) goes to 0.

Moment	**608**	in*kip
Target Moment	**607**	in*kip
Error (2)	0%	
Error in Equilibrium	0.000	

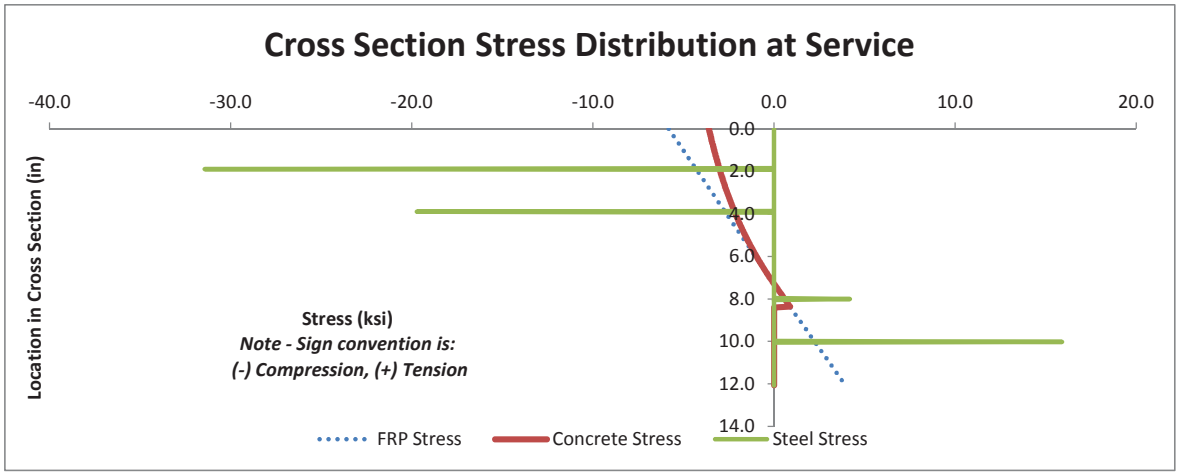

Zones with Steel Reinforcement:

Effective web width, bv	11.60	in
Effective shear depth, dv	8.69	in
Av = bv * dv	100.79	in^2
εs	-0.00025	
beta	5.917	
theta	28.12	deg
Shear contribution of concrete, Vc	**46.2**	kip
Strength reduction factor for shear, ϕ	0.75	
Limit for requirement of shear reinforcement, 0.5*ϕ*Vc	17.3	kip

Shear Reinforcement Required!

Calculate Steel contribution to shear capacity, Vs

Pitch of spirals, S	4.0	in
Area of spirals within distance S, Av	0.31	in^2
Shear contribution of Spirals, Vs	**75.6**	kip

Determine Hoop Strain due to shear:

dv at section of interest:	9.65	in
Hoop strain due to shear, εfv	0.000	
Allowable hoop strain if shell used as shear reinforcement:	0.004	
Effective hoop strain of shell reduced for shear, εfe:	0.00358	
Maximum confining stress in shell:	0.289	ksi
Strain at max stress for unconfined concrete:	0.00249	
Maximum allowable compression strain in core:	**0.00543**	

Set Analysis Case:

Controlling Limit	Compression
Axial Load Case	Maximum

Check that limit state is appropriate based on extreme fiber strains:

	Tension	Compression
Actual	0.0045	0.0054
Limit	0.0115	0.0054
	OK	OK

Solve for Equilibrium of Section by iterating on NA Depth:

Total Force due to FRP	-15.2	kip
Total Force due to Concrete	-229.7	kip
Total Force Due to Steel	-24.0	kip
Axial Force	268.8	kip
Sum of forces	-0.06	kip
Percent Error	-0.01%	

NA Depth	6.627	in

Solve for NA (Bending)

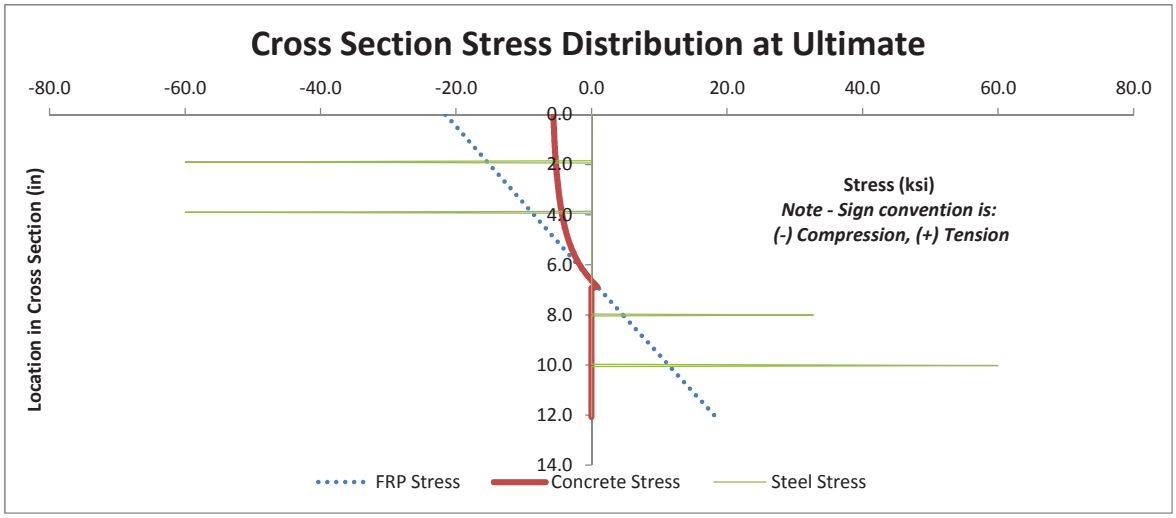

Determine Moment in Section:

Moment due to FRP	508.3	in*kip
Moment due to Concrete	770.4	in*kip
Moment due to axial load	-159.4	in*kip
Moment Due to Steel	398.1	in*kip
Nominal Flexural Capacity, Mn	1517.4	in*kip
Maximum strain in tension steel	0.0028	
Strength Reduction Factor, ϕ	0.55	
Reduced Nominal Flexural Capacity, ϕMn	**834.6**	in*kip
Ultimate Factored Moment, Mu	**835.0**	in*kip
Strength Ratio	**1.00**	

Reinforced Section - Shear Capacity:

Calculate concrete contribution to shear capacity, Vc		
Shear contribution of concrete, Vc	**46.2**	kip
Calculate FRP contribution to shear capacity, Vf		
Hoop tensile strength of tube, ffe	8.00	ksi
Minimum tube thickness, tfmin	0.018	in
	OK	
Effective depth for FRP capacity, dv	9.65	in
Shear contribution of FRP, Vf	**36.1**	kip
Shear contribution of Spirals, Vs	**75.6**	kip
Check Shear capacity limit of AASHTO Eq. 5.8.3.3-2		
Vn shall not exceed:	151.2	kip
Nominal Shear Capacity, Vn	**157.9**	kip
Strength reduction factor, ϕ	0.75	
Reduced Nominal Shear Capacity, ϕVn	**118.4**	
Ultimate Factored Shear, Vu for section of interest	21.9	
Strength Ratios	**5.40**	

Advanced Infrastructure Technologies
20 Godfrey Drive, Orono, ME 04473
Telephone: 207-866-6526
Fax: 207-866-6501

Tube Embedment Requirements

Determine tube embedment requirements (Reference AASHTO Guide Spec.)

Moment to be developed by CFFT	1039.9	in*kip	
Minimum embedment length to result in CFFT failure	11.7	in	*(no axial load case)*
Minimum embedment length to result in CFFT failure	6.3	in	*(with axial contribution)*
Additional safety factor on embedment length	1.5		
Required Minimum Embedment Length, X	**12**	in	

**Note: Embedment length requirements based on [Sadeghian & Fam, 2010]*

Tube Embedment measured as such:

Straight Tube

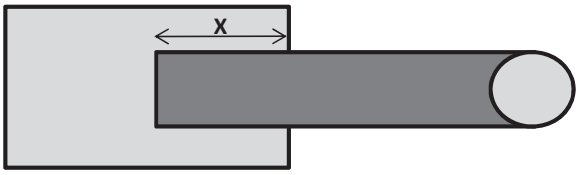

Arch, X measured along spine

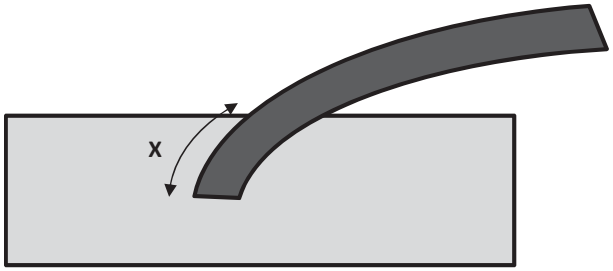

Steel Rebar Sizes and Development Length Requirements

Bar Size	Bar Diameter (in)	Bar Area (in^2)	Basic Development Length, ld (in)	Minimum Development Length, ld (in)	Required Development Length (in)
#3	0.375	0.11	3.4	9.0	**9.0**
#4	0.500	0.20	6.1	12.0	**12.0**
#5	0.625	0.31	9.5	15.0	**15.0**
#6	0.750	0.44	13.5	18.0	**18.0**
#7	0.875	0.60	18.4	21.0	**21.0**
#8	1.000	0.79	24.2	24.0	**24.2**
#9	1.128	1.00	30.6	27.1	**30.6**
#10	1.270	1.27	38.9	30.5	**38.9**
#11	1.410	1.56	47.8	33.8	**47.8**

Note:
If spirals of #3 or larger with pitch of 4.0 in or less are provided, ld may be multiplied by 0.75
If greater than the required steel is provided, ld may be reduced by (As provided) / (As Required)

```
function arch_fill_driver

%=========================================================================
%Inputs for this analysis are divided into types of input. For global
%geometry, span is the centerline distance between supports (in feet) and
%theta is the degree measure turned between supports (degrees).
%For local (cross section) geometry, diameter is the diameter of the tube
%wall, thick is the wall thickness (in), ex is the longitudinal modulus
%(ksi), ey is the transverse modulus (ksi), gxy is the shear modulus (ksi)
%and v is the poisson's ratio.
%num_els determines how many elements the arch is made
%with (more elements makes straight segments closer to an arch), num_steps
%is the number of different concrete heights that is to be checked, and
%fill_type is the way concrete volume is distributed before it overtops the
%apex.  For fill_type 0 means one-sided, 1 means even, and 2 means 2-ft arc
%length variation in volume between sides. There are 3 surcharge variables:
%surcharge_s is static surcharge; point load mid span(men and equipment in
%kips), surcharge_l; line load for self weight and decking and surcharge_c;
%for concrete collecting at crown. Surcharge s and c are in kips and l is
%in kips/inch arclength. It is recommended that surcharge c is not used
%without further development.

%==========================================================================

clear global
global volume
global forces
global NODES
global Ex
global Gxy
global h
global radius
global BOUNDARIES
global diam
global PROPERTIES
global TYPE
global total_volume
global geom_store
global zero_volume
global Ey
global nu

span = 36.18; %Arch span (ft)
rise = 7.53; %Arch rise (ft)
diam = 12; %Arch diameter (in)
thick = 0.2340; %Tube wall thickness (in)
ex = 4109; %Longitudinal MOE of tube wall (ksi)
ey = 2000; %Circumferential MOE of tube wall (ksi)
gxy = 1000; %Shear modulus of tube wall (ksi)
v = 0.37; %Poisson's ratio of tube wall
num_els = 60; %Number of elements
```

```
num_steps = 60; %Number of different concrete heights to be checked
fill_type = 0; %Type of filling: 0-one sided, 1-even, 2- 2ft unbalanced
surcharge_s = 1.0; %Construction point load at apex of arch (kip)
deck_weight = 68/60*.00156; %Deck weight tributary to arch (kip/in) ex. 0.00156 for
ATLAS with 60" o.c. arch spacing
%_____________________________________________________________________________
```

Advanced Infrastructure Technologies

20 Godfrey Drive
Orono, Maine 04473
Telephone: (207) 866-6526
Fax: (207) 866-6501
www.aitbridges.com

Project: Fairfield, VT

Task: Analyze Fill Buckling of Hollow Arches

References

1. *Arch Fill Driver Inputs*
2. *Arch Fill Driver Results*
3. *Response of Concrete-Filled Tubular FRP Arches to Construction-Induced Loading*
4. *Project Drawings*

Buckling equation parameters [Ref. 1]:

$Ex := 4109ksi$ $Ey := 2000ksi$ $nu := 0.37$ $r := 6.035in$ $t := 0.234in$

Inputs from Matlab Analysis [Ref. 2]:

$apex_stress := 1.679ksi$ $foot_stress := 1.3516ksi$

$$\sigma := \frac{2 \cdot t \cdot \sqrt{2Ex \cdot Ey}}{9 \cdot r \cdot \sqrt{1 - nu^2}} = 37.6 \cdot ksi$$ [Ref. 3]

$\sigma mean := \sigma \cdot 0.4 = 15.04 \cdot ksi$

$\sigma low := \sigma mean \cdot 0.8 = 12.032 \cdot ksi$ $ExRatio := \frac{6.5}{1.75} = 3.714$ $UseRatio := 2 \cdot \frac{r}{2.5in} = 4.828$

$reducest := 0.5 \cdot \frac{UseRatio}{ExRatio} = 0.65$

$\sigma hole := \sigma low \cdot 0.5 = 6.016 \cdot ksi$ $\sigma holemod := reducest \cdot \sigma low = 7.82 \cdot ksi$

Note: Apex hole reduction formula only valid for diameters between 12" and 15" equation needs to be adjusted to be used for other diameters.

Note: Factors of safety must be above 1.25

$$FSapexmod := \frac{\sigma holemod}{apex_stress} = 4.658$$

$$Fsfoot := \frac{\sigma low}{foot_stress} = 8.902$$

Advanced Infrastructure Technologies

20 Godfrey Drive
Orono, Maine 04473
Telephone: (207) 866-6526
Fax: (207) 866-6501
www.aitbridges.com

Project: *Fairfield, VT*

Task: *Determine details for steel end cage reinforcement*

References
1. *AASHTO LRFD Bridge Design Specifications, 2010*
2. *ACI 318*

Bar diameter: $d_b := \frac{6}{8}\text{in}$

Bar area: $A_b := \frac{\pi \cdot d_b^2}{4} = 0.44\,\text{in}^2$

Steel yield stress: $f_y := 60\text{ksi}$

Concrete compressive strength: $f'_{c_ARCH} := 6000\text{psi}$ *Specified arch compressive strength for l.d calculations*

Concrete compressive strength: $f'_{c_ABMT} := 4000\text{psi}$ *Specified abutment compressive strength for hook calculations*

Development Length within Tube

$\alpha := 1$ *Reinforcement Location Factor, > 12" cast below*

$\beta := 1.5$ *Coating Factor, epoxy coated with cover < 3d.b*

$\lambda := 0.8$ *Reinforcement Size Factor 0.8 for #6 or smaller 1.0 for #7 or larger*

$\sqrt{\frac{f'_{c_ARCH}}{\text{psi}}} = 77.46$ *must be < 100*

$$l_d := \frac{f_y \cdot \alpha \cdot \beta \cdot \lambda}{25 \cdot \sqrt{\frac{f'_{c_ARCH}}{\text{psi}}}\text{psi}} \cdot d_b = 27.89 \cdot \text{in}$$

ACI 318 Table 8-1 - Case 1 or 2 #6 and smaller

$$l_d := \frac{f_y \cdot \alpha \cdot \beta \cdot \lambda}{20 \cdot \sqrt{\frac{f'_{c_ARCH}}{\text{psi}}}\text{psi}} \cdot d_b = 34.86 \cdot \text{in}$$

ACI 318 Table 8-1 - Case 1 or 2 #7 and larger

Development Length within Abutment for 180 Deg. Hook

Minimum length of hook: $\max(4 \cdot d_b, 2.5in) = 3.00 \cdot in$

Minimum bend diameter: $6.0 \cdot d_b = 4.50 \cdot in$ *For #8 or less*

Epoxy Coating Factor $Epx := 1.2$ *1.2 for epoxy coating 1.0 for uncoated*

Clearance Factor $Clear := 0.7$ *for sidecover > 2.5"*

Basic development length:

$$\max\left(Epx \cdot Clear \frac{f_y \cdot d_b}{50 \cdot \sqrt{\frac{f'_{c_ABMT}}{psi}}\, psi}, 8d_b, 6in\right) = 11.95\, in$$

Ensure that rebar cage extends at least 28" above the top of abutment into arch.
Ensure that rebar cage extends at least 12" below the top of abutment into abutment.

CP248.part	REV. NO. 0

DATE	SYM	REVISION RECORD	AUTH.	DR.	CK.

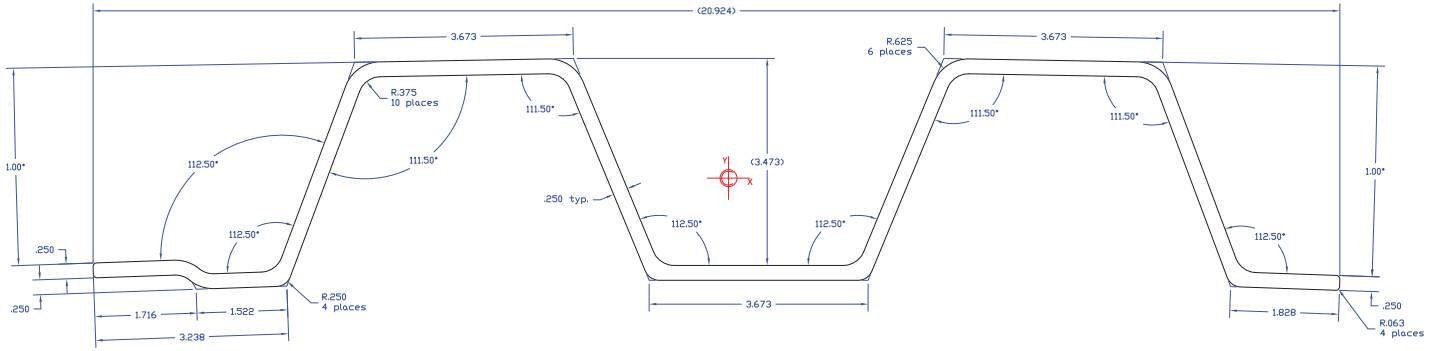

CROSS SECTION PROPERTIES		
Area	7.561	in^2
Ix	15.237	in^4
Iy	264.205	in^4
Ixy	0	in^4
Sx	7.619	in^3
Sy	24.773	in^3
rx	1.420	in
ry	5.911	in

Note: All tolerances per CPI Design Guide.

CREATIVE PULTRUSIONS

214 Industrial Lane, P.O. Box 6
Alum Bank, Pennsylvania 15521-0006
www.creativepultrusions.com

DRAWN BY	RVH	10-23-13
CHECKED		
APPROVED		
UNITS:	Imperial	
SCALE:	Full	
FRACTIONS	±	1/16"
DECIMAL	±	
ANGLES	±	

THIS PRINT IS THE PROPRIETARY PROPERTY OF CREATIVE PULTRUSIONS INC. (CPI) AND SHALL NOT BE REPRODUCED OR COPIED WITHOUT THE WRITTEN PERMISSION OF CPI.

PART NAME:
Atlas Composite Bridge Deck

CP248.part

REV. NO. 0

Average = 16,466 lbs
Standard Deviation = 574 lbs
Design Value (Avg-3xSD) = 14,745 lbs

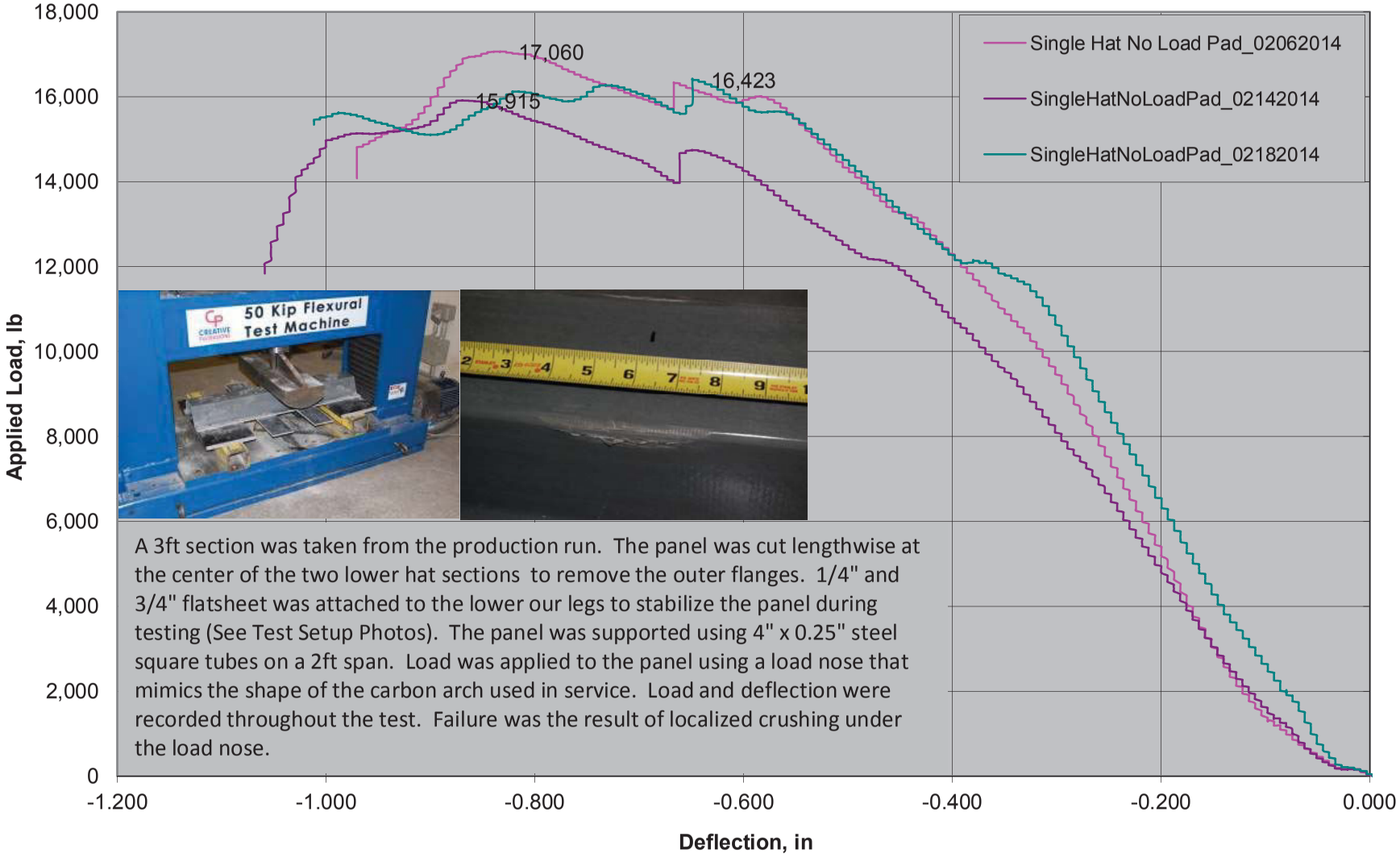

A 3ft section was taken from the production run. The panel was cut lengthwise at the center of the two lower hat sections to remove the outer flanges. 1/4" and 3/4" flatsheet was attached to the lower our legs to stabilize the panel during testing (See Test Setup Photos). The panel was supported using 4" x 0.25" steel square tubes on a 2ft span. Load was applied to the panel using a load nose that mimics the shape of the carbon arch used in service. Load and deflection were recorded throughout the test. Failure was the result of localized crushing under the load nose.

Advanced Infrastructure Technologies

20 Godfrey Drive
Orono, Maine 04473
Telephone: (207) 866-6526
Fax: (207) 866-6501
www.aitbridges.com

Project: Fairfield, VT BRO 1448(38)

Task: Calculate Soil Pressure Applied to Deck

Fairfield Vermont Design (Pressure at Base)

Inputs:

Angle of panel at base of arch: $\theta := 46deg$

Depth of soil above lowest panel: $d := 14ft$

Load factor for vertical earth: $\gamma_e := 1.35$ AASHTO LRFD Bridge Design Sec: 3.4.1

At-rest earth pressure coefficient: $K_o := 0.47$

Density of backfill: $\rho := 125 \frac{lbf}{ft^3}$

Horizontal projection of decking: $H_p := 1ft$

Vertical projection of decking: $V_p := 1ft \cdot \tan(\theta)$

Vertical pressure along horizontal projection: $Vert := \gamma_e \cdot \rho \cdot d \cdot H_p$ $Vert = 2362.5 \cdot \frac{lbf}{ft}$

Horizontal pressure along vertical projection: $Horiz := \gamma_e \cdot \rho \cdot d \cdot K_o \cdot V_p$ $Horiz = 1149.827 \cdot \frac{lbf}{ft}$

Portion of the pressure perpendicular to the deck panel contributed by the vertical pressure: $C_v := \cos(\theta) \cdot Vert$ $C_v = 1641.13 \cdot \frac{lbf}{ft}$

Portion of the pressure perpendicular to the deck panel contributed by the horizontal pressure: $C_h := \sin(\theta) \cdot Horiz$ $C_h = 827.116 \cdot \frac{lbf}{ft}$

Total resultant force perpendicular to the deck panel: $Total_Force := C_v + C_h$ $Total_Force = 2468.247 \cdot \frac{lbf}{ft}$

$$Factored_Pressure := \frac{Total_Force}{\sqrt{H_p^{\,2} + V_p^{\,2}}}$$

Factored pressure perpendicular to the deck panel: $Factored_Pressure = 11.907 \cdot psi$

Distributed load based on 9.75" trib deck width $w := Factored_Pressure \cdot 9.75in$

$w = 116.092 \cdot \frac{lbf}{in}$

Arch Spacing $sp := 68in$

Ultimate Reaction $R_u := 1.14 \cdot w \cdot sp$ Reaction equation 4-span continuous all spans loaded

$R_u = 8999 \cdot lbf$

Characteristic Reaction Value 24" bend tests $R_n := 14747lbf$ 24" span bending tests performed on decking simulated the reaction of the arch on decking. This value is mean -3sigma from three tests.

Compression Resistance Factor $\Phi_c := 0.7$

Moisture Reduction Factor $C_m := 0.9$

Design Reaction Value $\Phi R_n := \Phi_c \cdot C_m \cdot R_n$

$\Phi R_n = 9290.61 \cdot lbf$ > Ru = 8999lb

Pressure at Crown

This case looks at designing deck for pressure due to live load through 68" soil cover. The AASHTO 1:1.15 load trapezoid is used for live load distribution

Soil Cover $cover := 68in$ Measured from top of deck corrugation to road surface

Wheel Width Parallel to Deck Span $W_{par} := 20in$

Wheel Width Perpendicular to Deck Span $W_{per} := 10in$

Load Patch width 1 @ deck surface $Lw_1 := W_{par} + 1.15 \cdot cover$

Load Patch width 2 @ deck surface $Lw_2 := W_{per} + 1.15 \cdot cover$

Load Patch Area $L_A := Lw_1 \cdot Lw_2$ $L_A = 8661.24 \cdot in^2$

Impact Factor $IM := 1 + 0.33\left(1.0 - 0.125\frac{cover}{12in}\right)$ $IM = 1.096$

Maximum Wheel Load $P := 16kip$

Multiple Presence Factor $MPF := 1.2$

Live Load Factor $\gamma_{LL} := 1.75$

Factored Wheel Load $P_u := P \cdot \gamma_{LL} \cdot MPF \cdot IM$ $P_u = 36.834 \cdot kip$

Factored Live Load Pressure $PRL_u := \frac{P_u}{L_A}$ $PRL_u = 4.253 \cdot psi$

Factored Soil Pressure $PRE_u := cover \cdot \rho \cdot \gamma_e$ $PRE_u = 6.641 \cdot psi$

Total Factored Pressure $Factored_Pressure := PRL_u + PRE_u$ $Factored_Pressure = 10.893 \cdot psi$

Distributed Load based on 9.75in deck trib width $w := Factored_Pressure \cdot 9.75in$ $w = 106.21 \cdot \frac{lbf}{in}$

Arch Spacing $sp := 68in$

Ultimate Reaction $R_u := 1.22 \cdot w \cdot sp$ $R_u = 8811.207 \cdot lbf$ based on 4-span continuous equation with 3rd span unloaded (beam equation 40 in blue AISC manual) This is conservative.

$\Phi R_n = 9290.61 \cdot lbf$ > Ru = 8811.2 lbf

Creative Pultrusions, Inc.
Quality Assurance Laboratory
214 Industrial Lane
Alum Bank, PA 15521
(814) 839-4186

Part Number	CP248.758
Part Description	Atlas Composite Bridge Deck
Operator	D. Crawford
Date Produced	n/a
Date Tested	3/18/14
Machine Calibration Date	2/27/14
Crosshead Speed	0.0500 in/min
Temperature (deg F)	73
Humidity (%)	50
ASTM Test	ASTM D953
Specimen Orientation	Lengthwise

	Pin Diameter [in]	Thickness [in]	Area [in^ 2]	Bearing Load [lbf]	Bearing Stress [psi]
1	0.37500	0.25850	0.09694	-5,669	-58,476
2	0.37500	0.25450	0.09544	-6,053.0	-63,427
3	0.37500	0.25450	0.09544	-5,825	-61,038
4	0.37500	0.25700	0.09638	-5,595	-58,050
5	0.37500	0.25750	0.09656	-5,918	-61,289
6	0.37500	0.25850	0.09694	-5,661	-58,401
7	0.37500	0.25500	0.09562	-5,962	-62,350
8	0.37500	0.25550	0.09581	-5,821	-60,759.0
9	0.37500	0.25600	0.09600	-5,455	-56,825
10	0.37500	0.25450	0.09544	-5,328	-55,832
11	0.37500	0.25450	0.09544	-5,391	-56,488
12	0.37500	0.25550	0.09581	-5,595	-58,397
Mean	0.37500	0.25596	0.09598	-5,690	-59,278
Standard deviation	0.000	0.002	0.001	231.3	2,437.5
Coefficient of variation	0.00	0.60	0.60	-4.0650	-4.1121

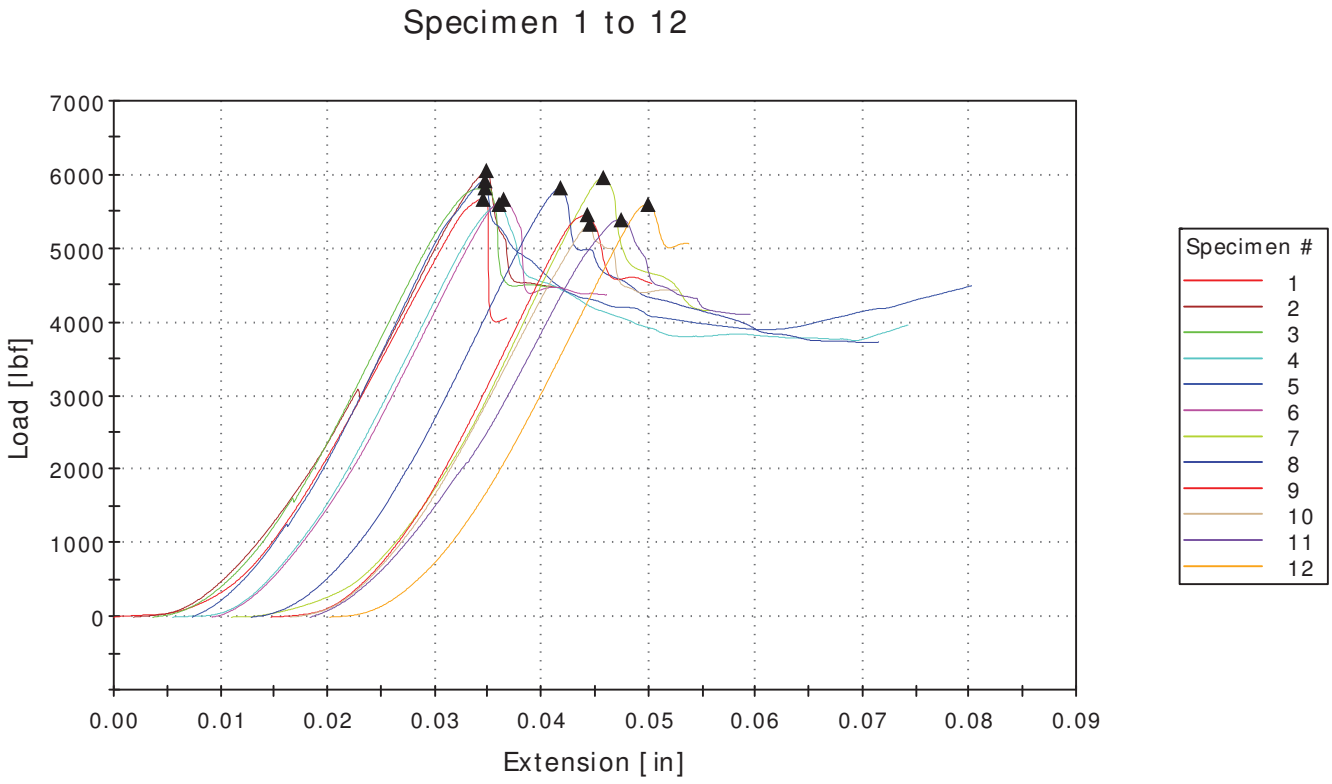

Comments

i	xi (psi)	MNR	Outlier?	xi^β_hat	ln(xi)	(xi^β_hat)*ln(xi)	Origin
1	58476.00	0.32888	FALSE	3.79590E+128	10.97637	4.16652E+129	
2	63427.00	1.70224	FALSE	3.39911E+129	11.05764	3.75861E+130	
3	61038.00	0.72217	FALSE	1.20676E+129	11.01925	1.32976E+130	
4	58050.00	0.50364	FALSE	3.11648E+128	10.96906	3.41848E+129	
5	61289.00	0.82514	FALSE	1.34801E+129	11.02336	1.48596E+130	
6	58401.00	0.35965	FALSE	3.66675E+128	10.97509	4.02429E+129	
7	62350.00	1.26041	FALSE	2.14165E+129	11.04052	2.36449E+130	
8	60759.00	0.60771	FALSE	1.06648E+129	11.01467	1.17470E+130	
9	56825.00	1.00619	FALSE	1.75315E+128	10.94773	1.91930E+129	
10	55832.00	1.41357	FALSE	1.08970E+128	10.93010	1.19106E+129	
11	56488.00	1.14445	FALSE	1.49328E+128	10.94178	1.63392E+129	
12	58397.00	0.36129	FALSE	3.65998E+128	10.97502	4.01683E+129	

n = 12

mean = 59277.67 psi

std dev = 2437.569 psi

(mean) - (2*std dev) = 54402.5287 psi

(mean) - (3*std dev) = 51964.9597 psi

CV = 2.365812

Max. likelihood estimate of scale parameter: α_hat = 60422.9361

Max. likelihood estimate of shape parameter: β_hat = 26.9729216

Equation 6 = 9.12585E-05

Γ(1+(2/β_hat) = 0.96229586

Γ(1+(1/β_hat) = 0.97991518

Coefficient of variation: COV = 0.0463411

Interpolation:

		COV		
n =	12	0.1	0.05	0.05
	Ω	0.913	0.956	0.956 = Ω

Data confidence factor: Ω = 0.956

Nominal value: x0.05 = 54122.8221 psi

Characteristic value: xchar = 51741.4179 psi

Key:
- user input
- run solver
- output

# of Specimens:	12
Mean Value:	59,278
St. Dev.:	2,438
COV:	0.046
Data confidence factor:	0.956
Nominal value:	54,123
Characteristic value:	51,741
5% LEL:	54,759

Creative Pultrusions, Inc.
Quality Assurance Laboratory
214 Industrial Lane
Alum Bank, PA 15521
(814) 839-4186

Part Number	CP248.758
Part Description	Atlas Composite Bridge Deck
Operator	D. Crawford
Date Produced	n/a
Date Tested	3/21/14
Machine Calibration Date	2/27/14
Crosshead Speed	0.0500 in/min
Temperature (deg F)	73
Humidity (%)	50
ASTM Test	ASTM D953
Specimen Orientation	Lengthwise

	Pin Diameter [in]	Thickness [in]	Area [in^ 2]	Bearing Load [lbf]	Bearing Stress [psi]
1	0.62500	0.25350	0.15844	-6,375	-40,240
2	0.62500	0.25450	0.15906	-8,520	-53,560
3	0.62500	0.25350	0.15844	-8,404	-53,040
4	0.62500	0.25550	0.15969	-8,261	-51,730
5	0.62500	0.25050	0.15656	-7,746	-49,480
6	0.62500	0.25500	0.15937	-8,102	-50,840
7	0.62500	0.25750	0.16094	-8,207	-51,000
8	0.62500	0.25500	0.15937	-8,980	-56,340
9	0.62500	0.25450	0.15906	-8,815	-55,420
10	0.62500	0.25350	0.15844	-9,352	-59,030
11	0.62500	0.25450	0.15906	-8,793	-55,280
12	0.62500	0.25450	0.15906	-9,062.0	-56,970
Mean	0.62500	0.25433	0.15896	-8,385	-52,740
Standard deviation	0.000	0.002	0.001	780.002	4,856.783
Coefficient of variation	0.00	0.64	0.64	-9.30	-9.21

Specimen 1 to 12

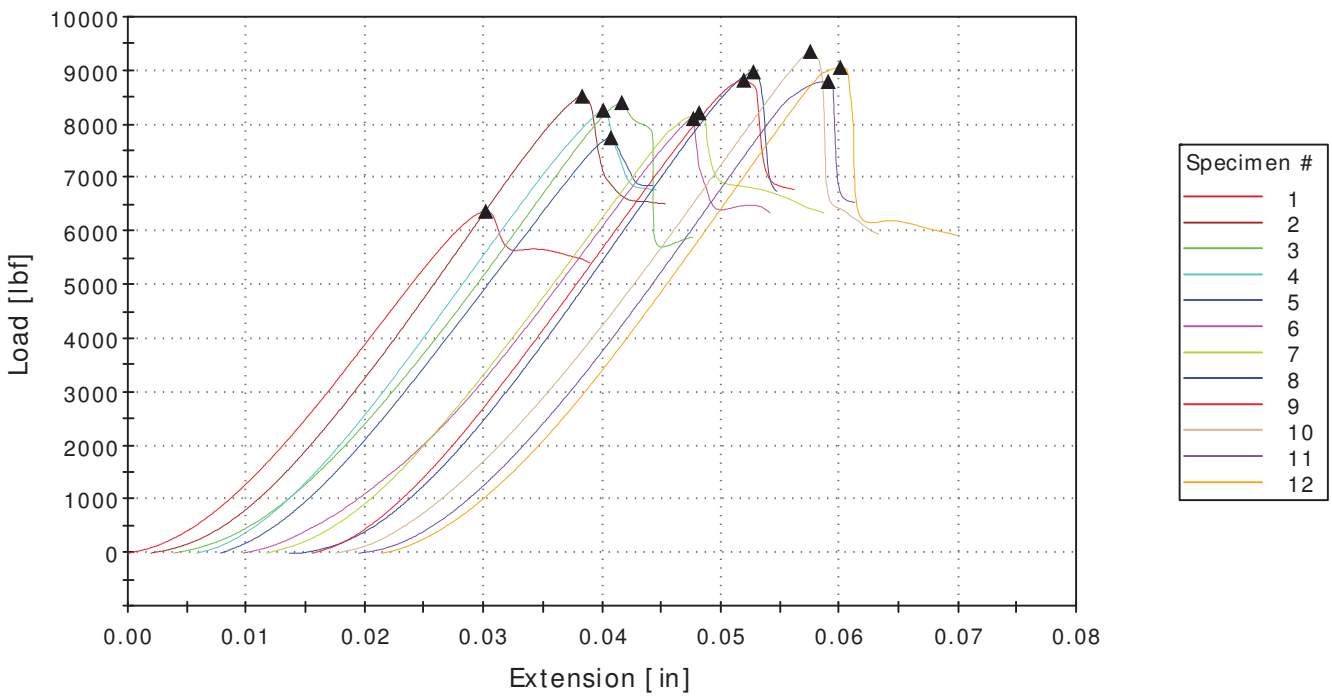

Comments

i	xi (psi)	MNR	Outlier?	xi^β_hat	ln(xi)	(xi^β_hat)*ln(xi)	Origin
2	53560.00	0.10770	FALSE	4.33848E+95	10.88856	4.72398E+96	
3	53040.00	0.28222	FALSE	3.56161E+95	10.87880	3.87460E+96	
4	51730.00	0.72188	FALSE	2.14778E+95	10.85379	2.33115E+96	
5	49480.00	1.47701	FALSE	8.73781E+94	10.80932	9.44498E+95	
6	50840.00	1.02058	FALSE	1.51203E+95	10.83644	1.63850E+96	
7	51000.00	0.96688	FALSE	1.61124E+95	10.83958	1.74651E+96	
8	56340.00	0.82531	FALSE	1.20723E+96	10.93916	1.32061E+97	
9	55420.00	0.51654	FALSE	8.65329E+95	10.92270	9.45173E+96	
10	59030.00	1.72811	FALSE	3.10065E+96	10.98580	3.40631E+97	
11	55280.00	0.46956	FALSE	8.22177E+95	10.92017	8.97831E+96	
12	56970.00	1.03675	FALSE	1.51169E+96	10.95028	1.65534E+97	

n = 11

mean = 53880.91 psi

std dev = 2979.6022 psi

(mean) - (2*std dev) = 47921.7048 psi

(mean) - (3*std dev) = 44942.1026 psi

CV = 2.303055

Max. likelihood estimate of scale parameter: α_hat = 55239.711

Max. likelihood estimate of shape parameter: β_hat = 20.2242677

Equation 6 = -0.000417139

Γ(1+(2/β_hat) = 0.95179876

Γ(1+(1/β_hat) = 0.97377325

Coefficient of variation: COV = 0.06131071

Interpolation:

		COV			
n =	11	0.1	0.05	0.06131071	
	Ω	0.906	0.953	0.94236793	= Ω

Data confidence factor: Ω = 0.94236793

Nominal value: x0.05 = 47694.955 psi

Characteristic value: xchar = 44946.1963 psi

Key:
user input
run solver
output

# of Specimens:	11
Mean Value:	53,881
St. Dev.:	2,980
COV:	0.061
Data confidence factor:	0.942
Nominal value:	47,695
Characteristic value:	44,946
5% LEL:	48,447

Shear Connection Calculations

Connection Shear Calculations			
3D Skew Model Link X-Y Spacing	8.37	inches	
Panel Corrugation Spacing	9.75	inches	
Scale Factor = panel spacing/model spacing	1.165		
Max Shear per corrugation = model x scale factor	2.43	kip	
Fastener Capacity			
Fastener Diameter, d	0.50	inches	
Area of Bolt, A.b	0.196	in^2	
Panel Thickness, t	0.25	inches	
Projected Bearing Area, A.pb = t*d	0.125	in^2	
Tension Strength, F.nt	60	ksi	Ref. 2 Table 8.2 for ASTM F593B
Shear Strength, F.nv	48	ksi	Ref. 2 Table 8.2 for ASTM F593B
Requried Shear Stress, f.v = Max Shear/A.pb	19.41	ksi	Ref. 2 Eqn. 8.3.2-2
Nominal Tensile Strength inc. shear, F.t.nt	45.64	ksi	Ref. 2 Eqn. 8.3.2-2
Phi for bearing strength	0.75		Ref. 2 Eqn. 8.3.2-2
Bearing Strength, Phi*Rn=Phi*1.8*F.y*Apb	6.72	kips	Ref. 2 Eqn. 8.3.2-2
Panel Bearing Capacity			
Characteristic Panel Bearing Capacity, F.pb	44.946	ksi	Ref. 1
Panel Moisture Reduction Factor, C.m	0.85		Ref. 2 Table 2.4-1 for Vinylester
Reduced Panel Bearing Strength = F.pb*Cm	38.204	ksi	
Phi for compression	0.8		Ref. 2 Eqn. 8.3.2-3
Bearing Strength, Phi*Rn=Phi*F.pb*A.pb	3.82	kips	Ref. 2 Eqn. 8.3.2-4
Bearing Strength Capacity/Demand Ratio	**1.57**	Must be > 1	

References:
(Ref. 1) Test results included in design package
(Ref. 2) ASCE Pre-Standard for Design of Pultruded Composites

Service Reactions Per Arch

Max Horizontal				Max Vertical				Max Moment				Min Moment			
	Horizontal (kips)	Vertical (kips)	Mmax (kip-in)		Horizontal (kips)	Vertical (kips)	Mmax (kip-in)		Horizontal (kips)	Vertical (kips)	Mmax (kip-in)		Horizontal (kips)	Vertical (kips)	Mmax (kip-in)
DC	3.1	2.7	7.2	DC	3.1	2.7	7.2	DC	3.1	2.7	7.2	DC	3.1	2.7	7.2
E	94.3	103.1	-244.6	E	94.3	103.1	-244.6	E	94.3	103.1	-244.6	E	91.3	102.4	-332.5
DW	4.0	3.5	6.4	DW	4.0	3.5	6.4	DW	4.0	3.5	6.4	DW	3.9	3.5	3.1
LL_Lane	5.2	4.5	10.3	LL_Lane	5.2	4.5	10.3	LL_Lane	2.7	1.0	59.6	LL_Lane	2.8	3.7	-45.4
LL_Veh	26.8	17.5	134.8	LL_Veh	23.1	19.6	20.8	LL_Veh	22.0	10.6	342.2	LL_Veh	10.2	15.9	-227.7
Total	133.5	131.4	-85.9	Total	129.9	133.5	-199.9	Total	126.2	120.8	170.9	Total	111.2	128.1	-595.3

Service Reactions Per ft

Max Horizontal				Max Vertical				Max Moment				Min Moment			
	Horizontal (kips/ft)	Vertical (kips/ft)	Mmax (kip-in/ft)		Horizontal (kips/ft)	Vertical (kips/ft)	Mmax (kip-in/ft)		Horizontal (kips/ft)	Vertical (kips/ft)	Mmax (kip-in/ft)		Horizontal (kips/ft)	Vertical (kips/ft)	Mmax (kip-in/ft)
DC	0.6	0.5	1.3	DC	0.6	0.5	1.3	DC	0.6	0.5	1.3	DC	0.6	0.5	1.3
E	16.7	18.2	-43.3	E	16.7	18.2	-43.3	E	16.7	18.2	-43.3	E	16.1	18.1	-58.8
DW	0.7	0.6	1.1	DW	0.7	0.6	1.1	DW	0.7	0.6	1.1	DW	0.7	0.6	0.5
LL_Lane	0.9	0.8	1.8	LL_Lane	0.9	0.8	1.8	LL_Lane	0.5	0.2	10.5	LL_Lane	0.5	0.6	-8.0
LL_Veh	4.7	3.1	23.8	LL_Veh	4.1	3.5	3.7	LL_Veh	3.9	1.9	60.5	LL_Veh	1.8	2.8	-40.3
Total	23.6	23.2	-15.2	Total	23.0	23.6	-35.4	Total	22.3	21.4	30.2	Total	19.7	22.7	-105.3

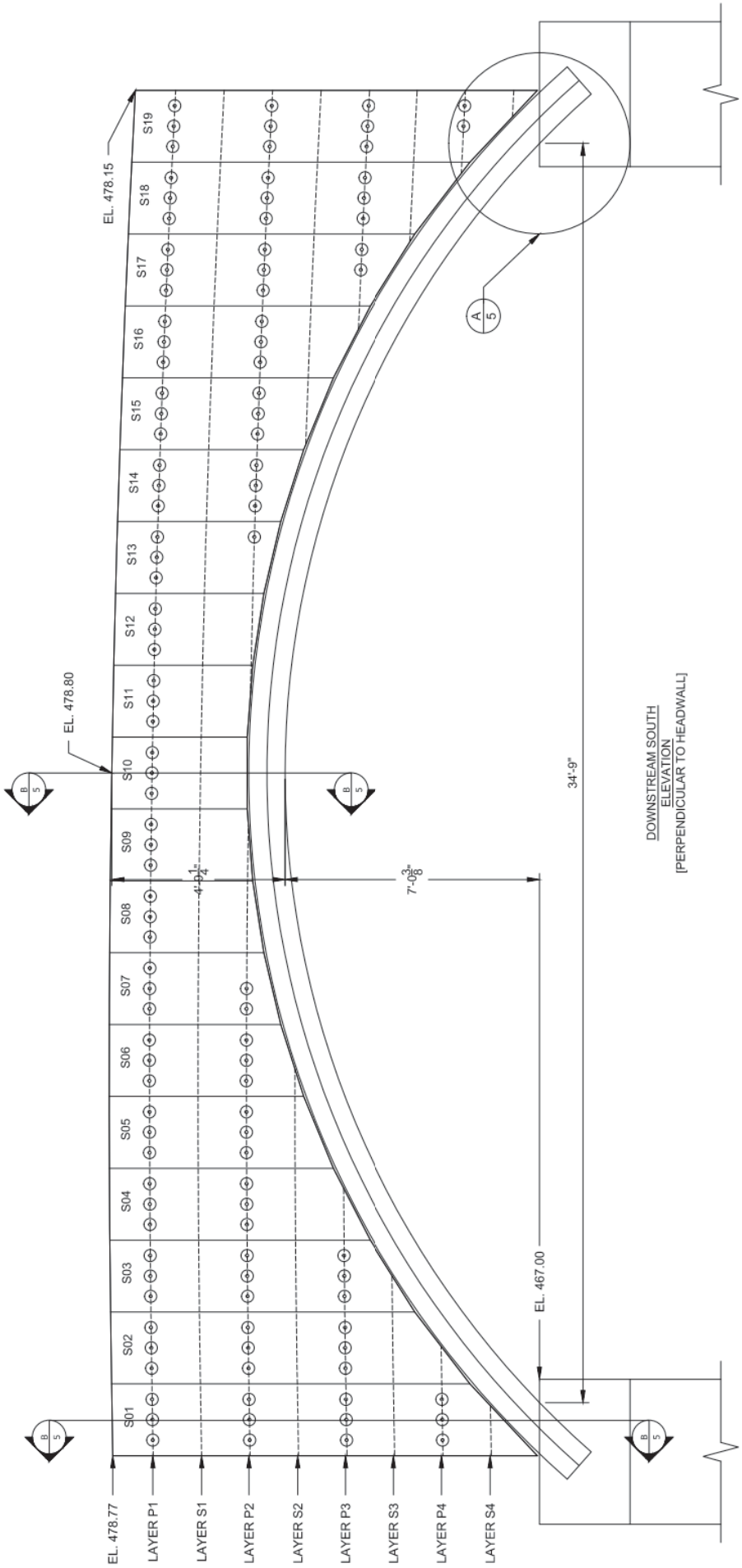
EL. 478.15
EL. 478.80
EL. 478.77
LAYER P1
LAYER S1
LAYER P2
LAYER S2
LAYER P3
LAYER S3
LAYER P4
LAYER S4
S01
S02
S03
S04
S05
S06
S07
S08
S09
S10
S11
S12
S13
S14
S15
S16
S17
S18
S19
4'-0 1/4"
7'-0 3/8"
34'-9"
EL. 467.00
A 5
B 5
DOWNSTREAM SOUTH
ELEVATION
[PERPENDICULAR TO HEADWALL]

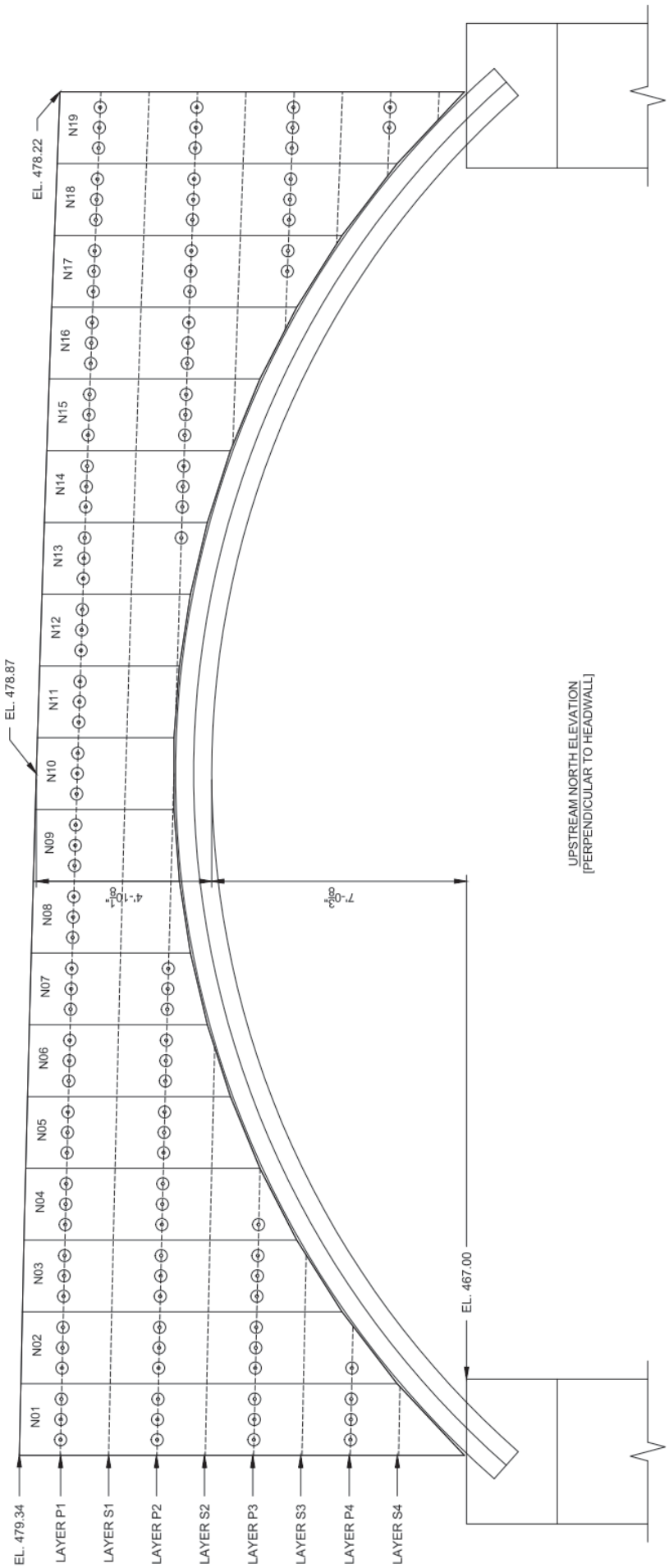
EL. 479.34
LAYER P1
LAYER S1
LAYER P2
LAYER S2
LAYER P3
LAYER S3
LAYER P4
LAYER S4
N01
N02
N03
N04
N05
N06
N07
N08
N09
N10
N11
N12
N13
N14
N15
N16
N17
N18
N19
EL. 478.87
EL. 478.22
4'-10 1/4"
7'-0 3/8"
EL. 467.00
UPSTREAM NORTH ELEVATION
[PERPENDICULAR TO HEADWALL]

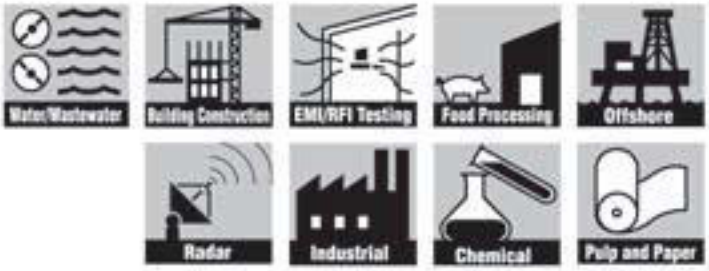

System Components

Mechanical Properties *(minimum)*

Properties	ASTM Test Method	Value	(MPa)
Flexural Strength, LW	D790	24.5 ksi	(169)
Flexural Strength, CW	D790	8.2 ksi	(57)
Flexural Modulus , LW	D790	885 ksi	(6102)
Flexural Modulus, CW	D790	646 ksi	(4454)
Tensile Strength	D638	31.1 ksi	(214)
Tensile Modulus	D638	2,486 ksi	(17140)
Short Beam Shear	D2344	3.19 ksi	(22)

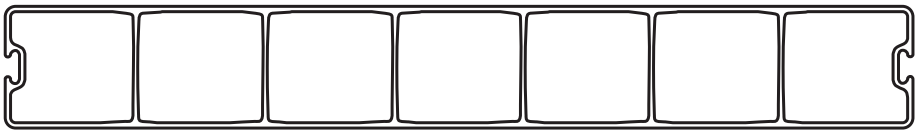

Panel
(3.16" x 23.80" nominal size — 80.26mm x 604.52mm actual) 7.48 lbs/ft (11.13 kg/m)

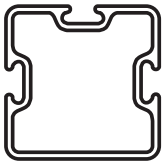

3-Way Connector
3" x 3" nominal size
(80mm x 80mm)
1.70 lbs/ft
(2.53 kg/m)

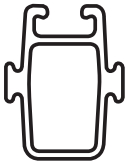

Hanger
1-1/2" x 3" nominal size
(80mm x 40mm)
1.59 lbs/ft
(2.37 kg/m)

Toggle
.33 lbs/ft
(0.49 kg/m)

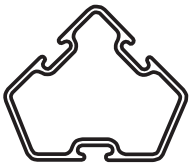

45º Connector
1.75 lbs/ft
(2.61 kg/m)

End Cap
.60 lbs/ft
(0.89 kg/m)

Advanced Infrastructure Technologies

20 Godfrey Drive
Orono, Maine 04473
Telephone: (207) 866-6526
Fax: (207) 866-6501
www.aitbridges.com

Project: *Fairfield, VT*

Task: *Design Headwall Panels*

References

1. *ASCE Pre-Standard for LRFD of Pultruded FRP Structures, November 9, 2010*
2. *Composolite Data Sheet*
3. *CP150.303 Test Data Values base on vinyl ester resin*
4. *Creative Pultrusions SuperLoc Series 1580 Data Sheet*
5. *Composolite DWG file from website*

Inputs:

Time effect factor	$\lambda := 0.4$	*[Ref.1 ASCE T2.3-1 FOR DEAD LOAD ONLY CASE 1.4D]*
Full width of the flange of one cell	$b_f := 3.37in = 3.37 \cdot in$	*[Ref.5]*
Full height of the member	$h := 3.149in = 3.149 \cdot in$	*[Ref.5]*
Thickness of the flange	$t_f := 0.118in = 0.118 \cdot in$	*[Ref.5]*
Thickness of the web	$t_w := 0.156in = 0.156 \cdot in$	*[Ref.5]*
Depth of the web	$d_w := h - t_f = 3.031 \cdot in$	
Radius of fillet between flange and web	$r := 0.118in$	*[Ref.5]*
Distance from the top of the member to the bottom of the fillet	$k := t_f + r = 0.236 \cdot in$	
Bearing Plate Diameter	$d_{plate} := 4.25in$	
Bearing plate thickness	$t_{plate} := 0.25in$	
Bearing Plate Center Hole Diameter	$d_{plate_hole} := \frac{13}{16} in$	*Only includes portion of plate width that spans from web to web*
Bearing plate effective width	$b_{plate} := \sqrt{d_{plate}^2 - (b_f - t_w)^2} - d_{plate_hole} = 1.968 \cdot in$	
Cells per panel	$cells := 7$	
Total Panel width	$w_{panel} := 23.8in$	
Shear area normalized per cell	$A_s := \frac{2.78in^2}{cells} = 0.397 \cdot in^2$	*[Ref.2]*
Section Modulus normalized per cell	$S_x := \frac{10.2in^3}{cells} = 1.457 \cdot in^3$	*[Ref.2]*

Characteristic long. strength of the flange	$F_{LT} := 31100psi = 31.1 \cdot ksi$	*[Ref.2]*
Characteristic long. strength (T or C)	$F_L := F_{LT} = 31.1 \cdot ksi$	*[Ref.2]*
Characteristic trans. strength of the web	$F_{Tw} := 9000psi = 9 \cdot ksi$	*[Ref.4]*
Characteristic trans. tensile strength of the flange	$F_{Tf} := 9000psi = 9 \cdot ksi$	*[Ref.4]*
Characteristic interlaminar shear strength	$F_{sh_int} := 3190psi = 3.19 \cdot ksi$	*[Ref.2]*
Characteristic long. modulus in the flange	$E_{Lf} := 2.486 \cdot 10^6 psi$	*[Ref.2]*
Characteristic long. modulus in the web	$E_{Lw} := 2.486 \cdot 10^6 psi$	*[Ref.2]*
Characteristic trans. modulus in the flange	$E_{Tf} := 1.45 \cdot 10^6 psi$	*[Ref.4]*
Characteristic trans. modulus in the web	$E_{Tw} := 1.45 \cdot 10^6 psi$	*[Ref.4]*
Characteristic in-plane shear modulus	$G_{LT} := 0.4 \cdot 10^6 psi$	*[Ref.1 - minimum value]*
Characteristic long. Poisson's ratio	$\nu_{LT} := 0.30$	*Assumed*

SECTION 5.2 Design of Members for Flexure

Equation 5.2.4 Nominal Strength of Members due to Lateral-Torsional Buckling

NOT APPLICABLE

Equation 5.2.3 Nominal Strength of Members due to Local Instability

Rotational spring constant

$$k_r := \frac{E_{Tw} \cdot t_w^3}{3 \cdot h} \left[1 - \left[\left(\frac{2 \cdot t_f^2 h^2 E_{Lf}}{11.1 \cdot b_f^2 t_w^2 E_{Lf}} \right) \left(\frac{\sqrt{E_{Lf} \cdot E_{Tf}} + E_{Tf} \cdot \nu_{LT} + 2G_{LT}}{1.25\sqrt{E_{Lw} \cdot E_{Tw}} + E_{Tw} \cdot \nu_{LT} + 2G_{LT}} \right) \right] \right] = 0.537 \cdot \frac{kip}{rad}$$

Coefficient of restraint

$$\zeta := \frac{1}{1 + \frac{4 \cdot E_{Tf} \cdot t_f^3}{5 \cdot k_r \cdot b_f}} = 0.487$$

Equations 5.2.3.4 Square and Rectangular Box Members

(a) Compression flange local buckling

$$f_{cr_flange} := \frac{4\cdot\pi^2\cdot t_f^{\,2}}{b_f^{\,2}}\cdot\left[\frac{\sqrt{E_{Lf}\cdot E_{Tf}\cdot(1+4.1\cdot\zeta)}}{6} + \left(2+0.62\zeta^2\right)\left(\frac{E_{Tf}\cdot\nu_{LT}}{12}+\frac{G_{LT}}{6}\right)\right] = 37.211\cdot ksi$$

(b) Web local buckling

$$f_{cr_web} := \frac{11.1\cdot\pi^2\cdot t_w^{\,2}}{6\cdot h^2}\cdot\left(1.25\sqrt{E_{Lw}\cdot E_{Tw}} + E_{Tw}\cdot\nu_{LT} + 2G_{LT}\right) = 161.686\cdot ksi$$

$$f_{cr_5234} := \min\left(f_{cr_flange}, f_{cr_web}\right) = 37.211\cdot ksi$$

$$\Phi_{523} := 0.80$$

$$M_{n_523} := f_{cr_5234}\cdot S_x = 54.222\cdot in\cdot kip$$

$$\boxed{\Phi M_{n_523} := \Phi_{523}\cdot M_{n_523}\cdot\frac{cells}{w_{panel}} = 153.098\cdot\frac{in\cdot kip}{ft}}$$

Equation 5.2.2 Nominal Strength of Members due to Material Rupture

$$\Phi_{522} := 0.65$$

$$M_{n_522} := F_L\cdot S_x = 45.317\cdot in\cdot kip$$

$$\boxed{\Phi M_{n_522} := \Phi_{522}\cdot M_{n_522}\cdot\frac{cells}{w_{panel}} = 103.963\cdot\frac{in\cdot kip}{ft}}$$

$$\boxed{\Phi M_n := \min\left(\Phi M_{n_522}, \Phi M_{n_523}\right) = 103.963\cdot\frac{in\cdot kip}{ft}}$$

Equation 5.2.1 Design Basis for Flexure

$$\boxed{M_u := \Phi M_n\cdot\lambda = 41.585\cdot\frac{in\cdot kip}{ft}}$$

SECTION 5.3 Design of Members for Shear

Equation 5.3.2 Nominal Strength of Members due to Material Rupture in Shear

$$\Phi_{532} := 0.65$$

$$V_{n_532} := F_{LT}\cdot A_s = 3.765\,m\cdot\frac{kip}{ft}$$

$$\boxed{\Phi V_{n_.532} := \Phi_{532}\cdot V_{n_532}\cdot\frac{cells}{w_{panel}} = 28.335\cdot\frac{kip}{ft}}$$

Equation 5.3.3 Nominal Strength of Members due to Web Shear Buckling

$\Phi_{533} := 0.80$

A $2 \cdot G_{LT} + E_{Tw} \cdot \nu_{LT} = 1235 \cdot ksi$

B $\sqrt{E_{Lw} \cdot E_{Tw}} = 1898.605 \cdot ksi$

If A < B use the following

$$k_{LT1} := 8.1 + 5.0 \cdot \frac{2 \cdot G_{LT} + E_{Tw} \cdot \nu_{LT}}{\sqrt{E_{Lw} \cdot E_{Tw}}} = 11.352$$

$$f_{cr_533} := \frac{t_w^{\,2} \cdot k_{LT1} \cdot \sqrt[4]{E_{Lw} \cdot E_{Tw}^{\,3}}}{3 \cdot h^2} = 15.409 \cdot ksi$$

$$V_{n_533} := f_{cr_533} \cdot A_s = 1.865\,m \cdot \frac{kip}{ft}$$

$$\boxed{\Phi V_{n_.533} := \Phi_{533} \cdot V_{n_533} \cdot \frac{cells}{w_{panel}} = 17.279 \cdot \frac{kip}{ft}}$$

Equation 5.3.1 Design Basis for Shear

$$\Phi V_n := \min\left(\Phi V_{n_.532}, \Phi V_{n_.533}\right) = 17.279 \cdot \frac{kip}{ft}$$

$$\boxed{V_u := \lambda \cdot \Phi V_n = 6.911 \cdot \frac{kip}{ft}}$$

SECTION 5.4 Design of Members for Concentrated Loads

Equation 5.4.2 Nominal Strength of Members due to Tensile Rupture of Webs

$\Phi_{542} := 0.65$

$l_{ten} := h = 3.149 \cdot in$

$R_{n_542} := l_{ten} \cdot F_{Tw} \cdot t_w = 4.421 \cdot kip$

$\boxed{\Phi R_{n_542} := \Phi_{542} \cdot R_{n_542} = 2.874 \cdot kip}$ *PER WEB*

DOES NOT OCCUR

Equation 5.4.3 Nominal Strength of Members due to Web Crippling

$\Phi_{543} := 0.70$

$$R_{n_543} := 0.7 \cdot h \cdot t_w \cdot F_{sh_int} \cdot \left(1 + \frac{2 \cdot k + 6 \cdot t_{plate} + b_{plate}}{d_w}\right) = 2.523 \cdot kip$$

$\boxed{\Phi R_{n_543} := \Phi_{543} \cdot R_{n_543} = 1.766 \cdot kip}$ *PER WEB*

Equation 5.4.4 Nominal Strength of Members due to Web Compression Buckling

$\Phi_{544} := 0.80$

$l_{eff} := d_w = 3.031 \cdot in$ *MUST BE CHANGED FOR WEB STIFFENERS*

$A_{eff} := l_{eff} \cdot t_w = 0.473 \cdot in^2$

$$f_{cr_544} := \frac{\pi^2 \cdot t_w^2}{6 \cdot l_{eff}^2} \cdot \left(\sqrt{E_{Lw} \cdot E_{Tw}} + E_{Tw} \cdot \nu_{LT} + 2 \cdot G_{LT}\right) = 13.654 \cdot ksi$$

$R_{n_544} := f_{cr_544} \cdot A_{eff} = 6.456 \cdot kip$

$\boxed{\Phi R_{n_544} := \Phi_{544} \cdot R_{n_544} = 5.165 \cdot kip}$ *PER WEB*

Equation 5.4.5 Nominal Strength of Members due to Flange Flexural Failure

$\Phi_{545} := 0.65$

$$l_e := \frac{b_f}{2} = 1.685 \cdot in$$

$b := l_e \cdot 2 = 3.37 \cdot in$

$$R_{n_545} := \frac{F_{Tf} \cdot b \cdot (t_f)^2}{6 \cdot l_e} = 0.042 \cdot kip$$

$\boxed{\Phi R_{n_545} := \Phi_{545} \cdot R_{n_545} = 0.027 \cdot kip}$ *PER WEB*

Flange Flexural Failure based on Steel bearing plate

Provide a steel bearing plate to draw load away from FRP flange

$P := 1.37kip$

$F_{plate} := 60ksi$

$$t_{steel} := \sqrt{\frac{P \cdot 6 \cdot l_e}{F_{plate} \cdot b_{plate}}} = 0.342 \cdot in$$

Equation 5.4.1 Design Basis

$$\Phi R_n := \min(\Phi R_{n_543}, \Phi R_{n_544}) = 1.766 \cdot kip$$

$$\Phi R_u := \lambda \cdot \Phi R_n = 0.706 \cdot kip$$

PER WEB

Design Capacity Summary

Allowable Moment Capacity

$$M_u := \Phi M_n \cdot \lambda = 41.585 \cdot in \cdot \frac{kip}{ft}$$

Allowable Shear Capacity

$$V_u := \lambda \cdot \Phi V_n = 6.911 \cdot \frac{kip}{ft}$$

Allowable Pull Through Capacity

$$\Phi R_{u_per_foot} := \Phi R_u \cdot \frac{12in}{b_f} \frac{1}{ft} = 2.515 \cdot \frac{kip}{ft}$$

capacities given for loads applied as a strip load per width of wall

Allowable Uniform Load Table (psf) (kPA)

SPAN	@Δ=Span/60			@Δ=Span/120			@Δ=Span/180		
(ft.) (m)	Δ (IN.) (mm)	Siding	Roofing	Δ (IN.) (mm)	Siding	Roofing	Δ (IN.) (mm)	Siding	Roofing
4 (1.22)	.8 (20.3)	*778 (37.3)	*774 (37.1)	.4 (10.2)	*778 (37.3)	*774 (37.1)	.27 (6.9)	*778 (37.3)	*774 (37.1)
5 (1.52)	1.0 (25.4)	*624 (29.9)	*620 (29.7)	.5 (12.7)	*624 (29.9)	*620 (29.7)	.33 (8.4)	490 (23.5)	486 (23.3)
6 (1.83)	1.2 (30.5)	*520 (24.9)	*516 (24.7)	.6 (15.2)	449 (21.5)	445 (21.3)	.40 (10.2)	299 (14.3)	295 (14.1)
7 (2.13)	1.4 (35.6)	*466 (22.3)	*466 (22.3)	.7 (17.8)	303 (14.5)	299 (14.3)	.47 (11.9)	204 (9.8)	200 (9.6)
8 (2.44)	1.6 (40.6)	*390 (18.7)	*386 (18.5)	.8 (20.3)	214 (10.2)	210 (10.1)	.53 (13.5)	142 (6.8)	138 (6.6)
9 (2.74)	1.8 (45.7)	311 (14.9)	308 (14.7)	.9 (22.9)	156 (7.5)	152 (7.3)	.60 (15.2)	104 (5.0)	100 (4.7)
10 (3.05)	2.0 (50.8)	233 (11.1)	229 (11.0)	1.0 (25.4)	116 (5.5)	112 (5.4)	.67 (17.0)	78 (3.7)	74 (3.5)
11 (3.35)	2.2 (55.9)	176 (8.4)	172 (8.2)	1.1 (27.9)	88 (4.2)	84 (4.0)	.73 (18.5)	59 (2.8)	55 (2.6)
12 (3.66)	2.4 (61.0)	140 (6.7)	136 (6.5)	1.2 (30.5)	70 (3.4)	64 (3.1)	.80 (20.3)	47 (2.3)	43 (2.1)
13 (3.96)	2.6 (66.0)	110 (5.3)	106 (5.1)	1.3 (33.0)	56 (2.7)	52 (2.5)	.87 (22.1)	37 (1.8)	33 (1.6)
14 (4.27)	2.8 (71.1)	90 (4.3)	86 (4.1)	1.4 (35.6)	48 (2.3)	44 (2.1)	.93 (23.6)	30 (1.4)	26 (1.2)
15 (4.57)	3.0 (76.2)	74 (3.5)	70 (3.4)	1.5 (38.1)	37 (1.8)	33 (1.5)	1.00 (25.4)	25 (1.2)	21 (1.0)
16 (4.88)	3.2 (81.3)	61 (2.9)	57 (2.7)	1.6 (40.6)	30 (1.4)	26 (1.2)	1.09 (27.7)	21 (1.0)	17 (0.8)
17 (5.18)	3.4 (86.4)	51 (2.4)	47 (2.3)	1.7 (43.2)	25 (1.2)	21 (1.0)	1.13 (28.7)	17 (0.8)	13 (0.6)
18 (5.49)	3.6 (91.4)	43 (2.1)	39 (1.9)	1.8 (45.7)	22 (1.1)	18 (.86)	1.20 (30.5)	14 (0.7)	10 (0.5)
19 (5.79)	3.8 (95.5)	36 (1.7)	32 (1.5)	1.9 (48.3)	18 (.86)	14 (.67)	1.27 (32.3)	12 (0.6)	8 (0.4)
20 (6.10)	4.0 (101.6)	32 (1.5)	28 (1.3)	2.0 (50.8)	15 (.71)	11 (.52)	1.33 (33.8)	11 (0.5)	7 (0.3)

**Controlled by strength with a factor of safety of 2.50 for flexural and 3.0 for shear. Note: All values are typical.*

Section Properties

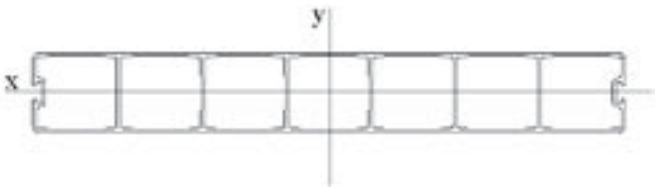

I_x =15.9 in.^{4} (6.62 x 10^6 mm^4)

S_x =10.2 in.^{3} (0.167 x 10^6 mm^3)

r_x =1.33 in. (33.8 mm)

I_y =422 in.^{4} (176 x 10^6 mm^4)

S_y =39.9 in.^{3} (0.654 x 10^6 mm^4)

r_y =6.88 in. (176 mm)

A =8.89 in.^{2} (5735 mm^2)

Aw_x =2.78 in.^{2} (1794 mm^2)

Aw_y=6.11 in.^{2} (3942 mm^2)

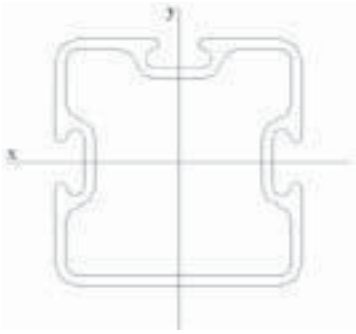

I_{xx} =2.73 in.^{4} (1.14 x 10^6 mm^4)

I_{yy} =2.69 in.^{4} (1.11 x 10^6 mm^4)

S_{xx} =1.80 in.^{3} (2.95 x 10^4 mm^4)

S_{yy} =1.71 in.^{3} (2.80 x 10^4 mm^4)

A =2.01 in.^{2} (1296 mm^2)

r_x =1.17 in. (30 mm)

r_y =1.17 in. (29 mm)

MATERIAL PROPERTIES

Pultex® Fiber Reinforced Polymer Structural Profiles
Rectangular Tubes, Channels, Angles, Square Tubes, Round Tubes

Includes all angles except 4" x 1/4", 4" x 3/8", 6" x 3/8" and 6" x 1/2", which are SuperStructurals.
Please consult the Pultex® Fiber Reinforced Polymer SuperStructural Profiles Angles Material Properties

1500 Series - Thermoset Polyester – Olive Green
1525 Series - Thermoset Polyester Class 1 FR – Slate Gray (Dark Gray)
1625 Series - Thermoset Vinyl Ester Class 1 FR – Beige

The following data was derived from ASTM coupon and full section testing. The results are average values based on random sampling and testing of production lots. Composite materials are not homogeneous; and therefore, the location of the coupon extraction can cause variances in the coupon test results. Creative Pultrusions publishes an average value of random samples from production lots.

Property (coupon values)	ASTM Test	Units	1500/1525 Series	1625 Series
Mechanical				
Tensile Strength (LW)	D638	psi	33,000	37,500
Tensile Strength (CW)	D638	psi	7,500	8,000
Tensile Modulus (LW)	D638	10^6 psi	2.5	3.0
Tensile Modulus (CW)	D638	10^6 psi	0.8	1.0
Compressive Strength (LW)	D695	psi	33,000	37,500
Compressive Strength (CW)	D695	psi	16,500	20,000
Compressive Modulus (LW)	D695	10^6 psi	3.0	3.0
Compressive Modulus (CW)	D695	10^6 psi	1.0	1.2
Flexural Strength (LW)	D790	psi	33,000	37,500
Flexural Strength (CW)	D790	psi	11,000	*12,500*
Flexural Modulus (LW)	D790	10^6 psi	1.6	2.0
Flexural Modulus (CW)	D790	10^6 psi	0.8	1.0
Modulus of Elasticity	Full Section[2]	10^6 psi	2.8-3.2	2.8-3.2
(Channels)	Full Section[2]	10^6 psi	2.8	2.8
(Square and Rectangular Tubes)	Full Section[2]	10^6 psi	3.2	3.2
Shear Modulus	Full Section[2]	10^6 psi	0.42	0.42
Interlaminar Shear (LW)[3]	D2344	psi	4,500	4,500
Shear Strength By Punch (PF)	D732	psi	5,500	6,000
Notched Izod Impact (LW)	D256	ft-lbs/in	28	30
Notched Izod Impact (CW)	D256	ft-lbs/in	4	5
Maximum Bearing Strength (LW)	D953	psi	30,000	30,000
Maximum Bearing Strength (CW)	D953	psi	18,000	18,000
Poisson's Ratio (LW)	D3039	in/in	0.35	0.35
Poisson's Ratio (CW)	D3039	in/in	0.15	0.15
In-plane Shear (LW)	Modified D2344[4]	psi	7,000	7,000

LW = lengthwise CW = crosswise PF = perpendicular to laminate face

Additional properties located on page 4

MATERIAL PROPERTIES

Pultex® Fiber Reinforced Polymer Structural Profiles
Rectangular Tubes, Channels, Angles, Square Tubes, Round Tubes

Includes all angles except 4" x 1/4", 4" x 3/8", 6" x 3/8" and 6" x 1/2", which are SuperStructurals.
Please consult the Pultex® Fiber Reinforced Polymer SuperStructural Profiles Angles Material Properties

Property (coupon values)	**ASTM Test**	**Units**	**1500/1525 Series**	**1625 Series**
Physical				
Barcol Hardness[1]	D2583		45	45
Water Absorption	D570	% Max	0.6	0.6
Density	D792	lbs/in^3	0.060-0.070	0.060-0.070
Specific Gravity	D792		1.66-1.93	1.66-1.93
Coefficient of Thermal Expansion (LW)	D696	10^{-6}in/in/°F	4.4	4.4
Thermal Conductivity (PF)	C177	BTU-in/ft^2/hr/°F	4	4
Electrical				
Arc Resistance (LW)	D495	seconds	120	120
Dielectric Strength (LW)	D149	KV/in	40	40
Dielectric Strength (PF)	D149	volts/mil	200	200
Dielectric Constant (PF)	D150	@60Hz	5.2	5.2

[1] Pultex® uses a synthetic surface veil that reduces the Barcol Hardness, but does not reflect lack of cure.
[2] Full section testing based on a 3-point bend with simply supported end conditions (Reference The *New and Improved* Pultex® Pultrusion Global Design Manual, Appendix B, for details).
[3] Tested on a 3:1, span to depth ratio.
[4] Follow ASTM D2344, but rotate coupon 90° (cut section of coupon length faces up).
[5] In-plane Shear (CW) values for square tubes and rectangular tubes = 2,500 psi; angles = 3,800 psi

	ASTM Test	**Value**	**Value**
Property		**1525**	**1625**
Flammability Classification	UL94	(VO)	(VO)
Tunnel Test	ASTM E-84	25 Max	25 Max
Flammability Extinguishing	ASTM D635	Self extinguishing	Self extinguishing
NBS Smoke Chamber	ASTM E662	650	650

Creative Pultrusions, Inc. believes the information put forth in this property sheet to be as accurate and reliable as of the date of publication. However, we assume no obligation or liability, which may arise as a result of its use. While Creative Pultrusions, Inc. has no knowledge that the information put forth infringes any valid patent, it assumes no responsibility with respect thereto and each user must satisfy oneself that one's intended application process or product infringes no patent.

Miragrid® 5XT

Miragrid® 5XT geogrid is composed of high molecular weight, high tenacity polyester multifilament yarns which are woven in tension and finished with a PVC coating. Miragrid® 5XT geogrid is inert to biological degradation and resistant to naturally encountered chemicals, alkalis, and acids.

TenCate Geosynthetics Americas is accredited by a2La (The American Association for Laboratory Accreditation) and Geosynthetic Accreditation Institute – Laboratory Accreditation Program (GAI-LAP). NTPEP test data.

Mechanical Properties	Test Method	Unit	Minimum Average Roll Value
			Machine Direction
Tensile Strength (at ultimate)	ASTM D6637	lbs/ft (kN/m)	4700 (68.6)
Tensile Strength (at 5% strain)	ASTM D6637	lbs/ft (kN/m)	1740 (25.4)
Creep Reduced Strength	ASTM D5262	lbs/ft (kN/m)	2975 (43.4)
Long Term Allowable Design Load[1]	GRI GG-4(b)	lbs/ft (kN/m)	2575 (37.6)

[1] NOTE: Long Term Allowable Design values are for sand, silt and clay

Physical Properties	Unit	Typical Value
Mass/Unit Area (ASTM D5261)	oz/yd^2 (g/m^2)	9.8 (332)
Roll Dimensions (width x length)	ft (m)	12 x 150 (3.6 x 46)
Roll Area	yd^2 (m^2)	200 (165)
Estimated Roll Weight	lbs (kg)	130 (59)

© 2012 TenCate Geosynthetics Americas
Miragrid® is a registered trademark of Nicolon Corporation

Disclaimer: TenCate assumes no liability for the accuracy or completeness of this information or for the ultimate use by the purchaser. TenCate disclaims any and all express, implied, or statutory standards, warranties or guarantees, including without limitation any implied warranty as to merchantability or fitness for a particular purpose or arising from a course of dealing or usage of trade as to any equipment, materials, or information furnished herewith. This document should not be construed as engineering advice.

Creep Reduced Strength (ASTM D5262), and Long Term Allowable Design Load (GRI GG-4(b)) is not covered by our current A2LA accreditation.

Made in USA

365 South Holland Drive
Pendergrass, GA 30567

Tel 706 693 2226
Tel 888 795 0808

Fax 706 693 4400
www.tencate.com

TENCATE Mirafi®

SOIL REINFORCEMENT

Miragrid® Geogrids
for Soil Reinforcement

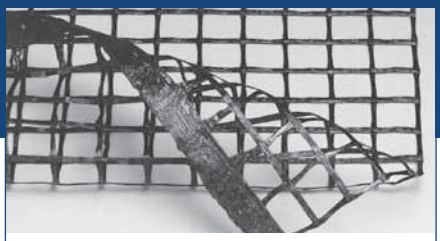

Miragrid® 5XT

TenCate develops and produces materials that function to increase performance, reduce costs and deliver measurable results by working with our customers to provide advanced solutions.

The Difference Miragrid® Geogrids Make:

- High long-term design strengths (LTDS). Miragrid® geogrids have more than 100,000 hours of tension creep testing performed at an independent test laboratory. Credible, dependable long term strength assured.
- Cost effective. Creep resistant polyester fibers provide higher allowable tensile strength, minimizing the required number of geogrid layers. Wide rolls significantly reducing placement time, lowering cost.
- Light weight, easy to handle. No sharp edges.
- Flexible, tough. Minimizes movement of soil structure.
- Custom fabrication. Rolls fabricated to meet your specific project requirements.
- Miragrid® geogrids provide the widest strength range, and are the highest strength geogrid material in the market today.

APPLICATIONS

Miragrid® geogrids can be used in most MSE applications for soil reinforcement including internally reinforced soil walls, segmental retaining wall reinforcement, steep reinforced slopes, and reinforcement in a variety of landfill applications including potential voids bridging and veneer stability. When a project specifies for long-term design strength for structure stability use Miragrid® geogrids.

INSTALLATION GUIDELINES

Before placing Miragrid® geogrids, the surface should be cleared of all debris and the foundation base proofrolled. The grids should be rolled out, cut to length, thus eliminating field connections and laid at the proper elevation, location and orientation. Since geogrids vary in strength with roll direction, Miragrid® geogrids should be laid in the direction of main reinforcement.

After rolling out, the geogrid should be tensioned by hand until it is taut, free of wrinkles, and lying flat. Adjacent geogrid rolls may be butted together side-by-side without overlap. Splices in the main reinforcement direction should be avoided.

Certain fill placement procedures may require the reinforcement to be held in place by stakes, sandbags, or fills, as directed by an engineer. A razor blade, sharp knife or scissors may be used to cut the geogrid. Fill placement should follow the standard practice, or as defined in the project specifications or directed by the Engineer. Care should be taken to prevent wrinkles and/or slippage of reinforcement during fill placement and spreading.

These guidelines serve as a general basis for installation. Detailed instructions are available from your TenCate representative.

TENCATE Mirafi®

Miragrid® Geogrids

for Soil Reinforcement

Property*	Test Method	Units	2XT[1]	3XT	5XT	7XT	8XT	10XT	20XT	22XT	24XT
Polymer (coating)	–	–	PET (PVC)	PET (PVC)	PET (PVC)	PET (PVC)	PET (PVC)	PET (PVC)	PET (PVC)	PET (PVC)	PET (PVC)
Tensile Strength @ Ultimate (MARV)	ASTM D6637	lbs/ft (kN/m)	2000 (29.2)	3500 (51.1)	4700 (68.6)	5900 (86.1)	7400 (108.0)	9500 (138.6)	13705 (200.0)	20559 (300.0)	27415 (400.0)
Creep Reduced Strength	ASTM D5262	lbs/ft (kN/m)	1266 (18.5)	2215 (32.3)	2975 (43.4)	3734 (54.5)	4684 (68.3)	6013 (88.0)	8674 (127.0)	13012 (190)	17351 (253)
Long Term Design Strength (In Type 3 Backfill) (sand, silt, clay)	GRI-GG4	lbs/ft (kN/m)	1096 (16.0)	1918 (28.0)	2575 (37.6)	3233 (47.2)	4055 (59.2)	5206 (76.0)	7510 (110.0)	11266 (164.0)	15023 (219.0)

Packaging	Units	2XT[2]	3XT[2]	5XT[2]	7XT[2]	8XT[2]	10XT	20XT	22XT	24XT
Roll Width	ft (m)	12 (3.6)	12 (3.6)	12 (3.6)	12 (3.6)	12 (3.6)	12 (3.6)	12 (3.6)	12 (3.6)	12 (3.6)
Roll Length	ft (m)	150 (46)	150 (46)	150 (46)	200 (61)	200 (61)	200 (61)	200 (61)	200 (61)	200 (61)
Estimate Roll Weight	lbs (kg)	101 (46)	119 (54)	130 (59)	163 (74)	187 (85)	223 (106)	387 (175)	499 (226)	628 (284)
Area	yd^2 (m^2)	200 (165)	200 (165)	200 (165)	267 (220)	267 (220)	267 (220)	267 (220)	267 (220)	267 (220)

[1]Note: Values shown for 2XT are both machine and cross-machine direction. Values for other Mirafi® products are machine direction only.
[2]Also available in 1.8m (6ft) wide by 45.7m (150ft) long rolls

Miragrid® Geogrids Typical Applications

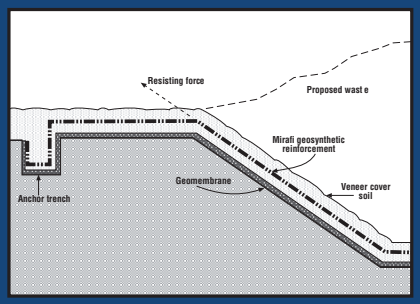

Veneer Reinforcement

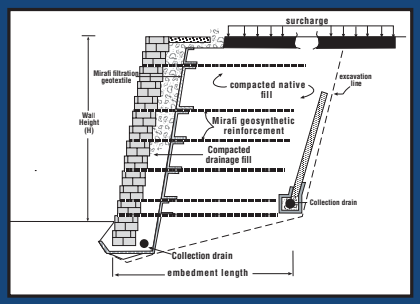

Retaining Wall

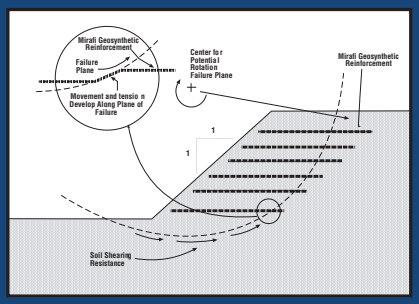

Steepened Slope

TenCate Geosynthetics Americas assumes no liability for the accuracy or completeness of this information or for the ultimate use by the purchaser. TenCate Geosynthetics Americas disclaims any and all express, implied, or statutory standards, warranties or guarantees, including without limitation any implied warranty as to merchantability or fitness for a particular purpose or arising from a course of dealing or usage of trade as to any equipment, materials, or information furnished herewith. This document should not be construed as engineering advice.

Mirafi® is a registered trademark of Nicolon Corporation.

© 2014 TenCate Geosynthetics Americas

PDS.GRID(M)0114

365 South Holland Drive Tel 800 685 9990 Fax 706 693 4400
Pendergrass, GA 30567 Tel 706 693 2226 www.mirafi.com

QUALITY ASSURANCE ACCREDITED LABORATORY GAI-LAP-25-07

GMA Geosynthetic Materials Association

BSI ISO 9001 FM 61026

TENCATE materials that make a difference

INEXTENSIBLE HEADWALL DESIGN WORKSHEET

Step 1: Establish Project Requirements

Exposed Wall Height			12.34	ft
Length of Wall			1	ft
Design Life			120	yrs
Panel Units		width	2	ft
		height	12.34	ft
		thickness	3.125	in
		angle	90	degrees
Type of Reinforcement	Gr.65 Steel bar mat with D11 bars		65	ksi
1 - Extensible (geogrid)	2 - Inextensible (steel)		1	
No Seismic considerations				

Step 2: Evaluate Project Parameters

Reinforced Backfill: ϕ'r=34°, gamma.r = pcf, C.u = 7.0 and meets AASHTO requirements for electrochemical properties			
	ϕ'r	34	degrees
	gamma.r	125	pcf
	C.u	7	
Retained backfill: ϕ'r=34°, gamma.f = 120 pcf			
	ϕ'f	34	degrees
	gamma.f	125	pcf
Foundation Soil:			
	ϕ'fd	34	degrees
	gamma.fd	125	pcf
Factored Bearing resistance of foundation soil:			
For service limit state for given settlement	q.nf-ser =		ksf
amount of settlement			in
For strength limit state:	q.nf-str =		ksf
Live Load Surcharge: per AASHTO T-3.11.6.4-2	h.eq	2	ft-soil

Step 3: Estimate Depth of Embedment and Length of Reinforcement

Foot of headwall is situated on footing and grouted into keyway, use 0" embedment for calcs							
per AASHTO Table C.11.10.2.2.-1					d	0	ft
					H=H.e+d	12.34	ft
Sloped backfill conditions suggests 0.9H embedment length							
Slope Run	4.5	ft	slope		L	12	ft
Slope Height, c	2.25	ft		26.6 degrees	suggested	12	ft
Total Height (H+c)	14.59	ft					

Step 4: Estimate Unfactored Loads

Coefficients of Lateral Earth Pressure	K.ar	0.283
K=(1-sin(phi))/(1+sin(phi))	K.af	0.283

Figure 1

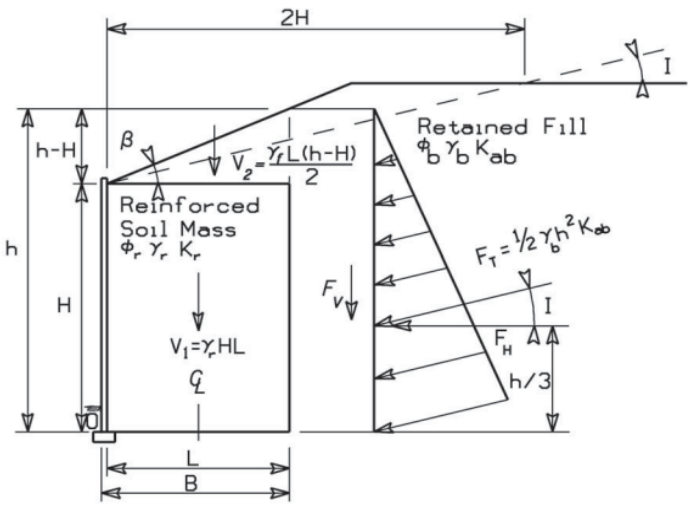

Figure 4-4. External analysis: earth pressure; broken backslope case (after AASHTO, 2007).

I=β=atan(c/2H)	5.2	degrees
Γ	2.42	
Active Earth Pressure Coefficient, Kab	0.286	

$$K_{ab} = \frac{\sin^2(\theta + \phi_b')}{\Gamma \sin^2\theta \sin(\theta - \delta)}$$

F.1 = 1/2*gamma.f*h^2*Kab = Retained Soil Load	3.80	k/lft
F.2 = gamma.f*LLS_height*h*Kab= Live Load Surcharge	1.04	

Table 1: Equations of computing unfactored vertical forces and moments

Vertical Force (Force/length units)	LRFD Load Type	Moment Arm (Length units) @Pt.O
V.1 = gamma.r*H*L	EV	L/2
V.2 = 1/2*gamma.r*(h-H)*L	EV	L*2/3
F.v1 = F.1*sin(I)	LL	L
F.v2 = F.2*sin(I)	LL	L
Note: h.eq is the equivalent height of soil such that q=gamma.f*h.eq		

Table 2: Equations of computing unfactored horizontal forces and moments

Horizontal Force (Force/length units)	LRFD Load Type	Moment Arm (Length units) @Pt.A
F.h1 = F.1*cos(I)	EH	h/3
F.h2 = F.2*cos(I)	LL	h/2

Table 3: Unfactored vertical forces and moments

Force	Value k/ft	Moment Arm @Pt.A (ft)	Moment	Moment @Pt.A (k-ft/ft)	LRFD Load Type
V.1	18.51	6	MV.1	111.1	EV
V.2	1.69	8	MV.2	13.5	EV
F.v1	0.35	12	MF1	4.1	EH
F.v2	0.09	12	MF2	1.1	LL

Table 4: Unfactored horizontal forces and moments

Force	Value k/ft	Moment Arm @Pt.A (ft)	Moment	Moment @Pt.A (k-ft/ft)	LRFD Load Type
F.h1	3.79	4.11	MF.1	15.6	EH
F.h2	1.04	6.17	MF.2	6.4	LL

Step 5: Summarize Applicable Load and Resistance Factors

Table 5: Summary of applicable load factors

Load Combination	AASHTO 3.4.1-1,2		
	EV	EH	LL
Strength 1 (max)	1.35	1.50	1.75
Strength 1 (min)	1.00	0.90	1.75
Service 1	1.00	1.00	1.00

Table 6: Summary of resistance factors for evaluation of resistances

Item	Resistance Factors	
Sliding of MSE wall on foundation soil	phi.s	1.00
Bearing resistance	phi.b	0.65
Tensile resistance (for steel bar mats)	phi.t	0.65
Tensile resistance (for geosynthetic)	phi.t	0.90
Pullout resistance	phi.p	0.90

Step 6: Evaluate External Stability of MSE Wall

6.1 Sliding Resistance at Base of MSE Wall

The purpose of these computations is to evaluate the sliding resistance at the base of the MSE wall. Since the computations are related to sliding resistance, the beneficial contribution of live load to resisting forces and moments is neglected. The computations for sliding resistance at the base of the MSE wall are illustrated in Table E4-6.1. Note that sliding resistance is a strength limit state check and therefore service limit state calculations are not performed. Since the friction angle of foundation soil, ϕ'_{fd}, is less than the friction angle for reinforced soil, ϕ'_r, the sliding check will be performed using ϕ'_{fd}. The critical values based on max/min result in the extreme force effect and govern the sliding mode of failure.

Table 7: Computations for evaluation of sliding resistance of MSE wall

Item	Unit	Str1(max)	Str1 (min)	Ser1
Lateral load on the MSE wall, H.m=F.1+F.2	k/ft	7.50	5.22	-
Vertical load at base of MSE wall without LL surcharge = V.1	k/ft	27.78	20.51	-
Nominal sliding resistance at base of MSE wall, V.Nm = tan(phi.fd)(V.1)	k/ft	18.74	13.83	-
Sliding resistance at base of MSE wall, V.Fm=phi.s*V.Nm	k/ft	18.74	13.83	-
Is V.Fm > H.m?	-	YES	YES	-
Capacity: Demand Ratio (CDR) = V.Fm:H.m		2.50	2.65	-
CRITICAL VALUES BASED ON MAX/MIN				
Minimum V.Fm (V.Fmmin)	k/ft	13.83		-
Maximum H.m (Hmmax)	k/ft	7.50		-
Is V.Fmmin > H.mmax? Design OK?	-	**YES**		-
Capacity: Demand Ratio (CDR) = V.Fm:minH.max		**1.85**		-

6.2 Limiting Eccentricity at Base of MSE Wall

The purpose of these computations is to evaluate the limiting eccentricity at the base of the MSE wall. Since the computations are related to limiting eccentricity, the beneficial contribution of live load to resisting forces and moments is neglected. The computations for limiting eccentricity at the base of the MSE wall are illustrated in Table E4-6.2. Limiting eccentricity is a strength limit state check and therefore service limit state calculations are not performed. The critical values based on max/min result in the extreme force effect and govern the limiting eccentricity mode of failure.

Table 7: Computations for evaluation of sliding resistance of MSE wall

Item	Unit	Str1(max)	Str1 (min)	Ser1
Total vertical load at base of MSE wall w/o LL, V.A=V.1	k/ft	27.78	20.51	-
Resisting moments abt Pt.A w/o LL surcharge = M.RA = MV.1	k-ft/ft	174.37	128.29	-
Overturning moments abt Pt.A = M.OA = MF.1+MF.2	k-ft/ft	34.57	25.22	-
Net Moment abt Pt.A = M.A=M.RA-M.OA	k-ft/ft	139.80	103.06	-
Location of resultant force on base of MSE wall from Pt.A, a=M.A/V.A	ft	5.03	5.03	-
Eccentricity at base of MSE wall, e.L = L/2-a	ft	0.97	0.97	-
Limiting eccentricity, e=L/4 for strength limit state	ft	3.00	3.00	-
Is the resultant within limitng value of e?	-	YES	YES	-
Calculated e.L/L	-	0.08	0.08	-
CRITICAL VALUES BASED ON MAX/MIN				
Overturning moments abt Pt.A = M.OA-C	k-ft/ft	34.57		-
Resisting moments abt Pt.A, M.RA-C	k-ft/ft	128.29		-
Net Moment abt Pt.A, M.A-C=M.RA-C - M.OA-C	-	93.72		-
Vertical force, V.A-C	k/ft	20.51		-
Location of resultant from Pt.A, a.nl = M.A-C/V.A-C	ft	4.57		-
Eccentricity from center of wall base, e.L=0.5*L - a.nl	ft	1.43		-
Limiting eccentricity, e=3L/8 for strength limit state	ft	4.50		-
Is the limiting eccentricity criteria satisfied?	-	**YES**		-
Effective width of base of MSE wall, B'=L-2e.L	ft	9.14		-
Calculated e.L/L	-	**0.12**		-

NOTE: L/4 limit based on soil foundation 3L/8 for rock

6.3 Bearing Resistance at base of MSE Wall

For bearing resistance computations, the effect of live load is included since it creates larger bearing stresses. The bearing stress at the base of the MSE wall can be computed as follows:

$$\sigma_V = \frac{\Sigma V}{L - 2e_L}$$

where $\Sigma V = R = V_1 + V_S$ is the resultant of vertical forces and the load eccentricity e_L is calculated by principles of statics using appropriate loads and moments with the applicable load factors.

In LRFD, σ_v is compared with the factored bearing resistance when computed for strength limit state and used for settlement analysis when computed for service limit state. The various computations for evaluation of bearing resistance are presented in Table E4-6.3. The Strength I (max) load combination results in the extreme force effect in terms of maximum bearing stress and therefore governs the bearing resistance mode of failure. The Service I

load combination is evaluated to compute the bearing stress for settlement analysis.

DOES NOT APPLY TO THIS DESIGN

6.4 Settlement Analysis

DOES NOT APPLY TO THIS DESIGN

Step 7: Evaluate Internal Stability Analysis of MSE Wall

7.1 Estimate critical failure surface, variation of K.r and F* for internal stability

Figure 2

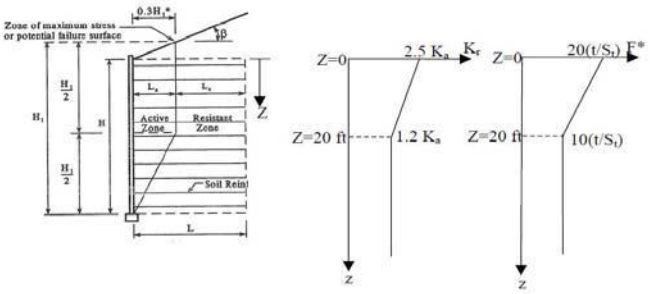

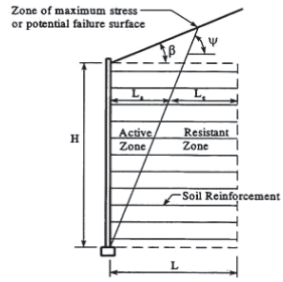

Inextensible

Extensible

Internal Lateral horizontal stress coefficient

At Z = 0', K.r =	0.283
At Z = 20', K.r =	0.283

S.eq, Equivalent uniform height of soil (ft)

2.16 must be < 2.25

Driven Posts? 0 - no; 1 - yes 0

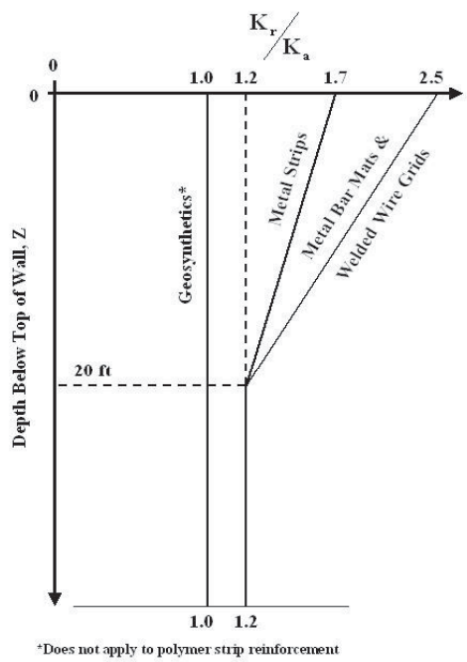

7.2 Establish vertical layout of soil reinforcements

Total wall height	12.34	ft
Spacing	32	in
	2.666667	ft
Num. Layers	5	
Initial depth	1.108	ft

Level	Z, depth (ft	Z.neg	Z.pos	S.vt (ft)	A.trib (sf)	Elev. From top of wall	Initial Depth
1	1.11	0.00	2.44	2.44	4.88	134.784	13.296
2	3.77	2.44	5.11	2.67	5.33	102.784	
3	6.44	5.11	7.77	2.67	5.33	70.784	
4	9.11	7.77	10.72	2.95	5.90	38.784	
5	12.34	10.72	12.34	1.62	3.23	0	
-							
-							
-							
-							
-							
-							
-							

7.3 Calculate horizontal stress and maximum tension at each reinforcement level

Sigma.H(Z)=K.r[gamma.r*(Z+h.eq)gamma.P-EV]

Level	K.r-neg	K.r-pos	Sigma.H (ksf)	T.max (k/ft)	T.max (k/panel)	kip/in/foot of wall
1	0.283	0.283	0.257	**0.627**	**1.253**	0.0214
2	0.283	0.283	0.379	**1.009**	**2.019**	0.0315
3	0.283	0.283	0.506	**1.349**	**2.697**	0.0421
4	0.283	0.283	0.640	**1.887**	**3.773**	0.0533
5	0.283	0.283	0.749	**1.210**	**2.420**	0.0624
-						
-						
-						
-						
-						
-						
-						

Total load on wall 6.08 kips/ft

Level	Z (ft)	Load (kip/pnl)	Ten. Cap (kip/pnl)	Plout Cap (kip/pnl)	Plout Le Rqrd (ft)	Plout Le Available (ft)	Tens. CDR	Plout CDR
1	1.11	1.253	4.02	NA	4.61	6.03	3.21	1.31
2	3.77	2.019	4.02	NA	3.15	7.45	1.99	2.36
3	6.44	2.697	4.02	NA	3.26	8.86	1.49	2.72
4	9.11	3.773	4.02	NA	3.72	10.28	1.07	2.77
5	12.34	2.420	4.02	NA	3.00	12.00	1.66	4.00
-								
-								
-								
-								
-								
-								
-								

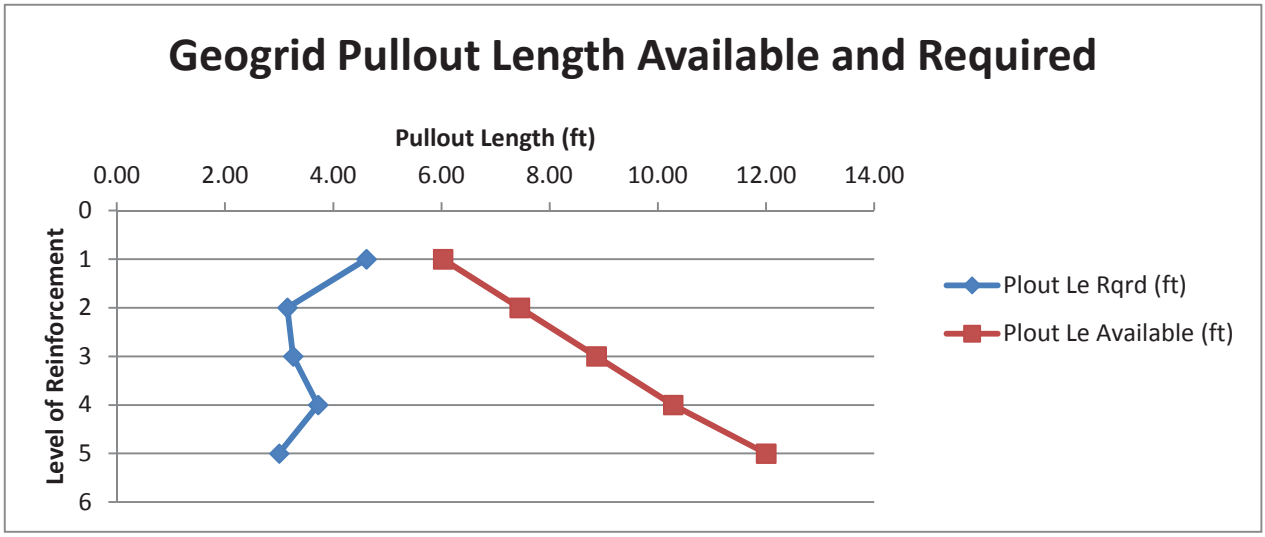
Geogrid Pullout Length Available and Required
Pullout Length (ft)
0.00
2.00
4.00
6.00
8.00
10.00
12.00
14.00
Level of Reinforcement
0
1
2
3
4
5
6
Plout Le Rqrd (ft)
Plout Le Available (ft)

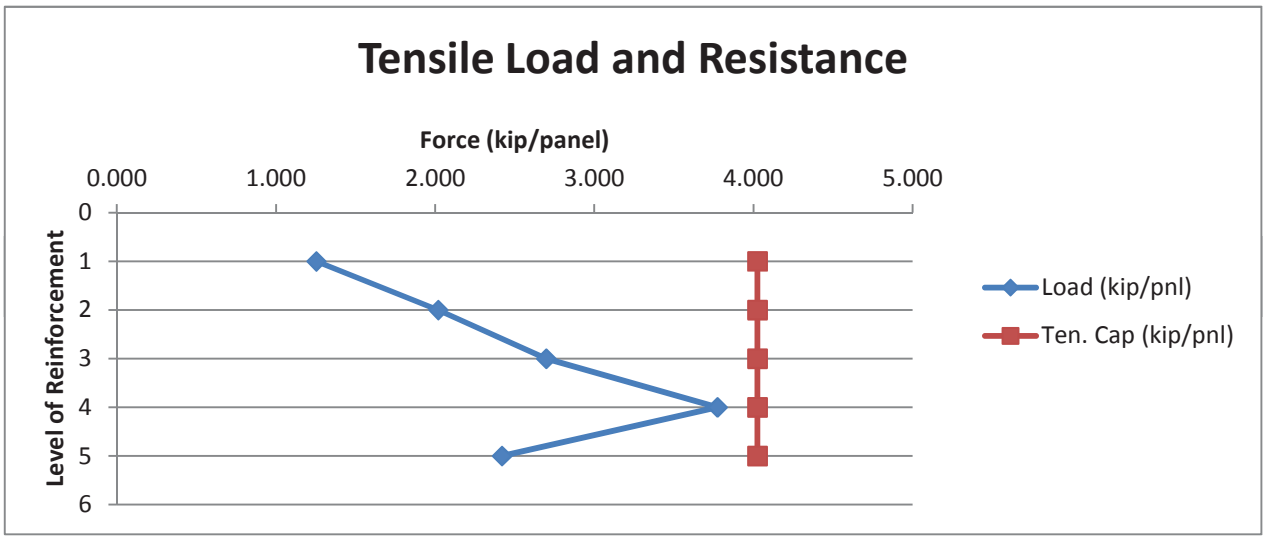
Tensile Load and Resistance
Force (kip/panel)
0.000
1.000
2.000
3.000
4.000
5.000
Level of Reinforcement
0
1
2
3
4
5
6
Load (kip/pnl)
Ten. Cap (kip/pnl)

EXTENSIBLE REINFORCEMENT ANALYSIS

7.4 Establish nominal and factored long-term tensile resistance of soil reinforcement

Design Life: 120 years

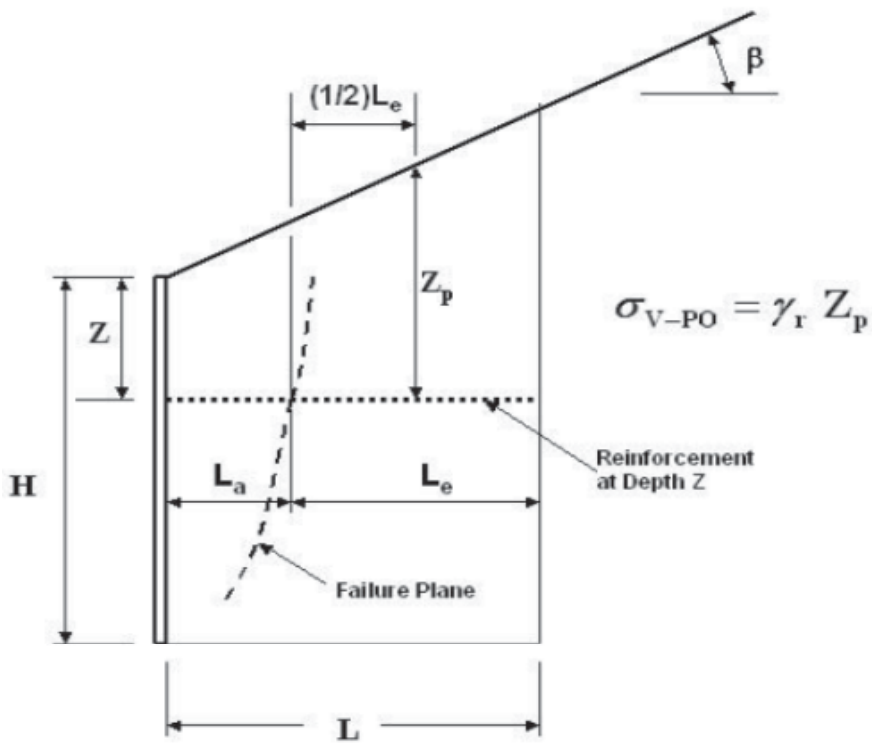

Table of geogrid properties

Type		T.ult	RF.CR	RF.D	RF.ID	T.al (kip/ft)	T.r (kip/ft)	T.r (kip/pnl)
1	Miragrid 2XT	2000	1.47	1.30	1.10	0.951	**0.856**	1.713
2	UX1100MSE	3970	2.60	1.00	1.05	1.454	**1.309**	2.618
3	Miragrid 3XT	3500	1.47	1.30	1.10	1.665	**1.499**	2.997
4	UX1400MSE	4800	2.60	1.00	1.05	1.758	**1.582**	3.165
5	Miragrid 5XT	4700	1.47	1.30	1.10	2.236	**2.012**	4.025
6	Miragrid 7XT	5900	1.47	1.30	1.10	2.807	**2.526**	5.052
7	UX1500MSE	7810	2.60	1.00	1.05	2.861	**2.575**	5.149
8	Miragrid 8XT	7400	1.47	1.30	1.10	3.520	**3.168**	6.337
9	UX1600MSE	9870	2.60	1.00	1.05	3.615	**3.254**	6.508
10	UX1700MSE	11990	2.60	1.00	1.05	4.392	**3.953**	7.905
11	Miragrid 10XT	9500	1.47	1.30	1.10	4.519	**4.067**	8.135
12	Miragrid 20XT	13705	1.47	1.30	1.10	6.520	**5.868**	11.735
13	Miragrid 22XT	20559	1.47	1.30	1.10	9.780	**8.802**	17.604
14	Miragrid 24XT	27415	1.47	1.30	1.10	13.042	**11.738**	23.475

7.5 Establish nominal and factored pullout resistance of soil reinforcement

Level	Z (ft)	L.a (ft)	Available Le (ft)	T.max	Z.p (ft)	σ.v unfctrd	Le.rqd (ft)	CDR
1	1.108	5.97	6.03	1.253	3.36	0.420	4.61	**1.31**
2	3.774666667	4.55	7.45	2.019	7.91	0.989	3.15	**2.36**
3	6.441333333	3.14	8.86	2.697	10.23	1.278	3.26	**2.72**
4	9.108	1.72	10.28	3.773	12.54	1.567	3.72	**2.77**
5	12.34	0.00	12.00	2.420	15.34	1.918	3.00	**4.00**
6	0	6.56	5.44	0.000	4.64	0.580	3.00	**1.81**
7	0	6.56	5.44	0.000	4.64	0.580	3.00	**1.81**
8	0	6.56	5.44	0.000	4.64	0.580	3.00	**1.81**
9	0	6.56	5.44	0.000	4.64	0.580	3.00	**1.81**
10	0	6.56	5.44	0.000	4.64	0.580	3.00	**1.81**
11	0	6.56	5.44	0.000	4.64	0.580	3.00	**1.81**
12	0	6.56	5.44	0.000	4.64	0.580	3.00	**1.81**

$$L_e \geq \frac{T_{MAX}}{\phi F^* \alpha \sigma_v C R_c} \geq 3 \text{ ft } (1 \text{ m})$$

F*, taken as 2/3*tan(ϕ)	0.45
α, scale correction factor	
0.6 for sheets and 0.8 for grids	0.8
C	2
C.R, coverage ratio	1

Level	Z (ft)	Layer Type	Load (kip/pnl)	Ten. Cap (kip/pnl)	Plout Le Rqrd (ft)	Plout Le Available(ft)	Tens. CDR	Plout CDR
1	1.108	5	1.25	4.02	4.61	6.03	3.21	1.31
2	3.774666667	5	2.02	4.02	3.15	7.45	1.99	2.36
3	6.441333333	5	2.70	4.02	3.26	8.86	1.49	2.72
4	9.108	5	3.77	4.02	3.72	10.28	1.07	2.77
5	12.34	5	2.42	4.02	3.00	12.00	1.66	4.00
6	0		0.00	#N/A	3.00	5.44	#N/A	1.81
7	0		0.00	#N/A	3.00	5.44	#N/A	1.81
8	0		0.00	#N/A	3.00	5.44	#N/A	1.81
9	0		0.00	#N/A	3.00	5.44	#N/A	1.81
10	0		0.00	#N/A	3.00	5.44	#N/A	1.81
11	0		0.00	#N/A	3.00	5.44	#N/A	1.81
12	0		0.00	#N/A	3.00	5.44	#N/A	1.81

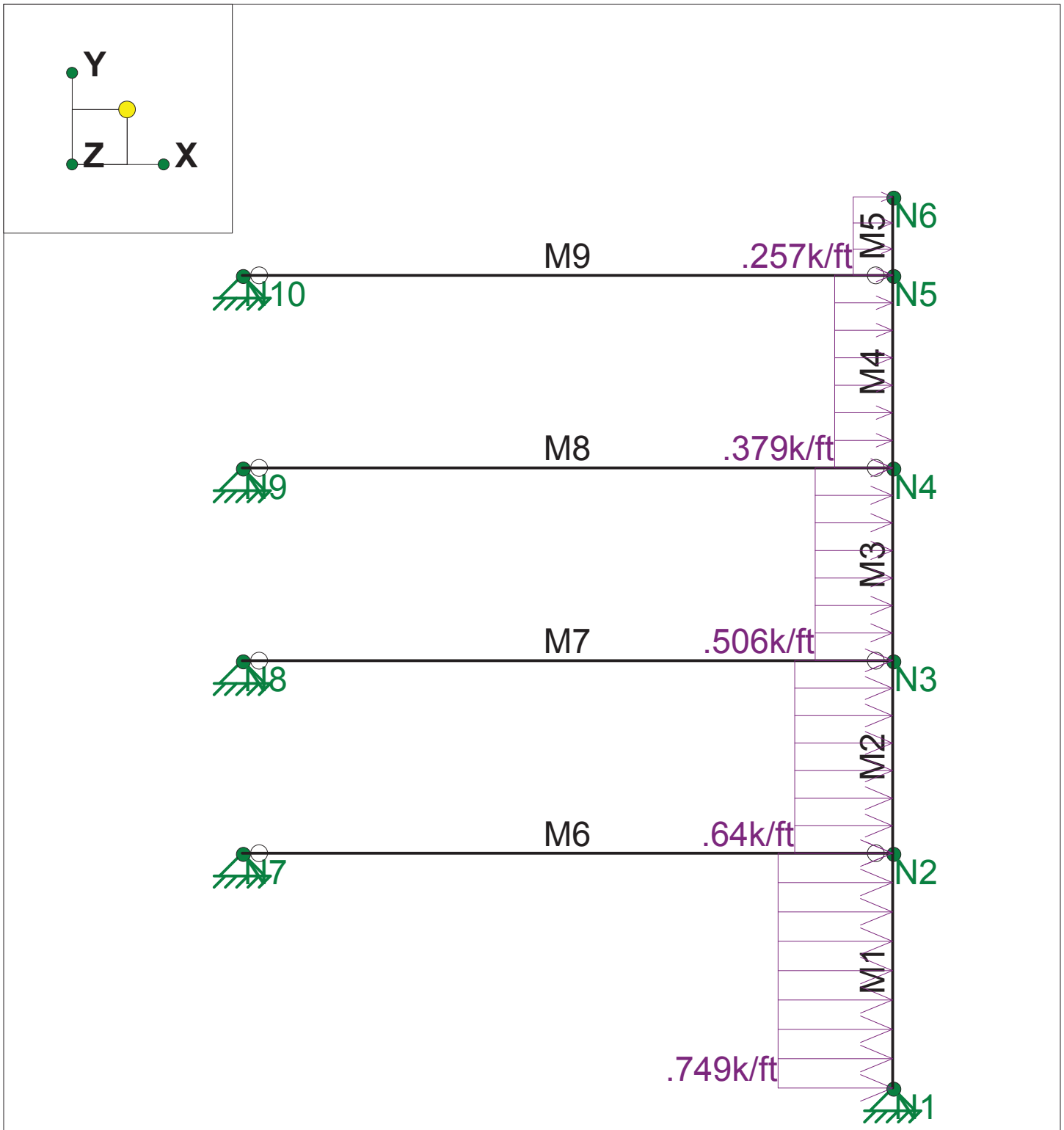

Loads: BLC 1,
Results for LC 1, 1

		SK - 2
		Apr 5, 2014 at 5:07 PM
		Headwall Shear, Moment, Reactio...

WARNING: Detail Report Based On Less Than 10 Sections!

Beam: ***M1***

Shape: **Composolite Panel**
Material: **FRP**
Length: **39 in**
I Joint: **N1**
J Joint: **N2**
LC 1: 1
Code Check: **0.000 (bending)**
Report Based On 5 Sections

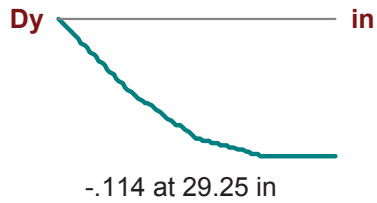

Dz — in

A — 0 at 0 in — k

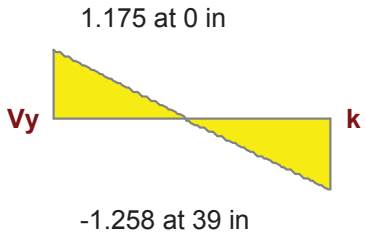

Vz — k

T — k-in

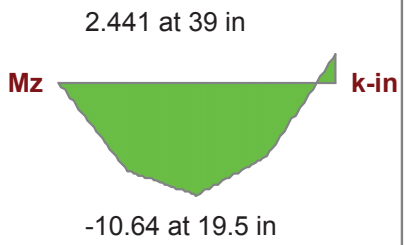

My — k-in

fa — 0 at 0 in — ksi

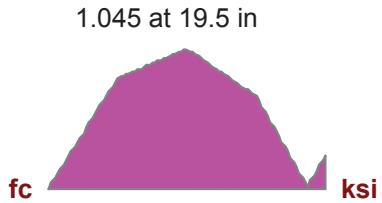

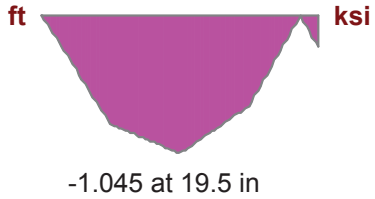

WARNING: Detail Report Based On Less Than 10 Sections!

Beam: ***M2***

Shape: **Composolite Panel**
Material: **FRP**
Length: **32 in**
I Joint: **N2**
J Joint: **N3**
LC 1: 1
Code Check: **0.000 (bending)**
Report Based On 5 Sections

Dy -.09 at 32 in / -.114 at 0 in **in**

Dz **in**

A 0 at 0 in **k**

Vy .816 at 0 in / -.89 at 32 in **k**

Vz **k**

T **k-in**

Mz 4.613 at 32 in / -3.297 at 16 in **k-in**

My **k-in**

fa 0 at 0 in **ksi**

fc .453 at 32 in / .003 at 25.333 in **ksi**

ft -.003 at 25.333 in / -.453 at 32 in **ksi**

WARNING: Detail Report Based On Less Than 10 Sections!

Beam: ***M3***

Shape: **Composolite Panel**
Material: **FRP**
Length: **32 in**
I Joint: **N3**
J Joint: **N4**
LC 1: 1
Code Check: **0.000 (bending)**
Report Based On 5 Sections

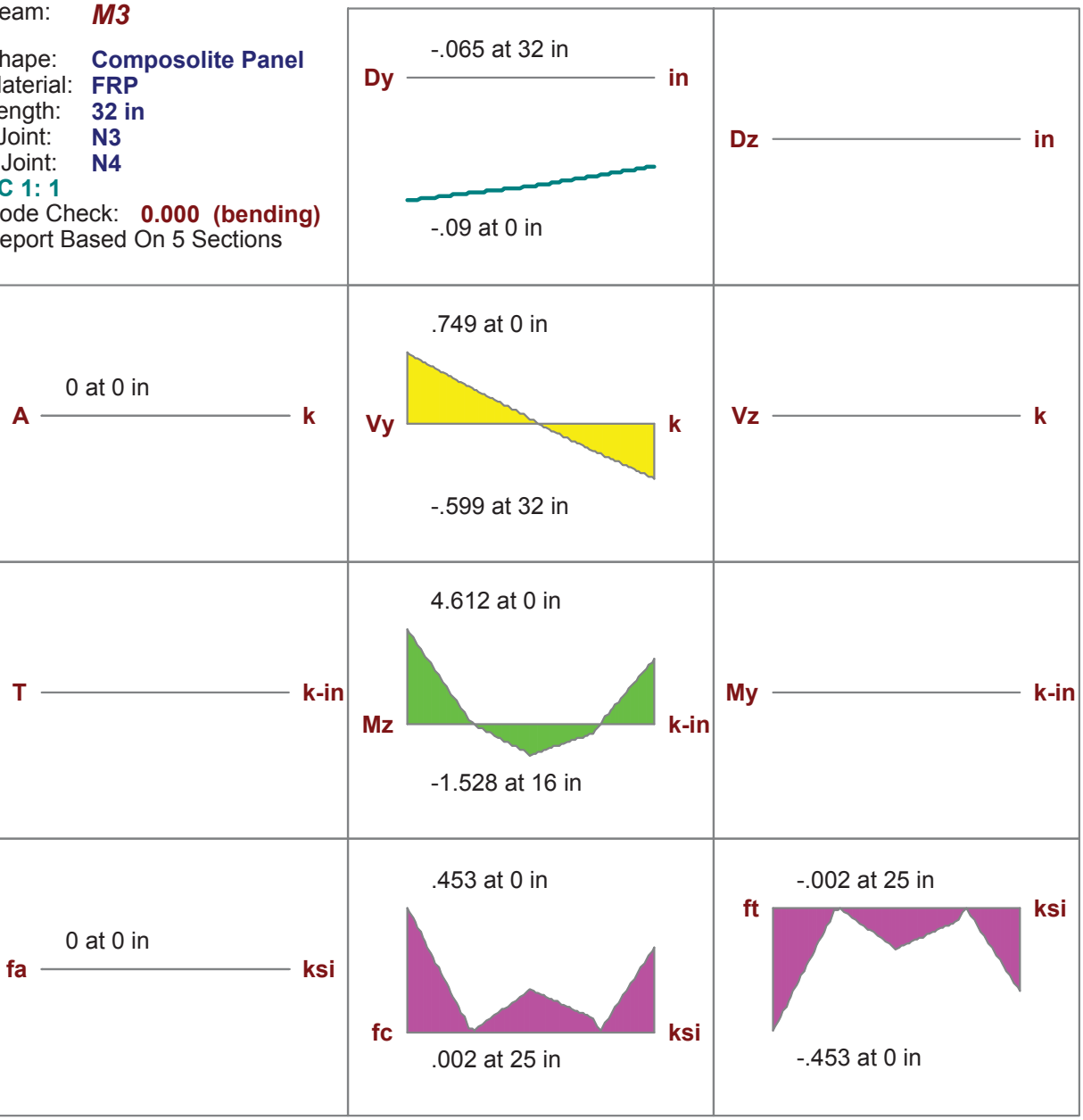

WARNING: Detail Report Based On Less Than 10 Sections!

Beam: ***M4***

Shape: **Composolite Panel**
Material: **FRP**
Length: **32 in**
I Joint: **N4**
J Joint: **N5**
LC 1: 1
Code Check: **0.000 (bending)**
Report Based On 5 Sections

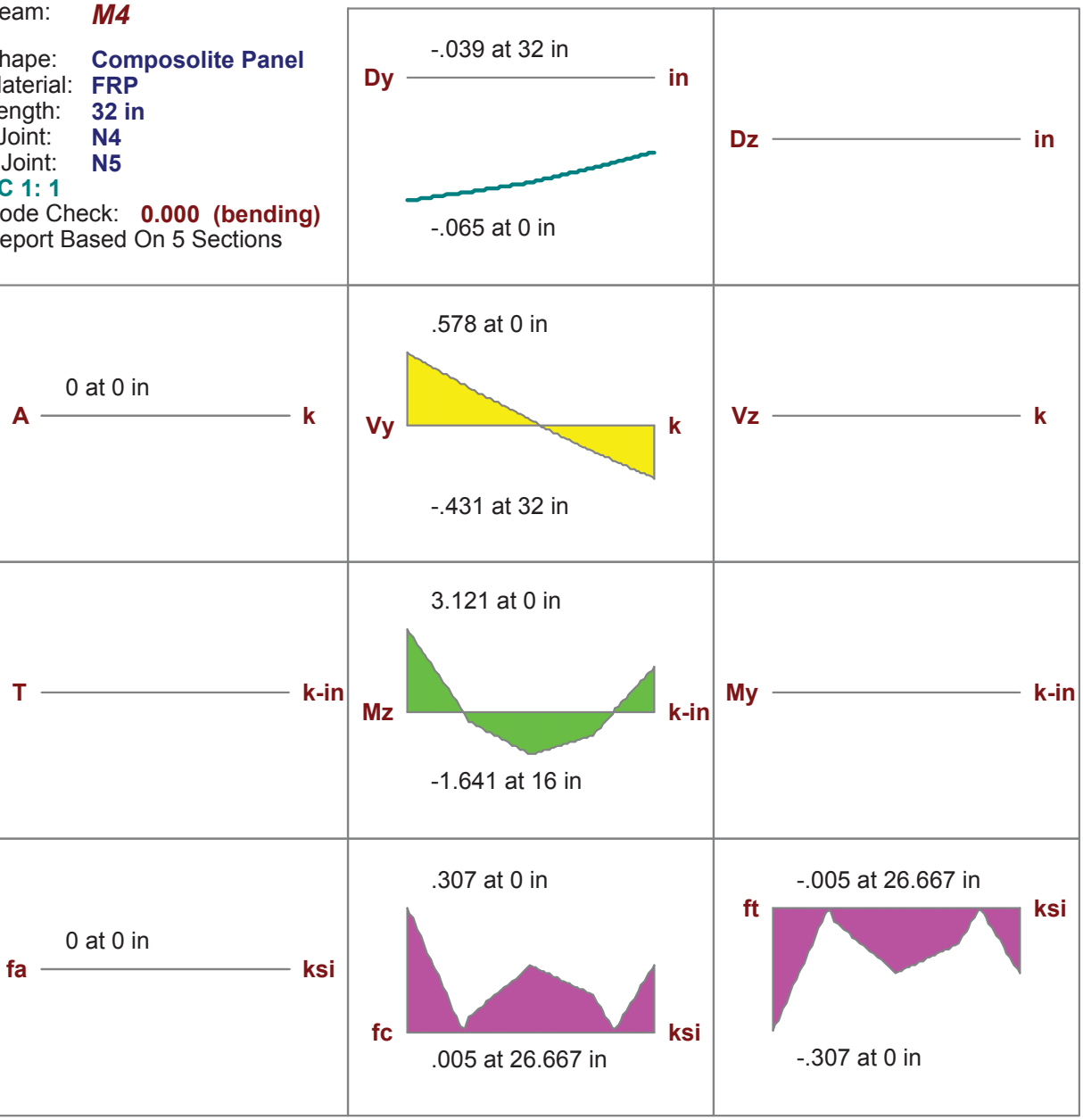

WARNING: Detail Report Based On Less Than 10 Sections!

Beam: ***M5***

Shape: **Composolite Panel**
Material: **FRP**
Length: **13 in**
I Joint: **N5**
J Joint: **N6**
LC 1: 1
Code Check: **0.000 (bending)**
Report Based On 5 Sections

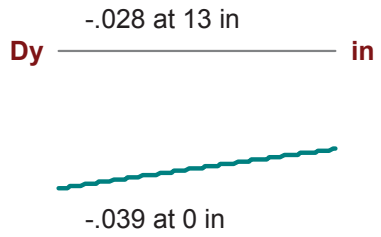

Dz — in

A — k

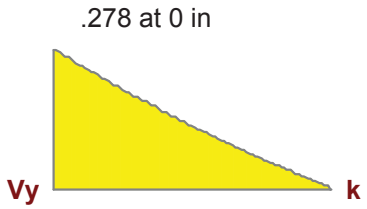

Vz — k

T — k-in

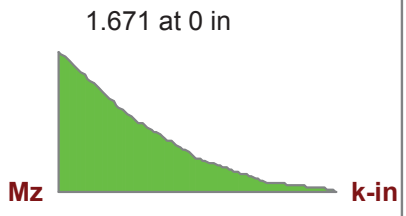

My — k-in

fa — ksi

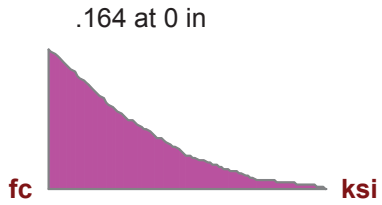

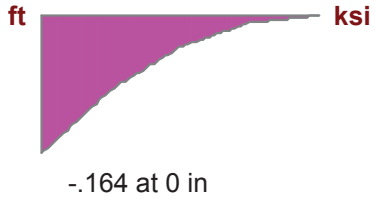

General Material Properties

	Label	E [ksi]	G [ksi]	Nu	Therm (\1E5 F)	Density[k/ft^3]
1	gen_Conc3NW	3155	1372	.15	.6	.145
2	gen_Conc4NW	3644	1584	.15	.6	.145
3	gen_Conc3LW	2085	906	.15	.6	.11
4	gen_Conc4LW	2408	1047	.15	.6	.11
5	gen_Alum	10600	4077	.3	1.29	.173
6	gen_Steel	29000	11154	.3	.65	.49
7	FRP	2486	1000	.28	0	0

General Section Sets

	Label	Shape	Type	Material	A [in2]	Iyy [in4]	Izz [in4]	J [in4]
1	COMPOSITE_PANEL	Composolite Panel	Beam	FRP	8.89	422	15.9	1.559

Joint Coordinates and Temperatures

	Label	X [in]	Y [in]	Z [in]	Temp [F]	Detach From Diaphragm
1	N1	0	0	0	0	
2	N2	0	39	0	0	
3	N3	0	71	0	0	
4	N4	0	103	0	0	
5	N5	0	135	0	0	
6	N6	0	148	0	0	
7	N7	-108	39	0	0	
8	N8	-108	71	0	0	
9	N9	-108	103	0	0	
10	N10	-108	135	0	0	

Joint Boundary Conditions

	Joint Label	X [k/in]	Y [k/in]	Z [k/in]	X Rot.[k-ft/rad]	Y Rot.[k-ft/rad]	Z Rot.[k-ft/rad]	Footing
1	N1	Reaction	Reaction	Reaction				
2	N2			Reaction				
3	N3			Reaction		Reaction		
4	N4			Reaction				
5	N5			Reaction				
6	N6			Reaction				
7	N7	Reaction	Reaction	Reaction				
8	N8	Reaction	Reaction	Reaction				
9	N9	Reaction	Reaction	Reaction				
10	N10	Reaction	Reaction	Reaction				

Member Primary Data

	Label	I Joint	J Joint	K Joint	Rotate(d...	Section/Shape	Type	Design List	Material	Design Rules
1	M1	N1	N2			Composolite Panel	Beam	None	FRP	Typical
2	M2	N2	N3			Composolite Panel	Beam	None	FRP	Typical
3	M3	N3	N4			Composolite Panel	Beam	None	FRP	Typical
4	M4	N4	N5			Composolite Panel	Beam	None	FRP	Typical
5	M5	N5	N6			Composolite Panel	Beam	None	FRP	Typical
6	M6	N2	N7			D11Bar	Beam	Round Default	A36 Gr.36	Typical
7	M7	N3	N8			D11Bar	Beam	Round Default	A36 Gr.36	Typical
8	M8	N4	N9			D11Bar	Beam	Round Default	A36 Gr.36	Typical
9	M9	N5	N10			D11Bar	Beam	Round Default	A36 Gr.36	Typical

Member Advanced Data

	Label	I Release	J Release	I Offset[in]	J Offset[in]	T/C Only	Physical	TOM	Inactive
1	M1						Yes		
2	M2						Yes		
3	M3						Yes		
4	M4						Yes		
5	M5						Yes		
6	M6						Yes		
7	M7						Yes		
8	M8						Yes		
9	M9						Yes		

Member Distributed Loads (BLC 1 :)

	Member Label	Direction	Start Magnitude[k/ft,deg]	End Magnitude[k/ft,deg]	Start Location[i...	End Location[in,%]
1	M5	X	.315	.198	0	0
2	M4	X	.442	.315	0	0
3	M3	X	.569	.442	0	0
4	M2	X	.71	.569	0	0
5	M1	X	.787	.71	0	0

Joint Reactions (By Combination)

	LC	Joint Label	X [k]	Y [k]	Z [k]	MX [k-in]	MY [k-in]	MZ [k-in]
1	1	N1	-1.175	0	0	0	0	0
2	1	N2	0	0	0	0	0	0
3	1	N3	0	0	0	0	0	0
4	1	N4	0	0	0	0	0	0
5	1	N5	0	0	0	0	0	0
6	1	N6	0	0	0	0	0	0
7	1	N7	-2.075	0	0	0	0	0
8	1	N8	-1.639	0	0	0	0	0
9	1	N9	-1.178	0	0	0	0	0
10	1	N10	-.709	0	0	0	0	0
11	1	Totals:	-6.775	0	0			
12	1	COG (in):	NC	NC	NC			

Member Section Forces (By Combination)

	LC	Member Label	Sec	Axial[k]	y Shear[k]	z Shear[k]	Torque[k-in]	y-y Moment...	z-z Moment[k-in]
1	1	M1	1	0	1.175	0	0	0	0
2			2	0	.543	0	0	0	-8.362
3			3	0	-.073	0	0	0	-10.64
4			4	0	-.673	0	0	0	-6.988
5			5	0	-1.258	0	0	0	2.441
6	1	M2	1	0	.816	0	0	0	2.441
7			2	0	.355	0	0	0	-2.228
8			3	0	-.083	0	0	0	-3.297
9			4	0	-.498	0	0	0	-.954
10			5	0	-.89	0	0	0	4.613
11	1	M3	1	0	.749	0	0	0	4.612
12			2	0	.38	0	0	0	.109
13			3	0	.032	0	0	0	-1.528
14			4	0	-.294	0	0	0	-.467
15			5	0	-.599	0	0	0	3.121
16	1	M4	1	0	.578	0	0	0	3.121
17			2	0	.294	0	0	0	-.354

Member Section Forces (By Combination) (Continued)

	LC	Member Label	Sec	Axial[k]	y Shear[k]	z Shear[k]	Torque[k-in]	y-y Moment...	z-z Moment[k-in]
18			3	0	.031	0	0	0	-1.641
19			4	0	-.211	0	0	0	-.91
20			5	0	-.431	0	0	0	1.671
21	1	M5	1	0	.278	0	0	0	1.671
22			2	0	.197	0	0	0	.901
23			3	0	.123	0	0	0	.384
24			4	0	.058	0	0	0	.092
25			5	0	0	0	0	0	0
26	1	M6	1	-2.075	0	0	0	0	0
27			2	-2.075	0	0	0	0	0
28			3	-2.075	0	0	0	0	0
29			4	-2.075	0	0	0	0	0
30			5	-2.075	0	0	0	0	0
31	1	M7	1	-1.639	0	0	0	0	0
32			2	-1.639	0	0	0	0	0
33			3	-1.639	0	0	0	0	0
34			4	-1.639	0	0	0	0	0
35			5	-1.639	0	0	0	0	0
36	1	M8	1	-1.178	0	0	0	0	0
37			2	-1.178	0	0	0	0	0
38			3	-1.178	0	0	0	0	0
39			4	-1.178	0	0	0	0	0
40			5	-1.178	0	0	0	0	0
41	1	M9	1	-.709	0	0	0	0	0
42			2	-.709	0	0	0	0	0
43			3	-.709	0	0	0	0	0
44			4	-.709	0	0	0	0	0
45			5	-.709	0	0	0	0	0

Member Section Deflections (By Combination)

	LC	Member Label	Sec	x [in]	y [in]	z [in]	x Rotate[rad]	(n) L/y Ratio	(n) L/z Ratio
1	1	M1	1	0	0	0	0	NC	NC
2			2	0	-.059	0	0	1287.953	NC
3			3	0	-.098	0	0	935.909	NC
4			4	0	-.114	0	0	1360.788	NC
5			5	0	-.114	0	0	NC	NC
6	1	M2	1	0	-.114	0	0	NC	NC
7			2	0	-.113	0	0	6327.927	NC
8			3	0	-.109	0	0	4576.049	NC
9			4	0	-.1	0	0	7898.47	NC
10			5	0	-.09	0	0	NC	NC
11	1	M3	1	0	-.09	0	0	NC	NC
12			2	0	-.084	0	0	NC	NC
13			3	0	-.079	0	0	NC	NC
14			4	0	-.072	0	0	NC	NC
15			5	0	-.065	0	0	NC	NC
16	1	M4	1	0	-.065	0	0	NC	NC
17			2	0	-.06	0	0	NC	NC
18			3	0	-.055	0	0	NC	NC
19			4	0	-.047	0	0	NC	NC
20			5	0	-.039	0	0	NC	NC
21	1	M5	1	0	-.039	0	0	1156.603	NC
22			2	0	-.036	0	0	1588.461	NC
23			3	0	-.033	0	0	2418.743	NC
24			4	0	-.03	0	0	4863.674	NC
25			5	0	-.028	0	0	NC	NC

Member Section Deflections (By Combination) (Continued)

	LC	Member Label	Sec	x [in]	y [in]	z [in]	x Rotate[rad]	(n) L/y Ratio	(n) L/z Ratio
26	1	M6	1	-.114	0	0	0	NC	NC
27			2	-.085	-.003	0	0	NC	NC
28			3	-.057	-.003	0	0	NC	NC
29			4	-.028	-.002	0	0	NC	NC
30			5	0	0	0	0	NC	NC
31	1	M7	1	-.09	0	0	0	NC	NC
32			2	-.067	-.018	0	0	6148.326	NC
33			3	-.045	-.02	0	0	5379.782	NC
34			4	-.022	-.013	0	0	8607.651	NC
35			5	0	0	0	0	NC	NC
36	1	M8	1	-.065	0	0	0	NC	NC
37			2	-.048	-.014	0	0	7891.213	NC
38			3	-.032	-.016	0	0	6904.811	NC
39			4	-.016	-.01	0	0	NC	NC
40			5	0	0	0	0	NC	NC
41	1	M9	1	-.039	0	0	0	NC	NC
42			2	-.029	-.018	0	0	6024.796	NC
43			3	-.019	-.02	0	0	5271.696	NC
44			4	-.01	-.013	0	0	8434.714	NC
45			5	0	0	0	0	NC	NC

RISA MODEL OUTPUT SUMARY

Location	Max Force		Capacities	Units	Capacity to Demand Ratios
M1@19.5"	Moment min =	-10.640	-41.59	kip-in/ft	3.91
M2@32"	Moment Max =	4.613	41.59	kip-in/ft	9.01
M1@39"	Shear max =	1.258	6.91	kips/ft	5.49
N7	Pull Through =	2.075	2.52	kips/ft	1.21
M1@29.25"	Max Deflection=	0.114	0.27	in	2.34

Deflection Tollerance based on L/120 where L = 32" = Geogrid conneciton spacing
Global panel movement may exceed L/120, but relative deflection between connections shall not

Advanced Infrastructure Technologies

20 Godfrey Drive
Orono, Maine 04473
Telephone: (207) 866-6526
Fax: (207) 866-6501
www.aitbridges.com

Project: *Fairfield, VT*

Task: *Size Connection bolts and washer plates*

References
1. *Headwall Loads to reinforcement*
2. *AISC LRFD*

Design of bolts

Factored Tensile Loads

Max load to headwall [Ref.1]: $w := 2.075 \frac{kip}{ft}$

Panel width: $width := 23.8in$

Bolts per panel: $spacing := 3$

Load per bolt: $P_u := w \cdot \frac{width}{spacing} = 1.37 \cdot kip$

Tensile Capacity

Use A307 J bolts

Strength Reduction Factor: $\Phi := 0.75$

Tensile capacity [Ref.2 Table J3.2]: $F_y := 36ksi$ $F_t := 45ksi$

Bolt diameter: $d_b := 0.25in$

Bar area: $A_b := \frac{d_b^2 \cdot \pi}{4} = 0.05 \cdot in^2$

Factored Capacity: $\Phi P_n := \Phi \cdot F_t \cdot A_b = 1.66 \cdot kip$

Tensile Strength Ratio: $\frac{\Phi P_n}{P_u} = 1.21$ *OK if greater than 1.0*

Design of washer plate

Design plate for simple span to distribute point load out to panel webs

Factored Plate Bending Loads

Distance between panel webs: $span := 3.37in$

Moment due to span: $M_u := P_u \cdot span \cdot 0.5 = 2.31 \cdot in \cdot kip$

Plate Bending Capacity

Plate dimensions: $depth := 0.375in$ $width := \left(4.25 - \frac{13}{16}\right)in$

Type A36 steel $F_y := 36ksi$ $F_u := 58ksi$

Plastic Section Modulus: $Z := \frac{width \cdot depth^2}{4} = 0.12 \cdot in^3$

Section Modulus: $S := \frac{width \cdot depth^2}{3} = 0.16 \cdot in^3$

Yielding Moment: $M_y := F_y \cdot S = 5.80 \cdot in \cdot kip$

Plastic Moment: $M_p := F_y \cdot Z = 4.35 \cdot in \cdot kip$

$M_n := \min(M_p, 1.5 \cdot M_y) = 4.35 \cdot in \cdot kip$

Factored Moment Capacity: $\Phi M_n := \Phi \cdot M_n = 3.26 \cdot in \cdot kip$

Strength Ratio: $\frac{\Phi M_n}{M_u} = 1.41$ *OK if greater than 1.0*

Design Summary:

- *Use A307 1/4" Diameter bolts or larger*
- *Use 4.25" diameter x 3/8" thick Bearing washer plate of A36 steel with up to a 13/16" diameter centered hole*

DESIGN WALER

LOADS USE CREATIVE PULTRUSIONS
PULTEX 1500 SERIES

- PUBLISHED VALUES ARE TEST AVERAGES
- ASSUME CHARACTERISTIC VALUE ON STRENGTHS ARE $0.7 \cdot AVG = \mu - 3\sigma$ WHERE COV = 10%

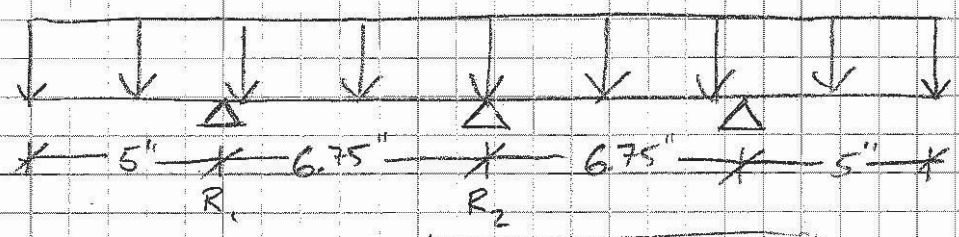

FROM RISA PANEL ANALYSIS

$R_{u_1} = 0.95$ k
$R_{u_2} = 1.56$ k

$M_u = 2.163$ in-k
$V_u = 0.766$ k
$R_u = 1.56$ k

FROM RISA MODEL

SECTION

USE 2"x1/4" SQUARE TUBE

FLEXURE

$$M_n = \frac{F_y I}{y} = \frac{26.25 \text{ ksi} \cdot 0.89 \text{ in}^4}{1 \text{ in}} = 23.36 \text{ in-k}$$

$$C_m \lambda \phi M_n = 4.86 \text{ in-k} > M_u$$ OKAY ✓

where $C_m = 0.8$ moisture
$\lambda = 0.4$ time effect
$\phi = 0.65$ material rupture

SHEAR

$$V_n = F_{LT} A_s = 4.9 \text{ ksi} \cdot 1 \text{ in}^2 = 4.9 \text{ kip}$$

$$C_m \lambda \phi V_n = 1.02 \text{ kip} > V_u$$ OKAY ✓

CONT →

CRUSHING

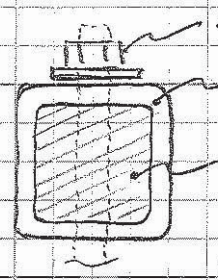

CV. BEARING STRENGTH = 32 ksi · 0.7 = 22.4 ksi

$R_n = F_{BS} \cdot A_{Bearing}$

$A_{Bearing}$ = WASHER AREA

$= \frac{\pi\, 1\frac{3}{8}^2}{4} - \frac{\pi\, 9/16^2}{4}$

$= \frac{\pi}{4}\left(1\frac{3}{8}^2 - \frac{9}{16}^2\right)$

$= 1.24\ in^2$

$R_n = 22.4\ ksi \cdot 1.24\ in^2$

$R_n = 27.7\ kip$

$C_m \lambda \phi R_n = 5.76\ kip > R_u$ ✓ OKAY

ANGLE DESIGN

MAX SPACING = 9.87" O.C. SPACING OF CORRUGATIONS

MAX LOAD = 1.175 k/ft

MAX LOAD TO ANGLE = 0.97 kip

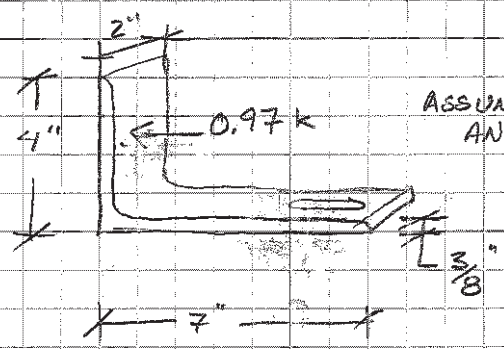

ASSUME FORCE ACTS HALFWAY UP ANGLE LEG

$$M_u = 0.97\,k \cdot 2'' = 1.94 \text{ in-k}$$

$$M_n = \frac{F_y I}{y} = \frac{60\,ksi \cdot \frac{2 \cdot \frac{3}{8}^3}{12}}{\frac{3}{8} \cdot \frac{1}{2}} = \frac{0.527}{3/16} = 2.81 \text{ in-k}$$

$$\boxed{\phi M_n = 2.53 \text{ in-k} > M_u}$$ OKAY FOR BENDING

USE GALV. STEEL

$7 \times 4 \times \frac{3}{8}$ ANGLE 2" WIDE

Simplified Modeling to Assess Soil-Structure Interaction Effects

AEWC Project 906F

Prepared for:

Advanced Infrastructure Technologies, LLC

AEWC Report Number
11 – 30

5/4/2011

Prepared by:

Joshua D. Clapp
Research Engineer

William G. Davids
Professor of Civil and Env. Engineering

Reviewed by:

Stephen Shaler, Ph.D.
Associate Director

An ISO 17025 accredited testing laboratory
Accredited by International Accreditation Service

AEWC Advanced Structures & Composites Center
5793 AEWC Bldg
University of Maine
Orono, ME 04469-5793

CONFIDENTIAL

Telephone: 207-581-2123
FAX: 207-581-2074
contactaewc@umit.maine.edu
www.aewc.umaine.edu

This report shall not be reproduced, except in full, without the written approval of the AEWC Advanced Structures & Composites Center.

Simplified Modeling to Assess Soil-Structure Interaction Effects

AEWC Project 906F

I. INTRODUCTION

Advanced Infrastructure Technologies (AIT) provides engineering and fabrication services for bridges that use composite arches as the primary structural members. All applications to date have been buried structures where transverse decking was placed across the arches to distribute soil loads, dead loads, and live loads to the arches. FRP decking may be used alone or as formwork for reinforced concrete decking. Present structural analysis methods consist of finite element (FE) models that utilize 2D Euler-Bernoulli beam elements to model the arch. Nonlinear moment-curvature relationships can be included. The axial and bending stiffnesses of the concrete deck, if present, are neglected. Soil loads are applied by assuming a constant lateral earth pressure coefficient, K (taken as the at-rest coefficient, K_o), to relate horizontal and vertical soil pressures.

This document is intended to summarize the work that was performed by the University of Maine AEWC Advanced Structures and Composites Center (AEWC) to develop new structural analysis software to analyze buried arch bridges that accounts for unbalanced backfilling and the potentially beneficial restraining effect of the compacted backfill on the arches. As with current AIT structural analysis software, all routines were written in MATLAB (MathWorks 2009) so that the user has full control over the analysis and may easily make changes to the analysis routines. The software incorporates four key capabilities:

1. The effect of staged construction was simulated by applying soil lifts sequentially on alternating sides of the arch.
2. A nonlinear soil constitutive relationship was incorporated by adding soil springs to the model corresponding to each layer of soil after it is placed.
3. Recognizing that the arches behave as stiff ribs supporting the more flexible deck, which may significantly affect soil-structure interaction, the decking was explicitly modeled using transverse elements perpendicular to the plane of the arch.
4. The effect of the axial and bending stiffness of the concrete deck, if present, in the longitudinal (span) direction was included in the model.

The net effect of these key features of the analysis methodology was investigated by modeling the backfilling of an example bridge which is proposed for construction in the near future. This allowed realistic parameters to be considered in a practical design scenario. Throughout this document references are made to this particular bridge project referred to as the Ellsworth Bridge. See Appendix A for more details describing the

This report shall not be reproduced, except in full, without the written approval of
the AEWC Advanced Structures & Composites Center.

example bridge and in general the work that was to be performed as part of the contract. See Appendix B for a collection of content specifically related to the programming aspect of the project.

II. FINITE ELEMENT MODEL

Three-dimensional (3D) elements were utilized in order to capture the effect of decking flexibility in the transverse direction (spanning between arches). A schematic view of the finite element mesh is shown in Figure 1. Three element types were used: arch elements (also includes longitudinal decking stiffness if applicable), transverse decking elements, and soil spring elements. Nonlinear 3D Euler-Bernoulli beam elements were used to model the arch in the longitudinal direction as well as the decking in the transverse direction. If a concrete deck is present, the stiffness of the deck in the longitudinal direction is added to the stiffness of the arch to arrive at the total non-composite stiffness for these elements. For this study, a cracked section was considered for the concrete deck in both the longitudinal and transverse directions. Soil spring elements were based on a compression-only constitutive relationship that is discussed later. The arch boundary conditions were taken as fully fixed at the ends, although other boundary conditions can be specified. Loads were applied to nodes defining the transverse decking elements and were then transferred to the arch.

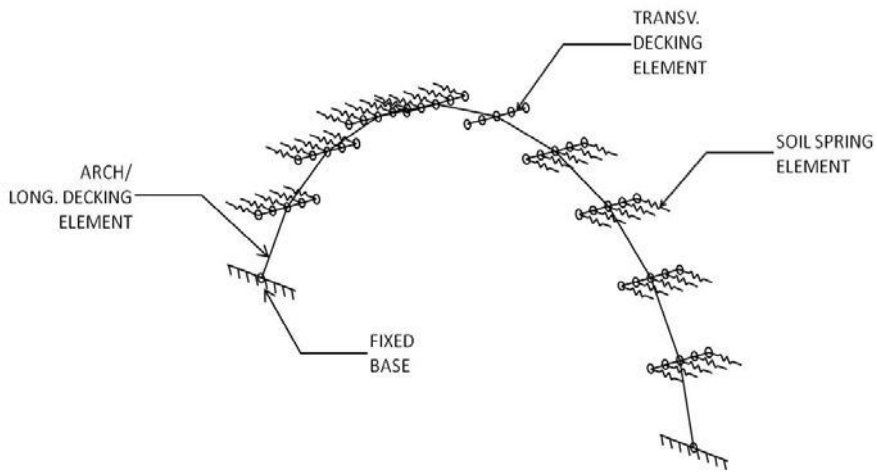

Figure 1 – Schematic 3D View of FE Mesh (Coarse Mesh Shown for Clarity)

I. Arch and Longitudinal Decking Elements

General nonlinear 3D Euler-Bernoulli beam elements were used to model the arch, although only in-plane deflections/member forces occurred since the arch was not subjected to out-of-plane loads in this study. The in-plane tangent bending stiffness, EI, and bending moment for the arch are a function of curvature and axial load level. These values were interpolated from relationships provided by AIT. If a concrete deck is

This report shall not be reproduced, except in full, without the written approval of
the AEWC Advanced Structures & Composites Center.

present, it is also necessary to account for the in-plane longitudinal bending and axial stiffness of this layer. In this study, two different values of EI corresponding to cracked sections were used depending on whether positive or negative bending was occurring. This was necessary since the location of reinforcement was non-symmetric through the depth of the deck. It is also possible for the user to specify a generic moment-curvature relationship for the decking in the longitudinal direction. The area used to calculate axial stiffness, EA, of the decking was taken as the full uncracked cross-sectional area of the concrete. Throughout analyses the total axial load was split into arch and decking components proportionally to their stiffnesses and only the arch component was used when interpolating for its bending stiffness and moment.

II. Transverse Decking Elements

General and specialized nonlinear 3D Euler-Bernoulli beam elements were used to model the decking in the transverse direction. These elements were only intended to capture the effect of transverse bending, which leads to variable soil pressures across the length of the decking elements. Longitudinal bending and axial stiffness of the decking was included with the arch elements. A single row of decking elements, which can contain any even number of elements, extends from –s/2 to s/2, where s is the center-to-center spacing of the arches. The local coordinate system [x′,y′,z′] of the decking elements is defined in Figure 2. The global coordinate system [X,Y,Z] is also shown for reference. Note that the x′ axis is parallel to the Z axis. For each element, the z′ axis was taken as being parallel to a line connecting the two adjacent arch nodes, as indicated by line A-B in Figure 2. The y′ axis was taken as perpendicular to the x′ and z′ axes. The actual bending stiffness of the deck was used for bending about the z′ axis. A large bending stiffness was applied for bending about the y′ axis to effectively prevent displacements in the x′-z′ plane. To model the symmetric bending of the decking, rotations about the z′ axis at each end of the decking must be prevented. Specialized elements were used to achieve this rotational restraint at coordinates Z = –s/2 and Z = s/2. This boundary condition was taken into account in the element formulation to arrive at a consistent element stiffness matrix, and it was not necessary to apply additional constraints in the model. General 3D Euler-Bernoulli beam elements were used for all other decking elements.

This report shall not be reproduced, except in full, without the written approval of
the AEWC Advanced Structures & Composites Center.

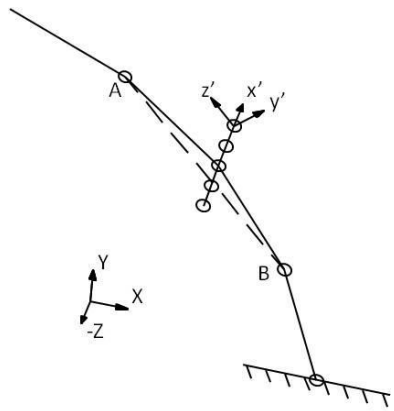

Figure 2 – Definition of Local Coordinate System for Transverse Decking Elements

III. Soil Spring Elements

Soil spring elements were oriented horizontally and only carried compressive axial loads. The axial load level F_{spring} depends on the tributary horizontal area A_h, the vertical pressure σ_v due to overburden and other loads, and the lateral earth pressure coefficient K as shown in Equation 1 below. Here, A_h was taken as the product of half of the elevation difference between the two adjacent nodes along the length of the arch and the z-spacing of decking nodes (or z-spacing/2 for nodes at the planes of symmetry).

$F_{spring} = A_h \times \sigma_v \times K$	Equation 1

Stiffness was estimated by using a forward difference approximation where a small deflection was applied. The tributary area for a particular element remained constant throughout the analysis, whereas σ_v and K changed as a function of additional loading and deflections, respectively. The lateral earth pressure coefficient K was defined based on Figure 3 below (see 'UMaine Model'), where deflections away from the soil were taken as positive. A curve reproduced from National Cooperative Highway Research Program (NCHRP 1991) is also shown for comparison. Note that the UMaine Model is just a simplified quadrilinear version of the NCHRP (1991) curve defined by the three pressure coefficients, except that K_o was taken as 0.45. This value represents a compromise between the NCHRP (1991) value of 0.4 and the value recommended by Maine DOT for culvert design of 0.47. Precedent for this approach can be found in literature on integral abutment bridges (Faraji et al. 2001; Ting and Faraji 1998) and in design procedures for earth retaining structures (USACoE 1994). Note that the UMaine model yields much softer behavior for the soil springs than the NCHRP curve, which was believed to be conservative. We note here that the MATLAB code developed as part of

This report shall not be reproduced, except in full, without the written approval of
the AEWC Advanced Structures & Composites Center.

this work is quite general, and should permit alternative soil spring load-deformation relationships to be implemented fairly easily.

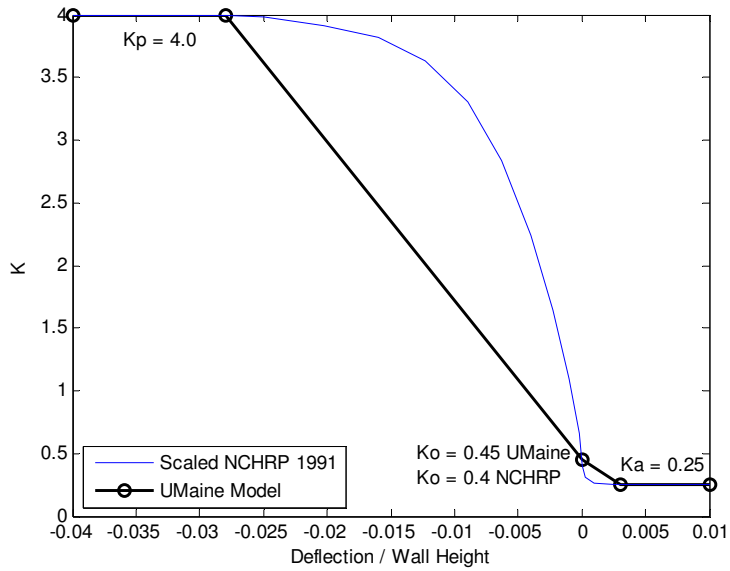

Figure 3 – Lateral Earth Pressure Coefficient as a Function of Relative Movement after NCHRP (1991) for Medium-Dense Backfill

The wall height for the example case was taken as the height of the arch, or 14 ft., which implies that deflections of approximately 0.5 in. away from and 4.7 in. into the soil are necessary to achieve the active and passive states, respectively. These deflections were defined relative to the horizontal displacement of the arch at the location of the spring after the applicable soil lift was applied (i.e. after a lift was placed that first caused a particular soil spring to be buried, the initial relative deflection for this soil spring was zero).

III. CONSIDERATION OF STAGED CONSTRUCTION

In the field, the backfilling process is performed after the arches are placed and decking is installed. Generally, based on recent bridge construction projects, the backfill is placed in lifts that do not exceed 12 in. in height and lifts are placed sequentially on alternating sides of the arch. Each lift is compacted before the next lift is placed. It was assumed for the analyses described in this document that a lift is in the at-rest state once it has been placed and compacted. After this point the state depends on deflections. Lifts were applied in 12 in. increments on alternating sides of the arch since this was believed to be the worst-case scenario for construction i.e. the scenario that causes the largest amount of side-sway. (The program allows lift heights of other than 12 in. to be specified.) The algorithm for the staged construction procedure, which takes place after the self-weight of arch and decking components are applied, was as follows:

This report shall not be reproduced, except in full, without the written approval of the AEWC Advanced Structures & Composites Center.

1. Apply a new lift of soil.
    a. Horizontal loads corresponding to the at-rest lateral earth pressure coefficient K_o are applied within the region of this lift in addition to vertical loads applied in all applicable regions.
    b. Element shape functions are used to calculate statically equivalent nodal loads for vertical and horizontal soil pressures that vary linearly over the length of an element.
    c. The tributary distance in the z-direction is taken as the z-spacing of decking elements (or z-spacing/2 for nodes at the planes of symmetry).
2. Adjust the vertical pressure for any lifts that are below the new lift.
3. Re-calculate the stiffness of each soil spring based on the additional vertical pressure as well as the change in relative deflection.
4. Utilize a nonlinear Newton-based solver to determine the position of equilibrium, while continually updating the stiffness of nonlinear elements in the model including the soil springs.
5. After a solution has been obtained, activate any springs that were buried by the lift that was just applied.
6. Set the zero relative displacement position of the newly activated springs to be at the X-coordinate of the current deflected position. This 'zero' position will be retained for all future load steps.
7. Repeat 1-6 until all lifts are applied.
8. Apply additional loads such as dead load of the wearing surface and vehicle live loads.

IV. CONSIDERATION OF LIVE LOADS

After backfilling was completed, the next step was to apply the wearing surface and then live loads were applied. Both a uniform lane load and a vehicular live load were considered per AASHTO. In this software, this process was broken into three steps: 1) dead load of the wearing surface DW, 2) AASHTO lane load, and 3) AASHTO vehicular loading. All analyses resume from the point at which the previous step was completed. For example, the DW analysis starts from the point at which the last backfilling step was applied. This was necessary since the principle of superposition does not apply for nonlinear analyses. The results of step (3) minus the results of step (1) represented the total effect of live loading. The lane load was applied separately from the live load only because it is a constant load and therefore it is not necessary to re-apply it for various truck positions in an envelope-type analysis. This may result in reduced computational time.

The loads and vertical stresses associated with the dead load of the wearing surface and the uniform lane load were simply based on tributary area. On the other hand, the loads for the vehicular live load were calculated using the integral solution to the Boussinesq

This report shall not be reproduced, except in full, without the written approval of
the AEWC Advanced Structures & Composites Center.

vertical stress equation. The vertical stress used to calculate soil spring forces due to vehicular live loads was taken as the calculated force divided by the tributary area.

V. SPECIFIC PARAMETERS USED FOR ANALYSES

All analyses conducted as part of this study were based on expected values for the proposed Ellsworth Bridge Project. A majority of these parameters were directly provided by AIT and are summarized in Table 1. Parameters not directly provided were calculated/ estimated based on drawings and other information provided by AIT. Supporting calculations are provided in Appendix C.

This report shall not be reproduced, except in full, without the written approval of
the AEWC Advanced Structures & Composites Center.

Table 1 – Specific Parameter Values for Analyses

Description	Variable	Units	Decking	
			Concrete	FRP
Diameter of CFRP tube	diam	in	11.8	
Rise of arch centerline	rise	ft	14	
Span of arch centerline	span	ft	34.33	
Depth of backfill above arch crown	depth_crown	ft	Variable, 3-12.5	
Depth of wearing surface	DW_depth	in	3	
Equivalent deck thickness for self-weight calculation	deck_thick	in	7.8	0.31
Arch spacing	spacing	in	60	
Strength of concrete in the arch	Fpc	psi	5000	
Soil density	rho	pcf	125	
Wearing surface density	rho_asphalt	pcf	140	
Design truck axle	Axle_space		Short	
Number of lanes loaded	num_lanes		2	
All load factors			1	
Number of arch elements	numels		60	
Number of deck elements (per section)	num_deck		8	
Effective height for which to apply soil springs	H_effective	ft	14	
Elastic modulus of deck	E_deck	ksi	3759	4200
Area of concrete deck, long.	A_deck	in^2/in	5	NA
Positive bending moment of inertia, long.	I_pos	in^4/in	0.592	NA
Negative bending moment of inertia, long.	I_neg	in^4/in	0.066	NA
Area of concrete deck, trans.	A_deck	in^2/in	7.68	0.303
Positive & negative bending moment of inertia, trans.	I_deck	in^4/in	3.2	0.93
Effective radial distance from arch centerline to soil	t_deck	in	14.4	7.9
Lateral pressure coefficient, active	Ka		0.25	
Lateral pressure coefficient, at-rest	Ko		0.45	
Lateral pressure coefficient, passive	Kp		4	
Deflection/H_effective, active	delta_Ka		0.003	
Deflection/H_effective, passive	delta_Kp		0.028	

This report shall not be reproduced, except in full, without the written approval of
the AEWC Advanced Structures & Composites Center.

The geometry of the circular arc-segment was provided by AIT. Another arch geometry, referred to as the "Bebo" or "ConSpan" arch was also provided by AIT. The geometry of this arch is based on an elliptical shape. It is steeper near the supports and flatter near midspan as compared to a circular arc-segment arch. The total span and rise were held constant. An intermediate multi-radius geometry was also considered. This was a symmetric 3-radius arch with interior (around midspan) curve defined by a radius of about 19.6 ft and included angle of about 77.4 degrees. The exterior (near supports) curves of this geometry were defined by a radius of about 13.3 ft and included angle of about 48.4 degrees. All three geometries are shown in Figure 4.

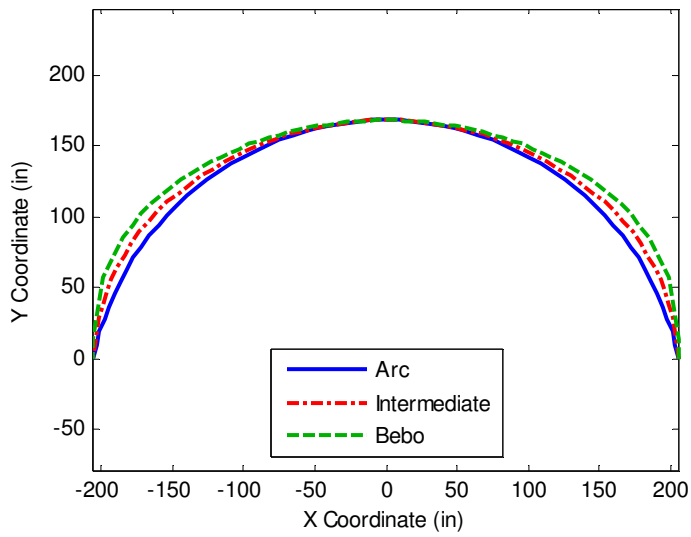

Figure 4 – Geometric Configurations for Analyses

VI. RESULTS: EFFECT OF STAGED BACKFILLING

Staged backfilling affects analysis results in several ways: 1) alternating soil lifts result in side-sway and non-symmetric response about midspan; 2) staged backfilling allows lateral earth pressure coefficients other than the at-rest coefficient to be rationally considered, which generally reduces critical response values; and 3) staged backfilling allows the structural response to be tracked throughout the construction period, which is important if the greatest response occurs prior to the final backfilling step.

The effect of staged backfilling was examined by running the matrix of analyses shown in Table 2. Three different arch bending stiffness relationships were considered, one of which utilized the nonlinear moment-curvature relationship provided for the arch tubes of

This report shall not be reproduced, except in full, without the written approval of
the AEWC Advanced Structures & Composites Center.

this study. The others were linear-elastic relationships intended to provide approximate bounds on the response that would be expected. Both FRP decking and concrete decking were considered. The concrete decking is placed on top of another type of FRP decking in actual bridge applications, but this type of FRP is much softer than the FRP decking that would be used instead of concrete, and its stiffness was neglected in analyses. Three different levels of backfilling were considered: 3, 6, and 12.5 ft. The 3 ft and 6 ft depths are similar to actual values that have been used for recently constructed bridges. The 12.5 ft depth is the specified depth for the proposed Ellsworth Bridge. All results shown here are for service (unfactored) loads.

Results of analyses are presented in Figure 5 through Figure 9 below for both types of decking and also for both arch moment and total foundation thrust. Envelope arch moments are presented, meaning that the values represent the maximum/minimum values for any point along the length of the arch at a particular load step (average backfill elevation).

Table 2 Matrix of Analyses to Examine the Effect of Staged Backfilling

Arch Bending Stiffness	Decking	Backfill Depth Above Centerline of Arch Crown (ft)
Nonlinear	Concrete	3
Linear, Uncracked Section	FRP-only	6
Linear, Cracked Section	--	12.5

This report shall not be reproduced, except in full, without the written approval of
the AEWC Advanced Structures & Composites Center.

I. Envelope Arch Moments

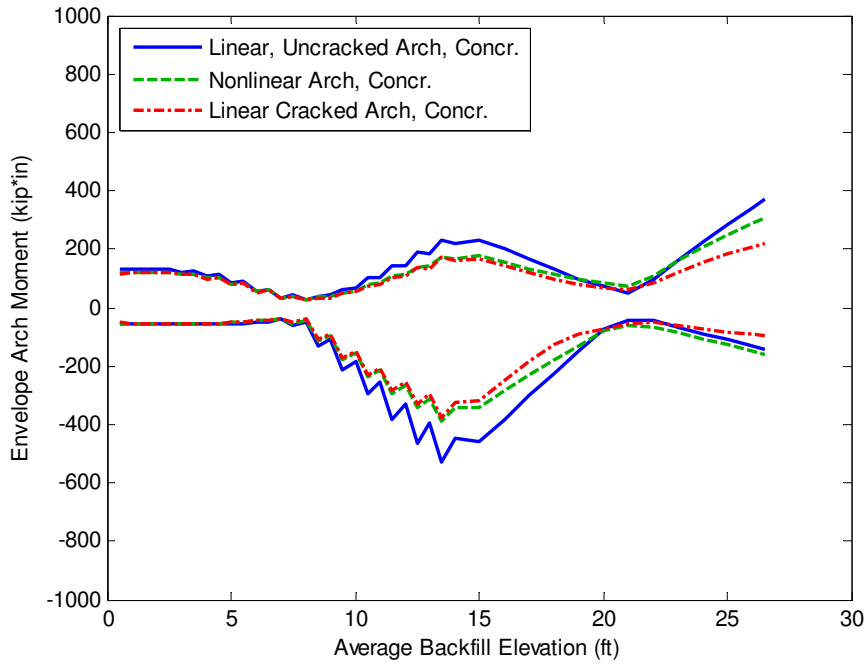

Figure 5 – Backfilling Envelope Arch Moment for Various Arch Bending Stiffness Relationships, Concrete Deck

This report shall not be reproduced, except in full, without the written approval of
the AEWC Advanced Structures & Composites Center.

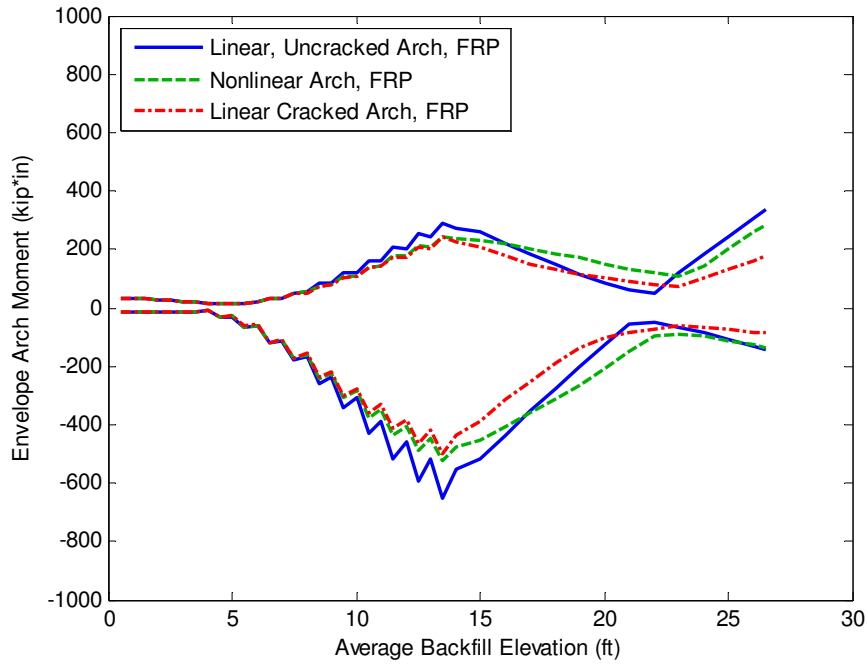

Figure 6 – Backfilling Envelope Arch Moment for Various Arch Bending Stiffness Relationships, FRP Deck

As shown in Figure 5 and Figure 6, the response of the nonlinear arch generally falls between those of the two corresponding linear models for arch bending moment. Generally the arch moments reach a peak at some point during construction near the point at which the backfill elevation approaches the height of the arch (14 ft). After which the magnitude of the moments generally decreases until the backfill elevation is around 21-22 ft, and then increases again. Thus, the critical construction moment may occur prior to the last load step, depending on the final backfill elevation.

The increased moment at elevations near 14 ft. stems from the fact that the alternating soil lifts cause side-sway and increased moments. The side-sway is depicted graphically in Figure 7 for the model with nonlinear arch bending stiffness relationship and a concrete deck. The original position of the arch is outlined in black. The deformed shape is indicated by the thick blue line (deflections are scaled by a factor of 10). It is apparent from this illustration that the deflections (and resulting moments) are much greater as the backfill level is near the top of the arch. However, at the final grade elevation, the deflections are relatively small and many of the soil springs (not shown) have increased in stiffness (i.e. $K > K_o$). This stiffness of the soil is expected to reduce live load moments in the arch.

This report shall not be reproduced, except in full, without the written approval of
the AEWC Advanced Structures & Composites Center.

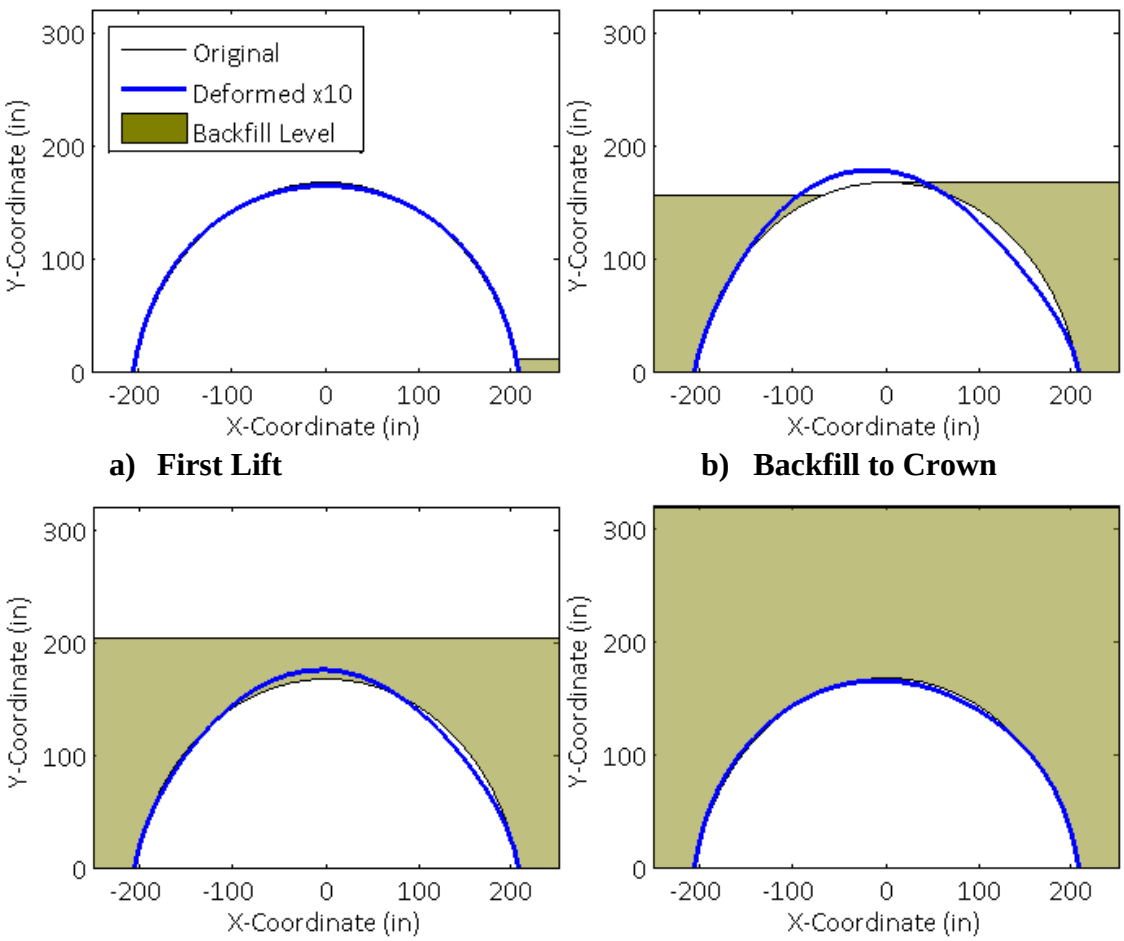

a) First Lift **b) Backfill to Crown**

c) 3 ft. Above Crown (Typical) **d) 12.5 ft. Above Crown**

Figure 7 – Deflected Shape of the Arch at Various Backfill Levels, Nonlinear Arch Bending Stiffness, Concrete Deck

This report shall not be reproduced, except in full, without the written approval of
the AEWC Advanced Structures & Composites Center.

II. Outward Foundation Thrust

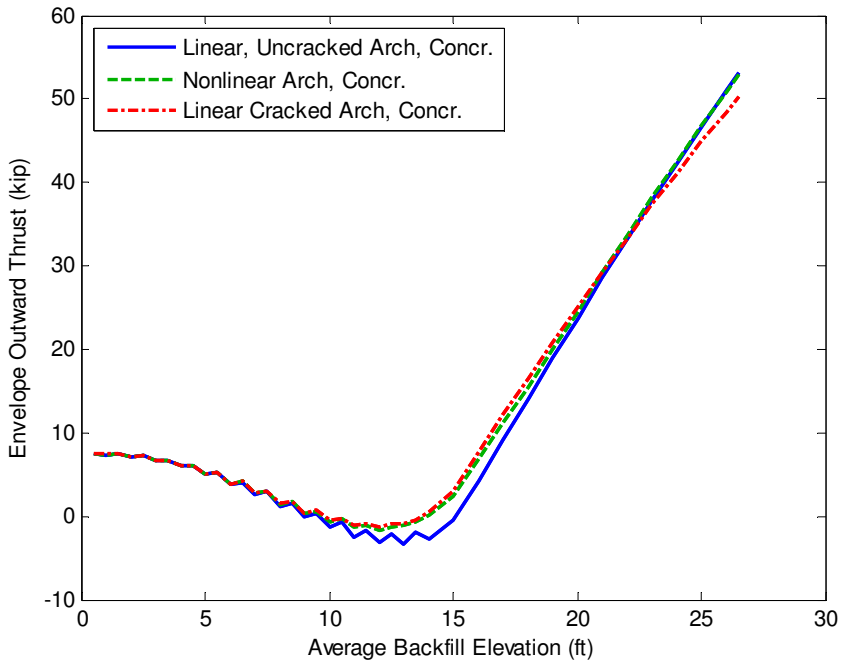

Figure 8 – Backfilling Envelope Outward Thrust for Various Arch Bending Stiffness Relationships, Concrete Deck

This report shall not be reproduced, except in full, without the written approval of
the AEWC Advanced Structures & Composites Center.

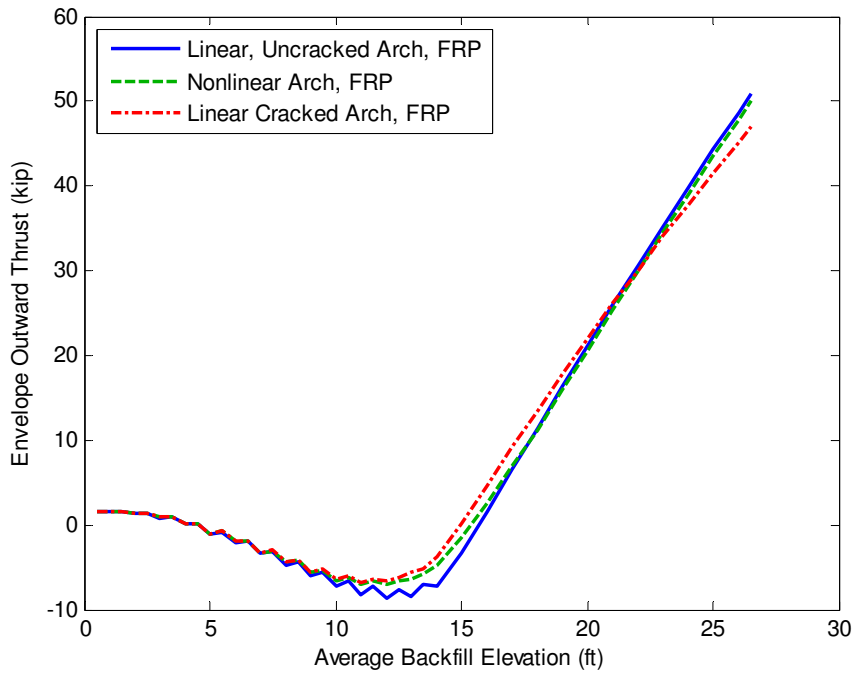

Figure 9 – Backfilling Envelope Outward Thrust for Various Arch Bending Stiffness Relationships, FRP Deck

As shown in Figure 8 and Figure 9, the response of the nonlinear arch again generally falls between the responses of the two corresponding linear models for arch outward thrust. Note that thrust values for the concrete-decked arches are initially much larger than those for FRP-decked arches due to the increased self-weight of the concrete. However, as the backfill elevation exceeds the approximate height of the arch, the thrust forces are dominated by the backfilling loads and both types of decking show similar results. It is important to note that the thrust force reported is not the total horizontal reaction, but rather the horizontal reaction at the base of the arch. The total reaction is the sum of the base reaction plus all of the horizontal spring forces.

This report shall not be reproduced, except in full, without the written approval of
the AEWC Advanced Structures & Composites Center.

III. Envelope Arch Axial Load

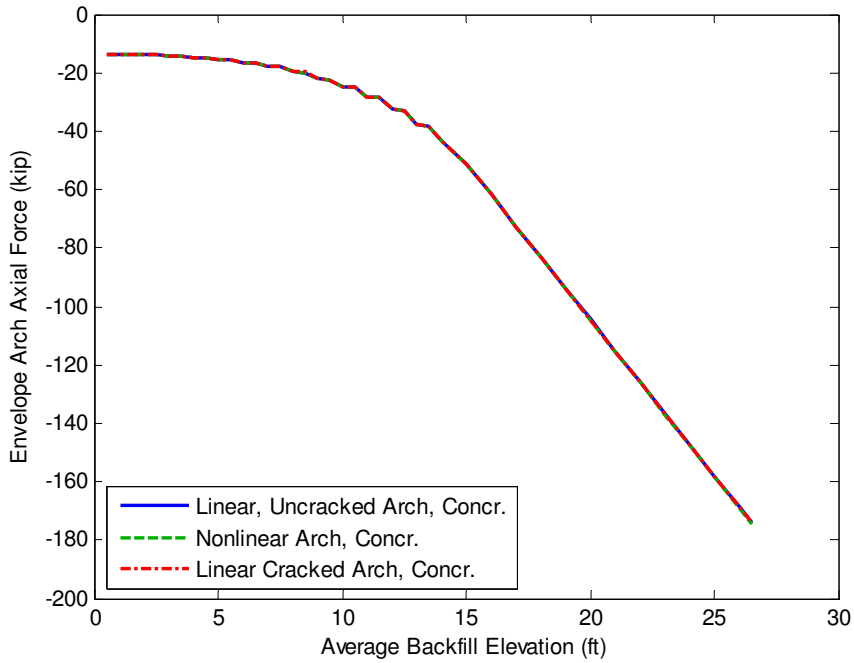

Figure 10 – Backfilling Envelope Arch Axial Load for Various Arch Bending Stiffness Relationships, Concrete Deck

This report shall not be reproduced, except in full, without the written approval of
the AEWC Advanced Structures & Composites Center.

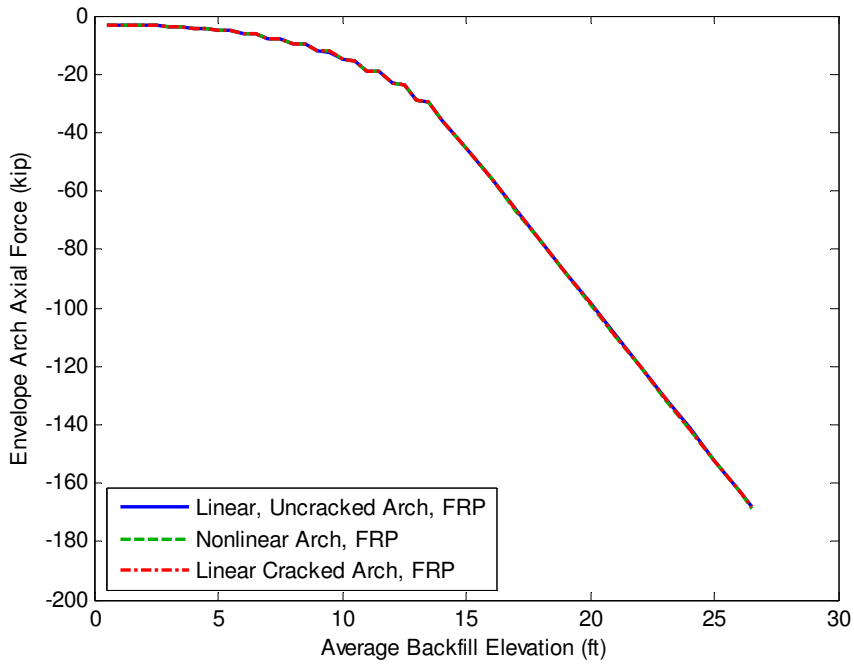

Figure 11 – Backfilling Envelope Arch Axial Load for Various Arch Bending Stiffness Relationships, FRP Deck

As shown in Figure 10 and Figure 11, the axial response of the arch is practically unaffected by the type of relationship used to describe the arch bending stiffness. The magnitude of the axial load in the concrete-decked arches is slightly more than for the FRP-decked arches due to the increased self-weight.

VII. RESULTS: EFFECT OF ARCH GEOMETRY

The geometry of the arches has a major effect on the way that the structure responds to a given set of loads. All bridges constructed to-date have utilized circular arc-segment arches. However, this configuration may not be ideal for all applications. Other geometric configurations are possible and have been considered for future projects. For example, one possible configuration is an arch that is relatively steeper near the supports and flatter near midspan as compared to a circular segment arc shape. This shape tends to result in decreased foundation thrust and increased arch member bending moments. Based on economic factors, the shape of the arch could be optimized to achieve a desired effect. In this study, the effect of arch geometry was investigated by analyzing the three geometric shapes described previously. The matrix of analyses conducted is shown below in Table 3.

This report shall not be reproduced, except in full, without the written approval of the AEWC Advanced Structures & Composites Center.

Table 3 Matrix of Analyses to Examine the Effect of Arch Geometry

Arch Geometry	Decking
Circular Segment Arc	Concrete
ConSpan Bebo Arch	FRP-only
Multi-radius (Intermediate)	--

I. Envelope Arch Moments

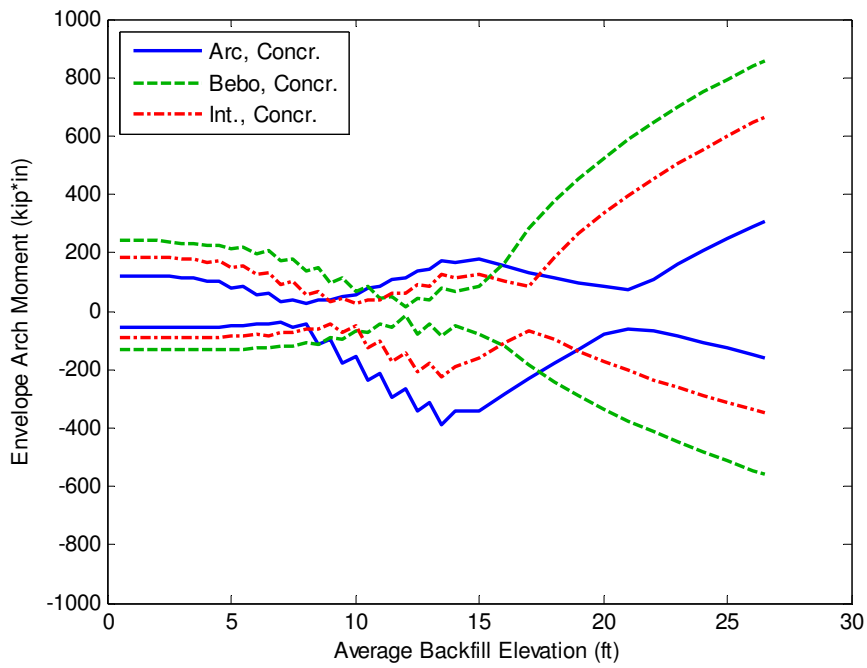

Figure 12 – Backfilling Envelope Arch Moments for Various Geometric Configurations, Concrete Deck, 12.5 ft of Total Fill Above the Crown

This report shall not be reproduced, except in full, without the written approval of the AEWC Advanced Structures & Composites Center.

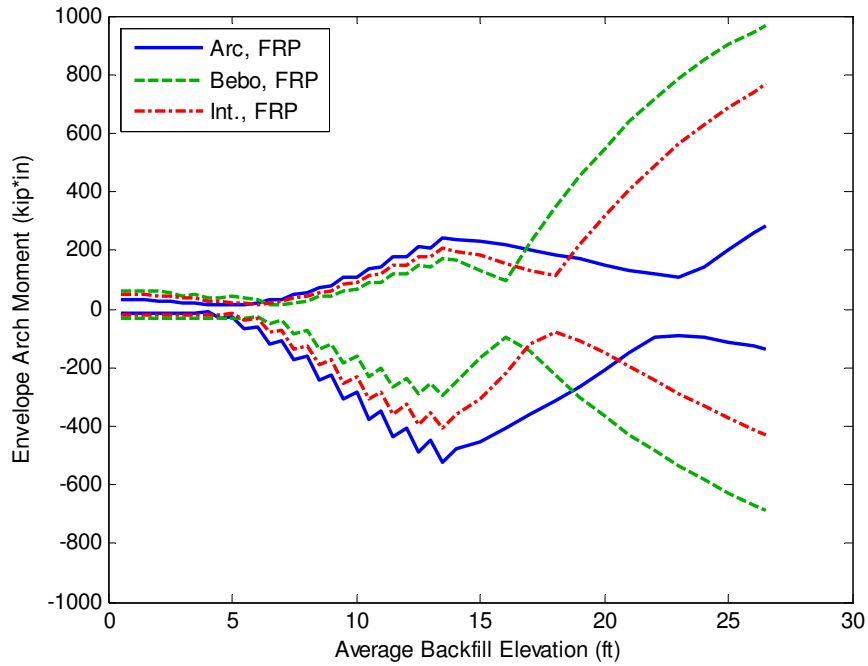

Figure 13 – Backfilling Envelope Arch Moments for Various Geometric Configurations, FRP Deck, 12.5 ft of Total Fill Above the Crown

It is apparent from Figure 12 and Figure 13 that the moment in the arch increases significantly at high backfill elevations going from the arc shape to the intermediate shape and again going from the intermediate shape to the Bebo shape. The reverse is true for the moment in the arch when the backfill elevation is near the height of the arch. This may indicate that shapes such as the Bebo arch are more appropriate for relatively small crown burial depths.

This report shall not be reproduced, except in full, without the written approval of
the AEWC Advanced Structures & Composites Center.

II. Outward Foundation Thrust

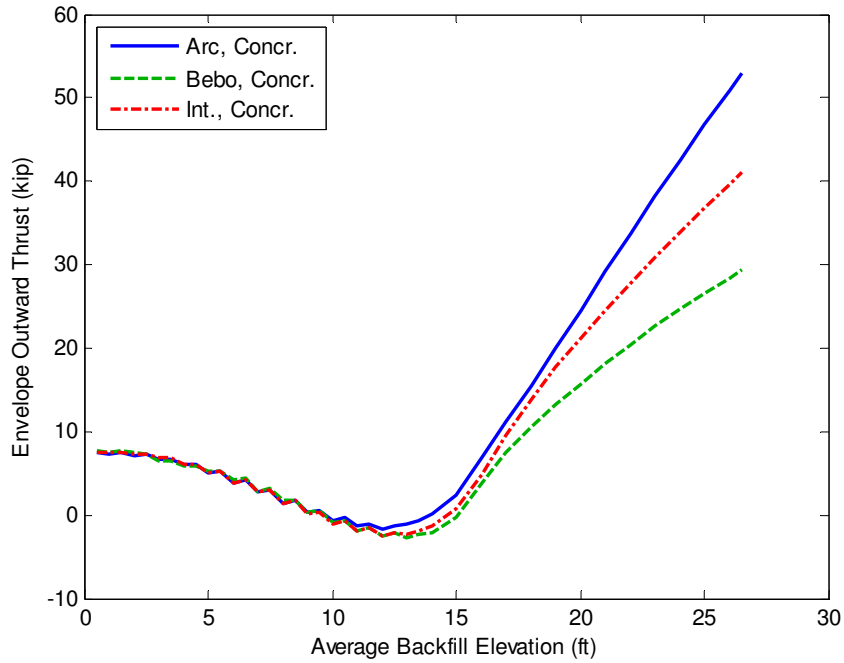

Figure 14 – Backfilling Envelope Outward Thrust for Various Geometric Configurations, Concrete Deck, 12.5 ft of Total Fill Above the Crown

This report shall not be reproduced, except in full, without the written approval of
the AEWC Advanced Structures & Composites Center.

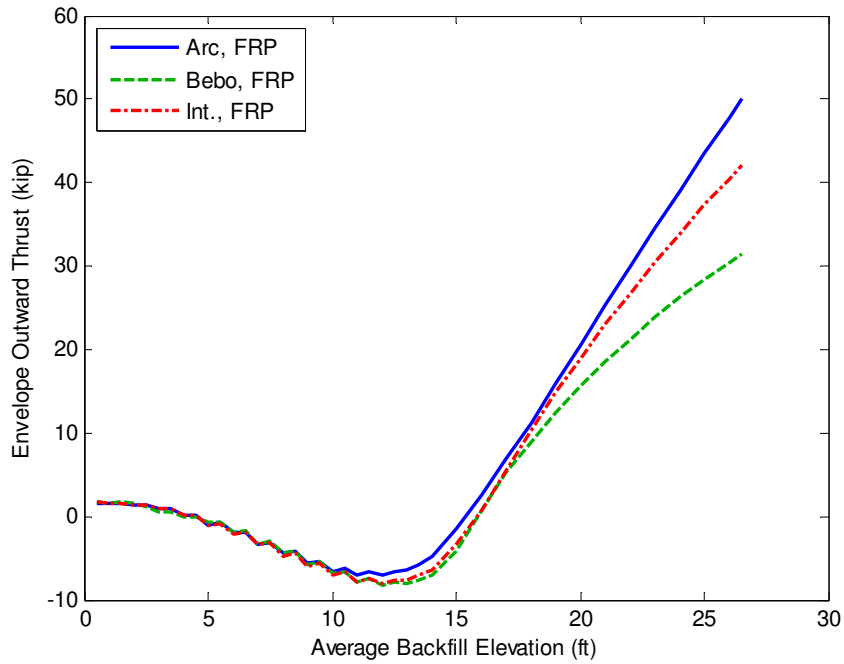

Figure 15 – Backfilling Envelope Outward Thrust for Various Geometric Configurations, FRP Deck, 12.5 ft of Total Fill Above the Crown

It is apparent from Figure 14 and Figure 15 that the outward thrust is generally greater for arc-shaped arches as compared to the Bebo arch for practically all levels of arch crown burial. Once again the response of the intermediate arch is in between the two others. This indicates that shapes that are relatively steeper near the supports and flatter near midspan are more effective at reducing foundation thrust loads.

This report shall not be reproduced, except in full, without the written approval of
the AEWC Advanced Structures & Composites Center.

III. Envelope Arch Axial Load

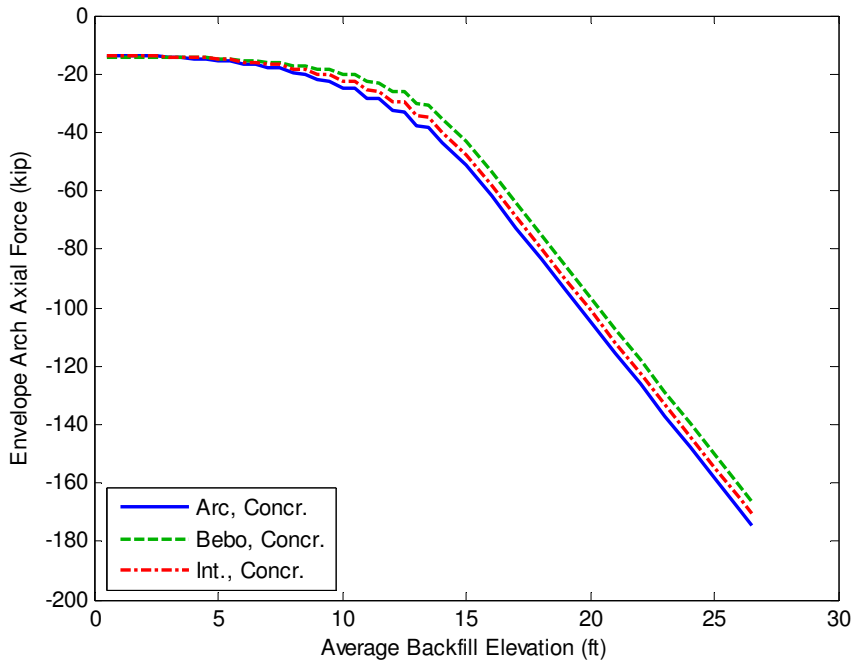

Figure 16 – Backfilling Envelope Arch Axial Load for Various Geometric Configurations, Concrete Deck, 12.5 ft of Total Fill above the Crown

This report shall not be reproduced, except in full, without the written approval of
the AEWC Advanced Structures & Composites Center.

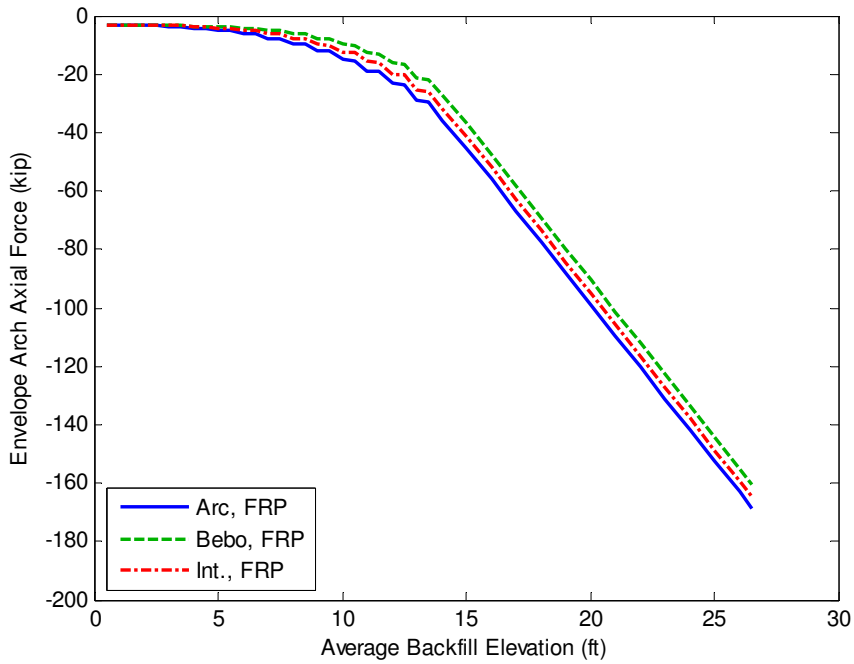

Figure 17 – Backfilling Envelope Arch Axial Load for Various Geometric Configurations, FRP Deck, 12.5 ft of Total Fill above the Crown

The maximum axial load level in the arch does not appear to be greatly affected by the shape of the arch based on Figure 16 and Figure 17, although the arc-shaped arch does carry slightly greater axial loads at all backfill levels.

VIII. RESULTS: EFFECT OF LIVE LOADING

The response due to live loading may control the design of the arch members, particularly for bridges with relatively low soil depth above the crown of the arch. The effect of soil-structure interaction on live loading was examined in this study by analyzing a variety of configurations as summarized in Table 4. Four different truck/position combinations provided by AIT were analyzed. The position refers to the front axle of the truck moving from left to right and the origin of the coordinate system is at midspan. Note that the positions referring to M+ in the right footing were actually applied with the truck mirrored about midspan to maximize M+ in the left footing of the model. This was done because the positive moment is larger at the left footing due to staged backfilling. If staged backfilling were not considered, the foundation moments on each side of the arch due to construction would be equal. All analyses with live loading considered a final

This report shall not be reproduced, except in full, without the written approval of the AEWC Advanced Structures & Composites Center.

backfilling elevation of 15 ft (3 ft crown burial depth) unless otherwise noted. Service (unfactored) loads are used for all analyses.

Table 4 Matrix of Analyses to Examine the Effect of Arch Geometry

Truck and Position of Front Axle	Maximizes	Arch Geometry	Decking
Short Design Truck at 130 in (266 in Rev.)	M+ at right footing (M+ at left footing)	Circular Segment Arc	Concrete
Short Design Truck at 466 in	M- at right footing	ConSpan Bebo Arch	FRP-only
Tandem at -38 in (86 in Rev.)	M+ at right footing (M+ at left footing)	--	--
Tandem at 154 in	M- at right footing	--	--

I. Envelope Arch Moments

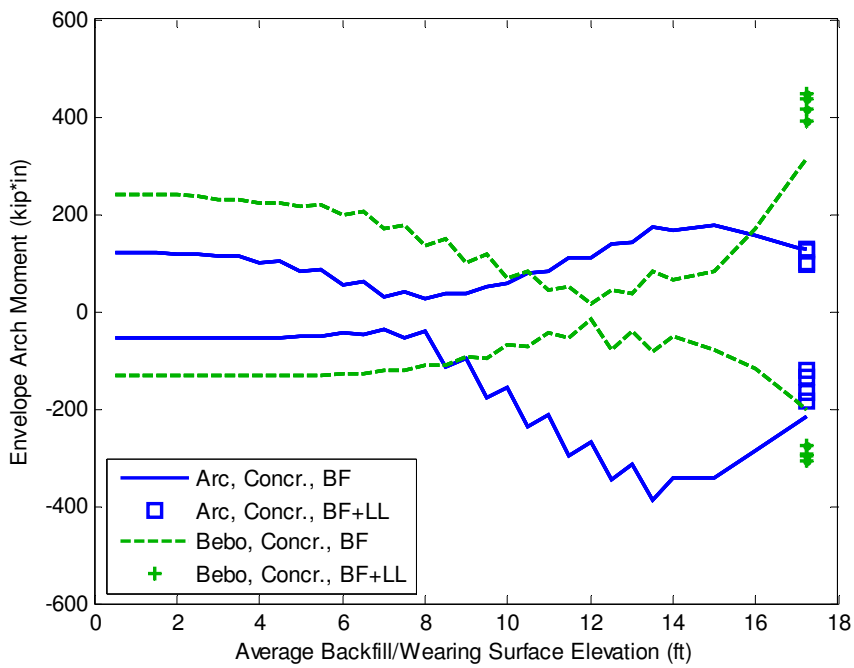

Figure 18 – Backfilling and LL Envelope Arch Moment for Arc and ConSpan (Bebo) Geometries (All 4 LL Analyses Shown for Each), Concrete Deck

This report shall not be reproduced, except in full, without the written approval of the AEWC Advanced Structures & Composites Center.

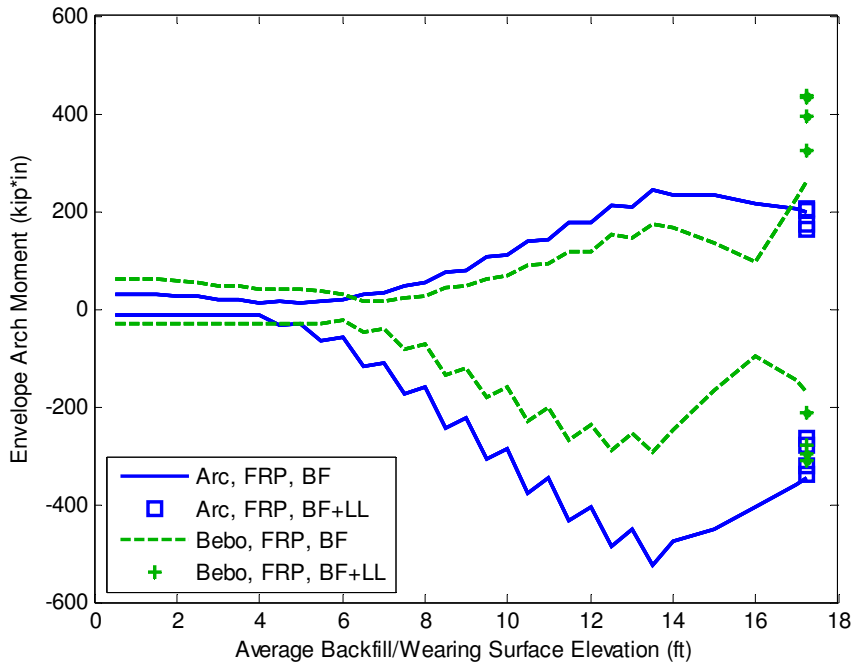

Figure 19 – Backfilling and LL Envelope Arch Moment for Arc and ConSpan (Bebo) Geometries (All 4 LL Analyses Shown for Each), FRP Deck

Interestingly, the magnitude of the arch moment due to live loading for the arc-shaped arches at all truck positions except one decreased as shown in Figure 18 and Figure 19. The one case that showed an increase in arch moment was only about 1%. This counter-intuitive result occurs because the crown burial depth is low (3 ft) and the arch is in such a position that it benefits from being "pushed back into place" by additional vertical loading (see Figure 7). On the other hand, the arch moment magnitudes increase for all possible scenarios with the Bebo arch. This indicates that the arc-shaped arch is more effective for resisting moment due to live loads at low crown burial depths.

This report shall not be reproduced, except in full, without the written approval of
the AEWC Advanced Structures & Composites Center.

II. Outward Foundation Thrust

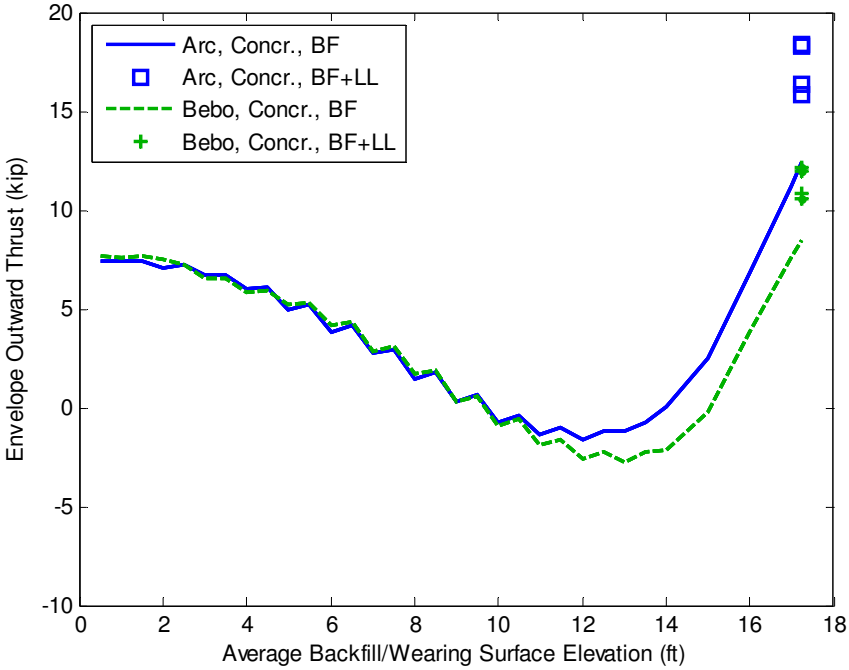

Figure 20 – Backfilling and LL Envelope Outward Thrust for Arc and ConSpan (Bebo) Geometries (All 4 LL Analyses Shown for Each), Concrete Deck

This report shall not be reproduced, except in full, without the written approval of
the AEWC Advanced Structures & Composites Center.

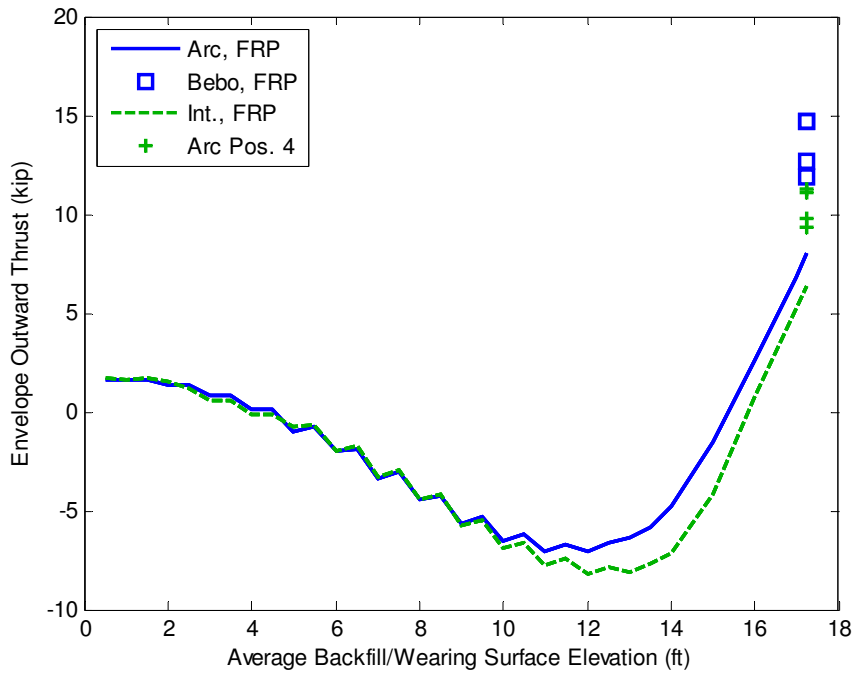

Figure 21 – Backfilling and LL Envelope Outward Thrust for Arc and ConSpan (Bebo) Geometries (All 4 LL Analyses Shown for Each), FRP Deck

It is apparent from Figure 20 and Figure 21 that the outward thrust is generally greater for arc-shaped arches as compared to the Bebo arch for practically all backfill and live load levels. This indicates that shapes that are relatively steeper near the supports and flatter near midspan are more effective at reducing foundation thrust loads due to backfilling and live loads.

This report shall not be reproduced, except in full, without the written approval of
the AEWC Advanced Structures & Composites Center.

III. Envelope Arch Axial Load

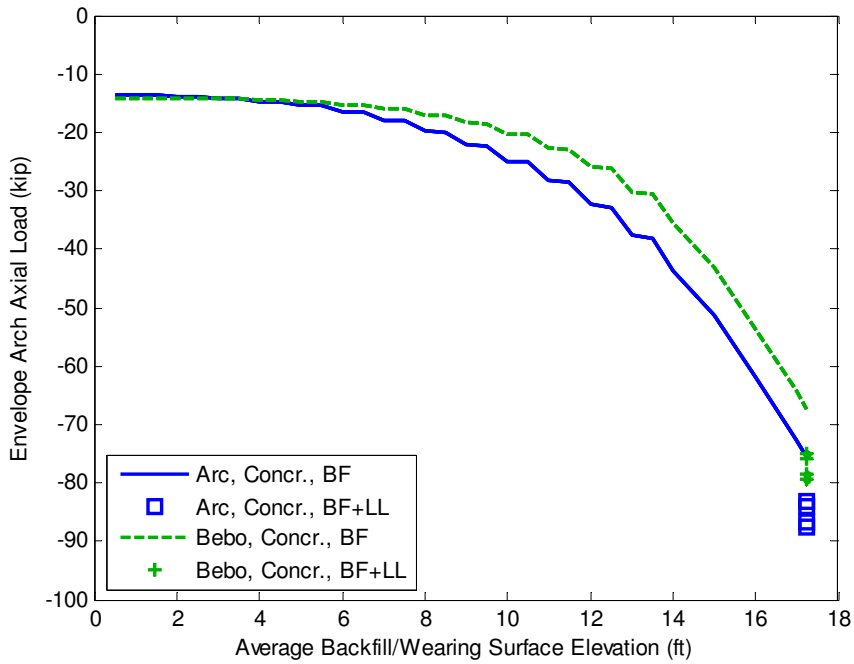

Figure 22 – Backfilling and LL Envelope Arch Axial Load for Arc and ConSpan (Bebo) Geometries (All 4 LL Analyses Shown for Each), Concrete Deck

This report shall not be reproduced, except in full, without the written approval of
the AEWC Advanced Structures & Composites Center.

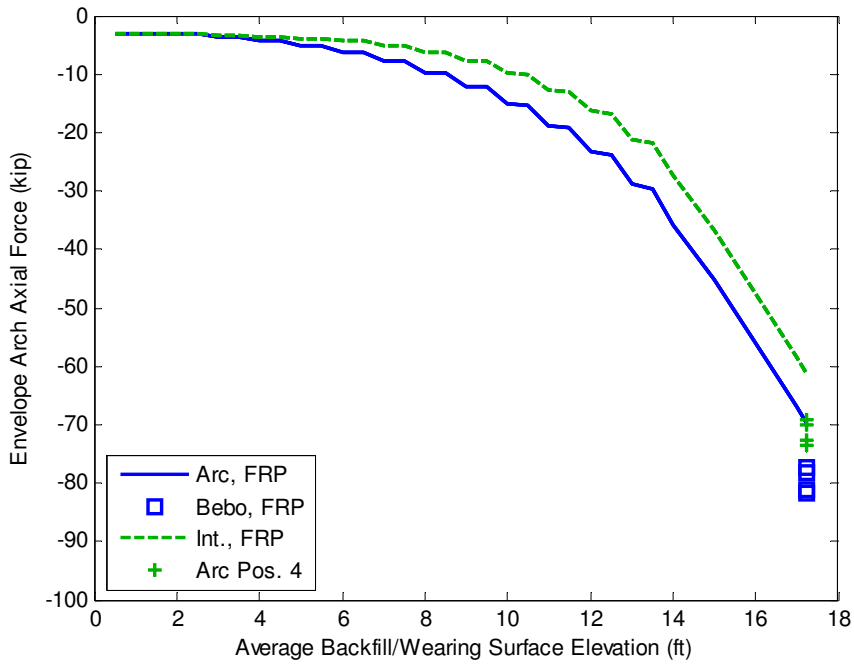

Figure 23 – Backfilling and LL Envelope Arch Axial Load for Arc and ConSpan (Bebo) Geometries (All 4 LL Analyses Shown for Each), FRP Deck

The change in axial load level in the arch due to live loading appears to be very similar for both arch shapes based on Figure 22 and Figure 23. Again the arc-shaped arch carries greater axial loads at all backfill levels.

IX. RELATIVE EFFECT OF SOIL SPRINGS

All analysis results presented to this point have utilized the procedure developed as part of this study with nonlinear soil springs. It is of interest to directly compare these results with those that would be generated with existing analysis code that does not consider nonlinear soil springs. A limited set of results is presented here to examine this.

This report shall not be reproduced, except in full, without the written approval of
the AEWC Advanced Structures & Composites Center.

I. Envelope Arch Moment

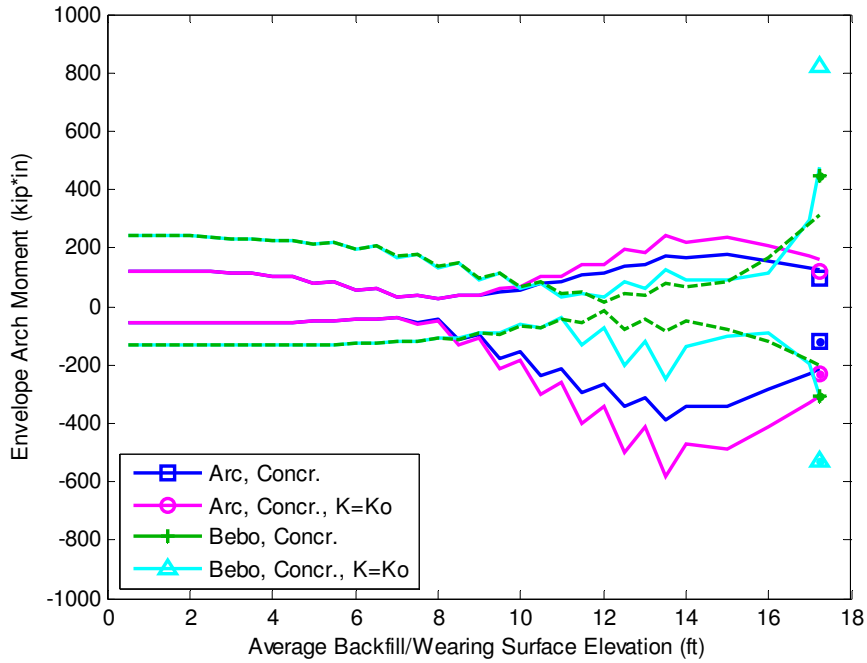

Figure 24 – Effect of Soil Springs on Backfilling and LL Moment, Concrete Deck, 3 ft of Backfill above the Crown

This report shall not be reproduced, except in full, without the written approval of
the AEWC Advanced Structures & Composites Center.

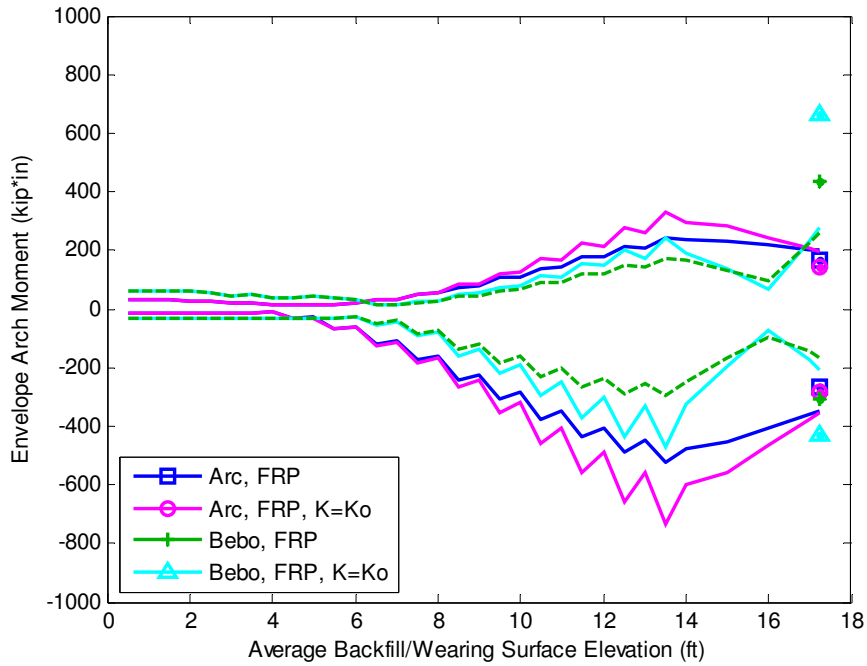

Figure 25 – Effect of Soil Springs on Backfilling and LL Moment, FRP Deck, 3 ft of Backfill above the Crown

It is apparent from Figure 24 and Figure 25 that the arch bending moment in both the arc-shaped arch and the Bebo arch are significantly reduced by considering the nonlinear soil spring relationship. The peak bending moment magnitudes and relative difference between the two types of arches are presented in Table 5. For all scenarios presented, the nonlinear soil spring relationship results in a reduction in arch bending moment of 26-46%.

Table 5 Peak Moment Magnitudes and Relative Differences Due to the Consideration of Nonlinear Soil Springs, 3 ft of Backfill above the Crown

		Arc			Bebo		
Deck	**Param**	**Nonlinear**	**K = Ko**	**Diff.**	**Nonlinear**	**K = Ko**	**Diff.**
Concr.	M+ (kip*in)	176	244	28%	447	823	46%
	M- (kip*in)	-386	-583	34%	-306	-532	42%
FRP	M+ (kip*in)	243	328	26%	436	666	35%
	M- (kip*in)	-523	-736	29%	-309	-470	34%

This report shall not be reproduced, except in full, without the written approval of the AEWC Advanced Structures & Composites Center.

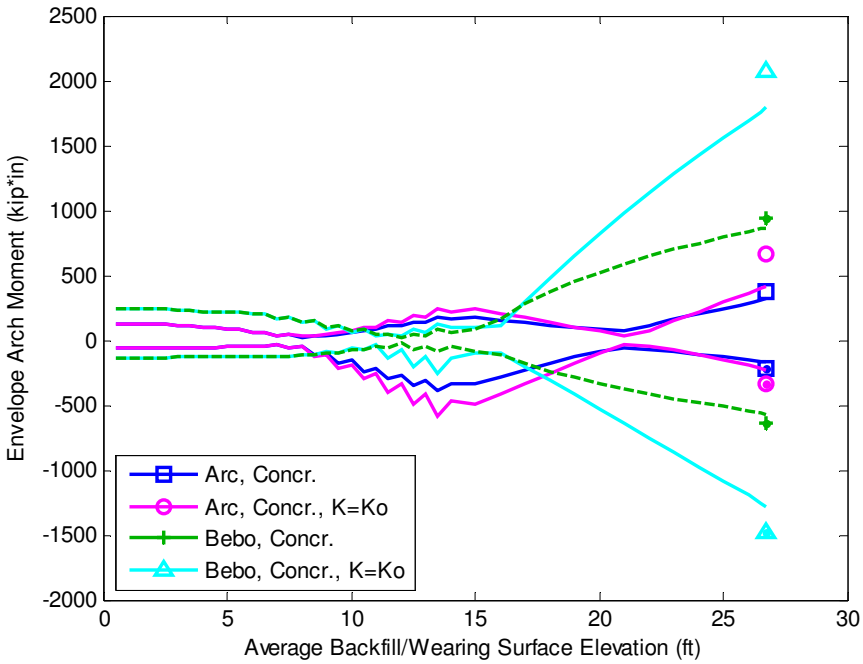

Figure 26 – Effect of Soil Springs on Backfilling and LL Moment, Concrete Deck, 12.5 ft of Backfill above the Crown

This report shall not be reproduced, except in full, without the written approval of
the AEWC Advanced Structures & Composites Center.

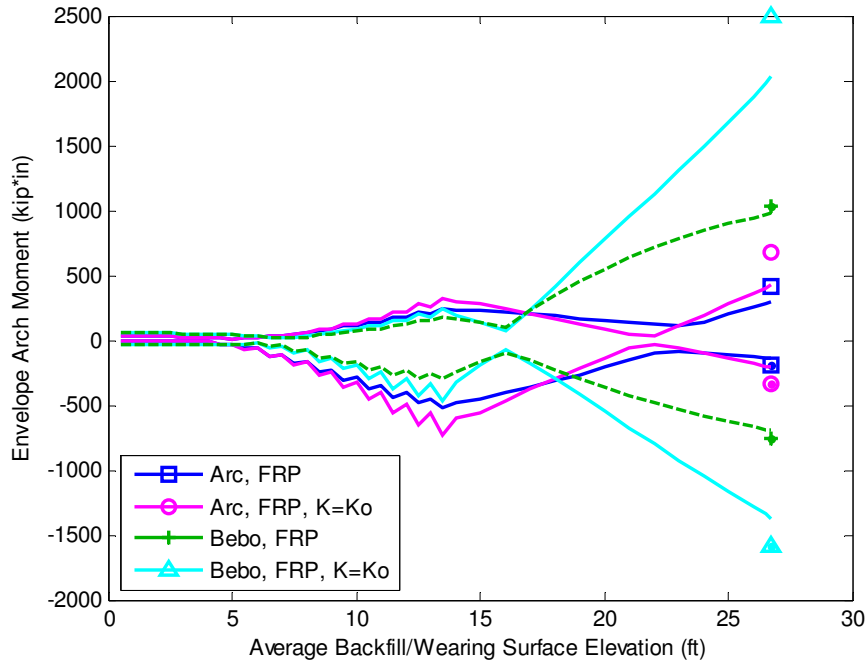

Figure 27 – Effect of Soil Springs on Backfilling and LL Moment, FRP Deck, 12.5 ft of Backfill above the Crown

It is apparent from Figure 26 and Figure 27 that the arch bending moment in both the arc-shaped arch and the Bebo arch are significantly reduced by considering the nonlinear soil spring relationship. The peak bending moment magnitudes and relative difference between the two types of arches are presented in Table 6. For all scenarios presented, the nonlinear soil spring relationship results in a reduction in arch bending moment of 37-59%.

Table 6 Peak Moment Magnitudes and Relative Differences Due to the Consideration of Nonlinear Soil Springs, 12.5 ft of Backfill above the Crown

		Arc			Bebo		
Deck	**Param**	**Nonlinear**	**K = Ko**	**Diff.**	**Nonlinear**	**K = Ko**	**Diff.**
Concr.	M+ (kip*in)	379	664	43%	935	273	55%
	M- (kip*in)	-212	-334	37%	-633	-1481	57%
FRP	M+ (kip*in)	417	674	38%	1032	2500	59%
	M- (kip*in)	-196	-340	42%	-762	--1581	52%

This report shall not be reproduced, except in full, without the written approval of the AEWC Advanced Structures & Composites Center.

II. Envelope Outward Thrust

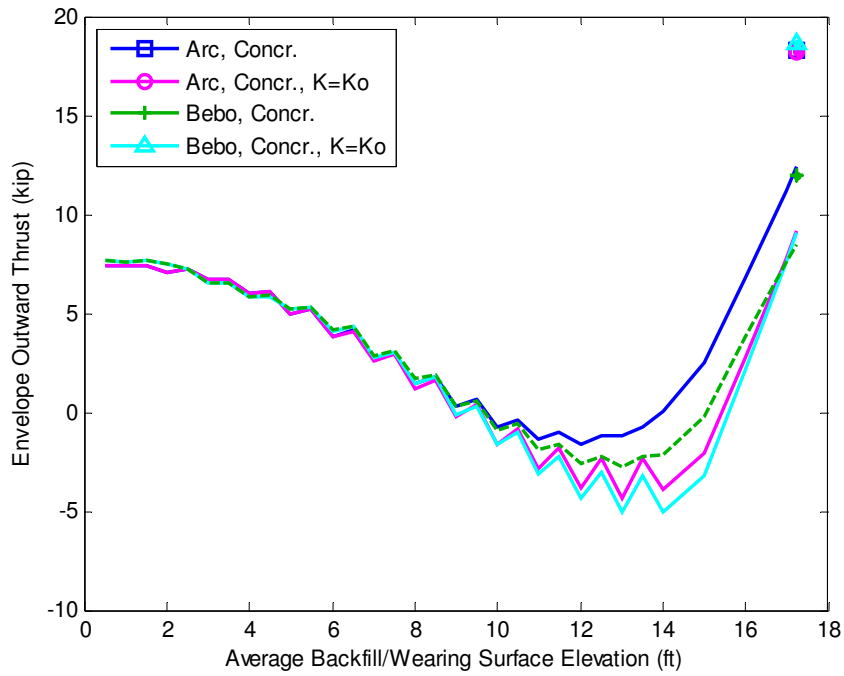

Figure 28 – Effect of Soil Springs on Backfilling and LL Thrust, Concrete Deck, 3 ft of Backfill above the Crown

This report shall not be reproduced, except in full, without the written approval of
the AEWC Advanced Structures & Composites Center.

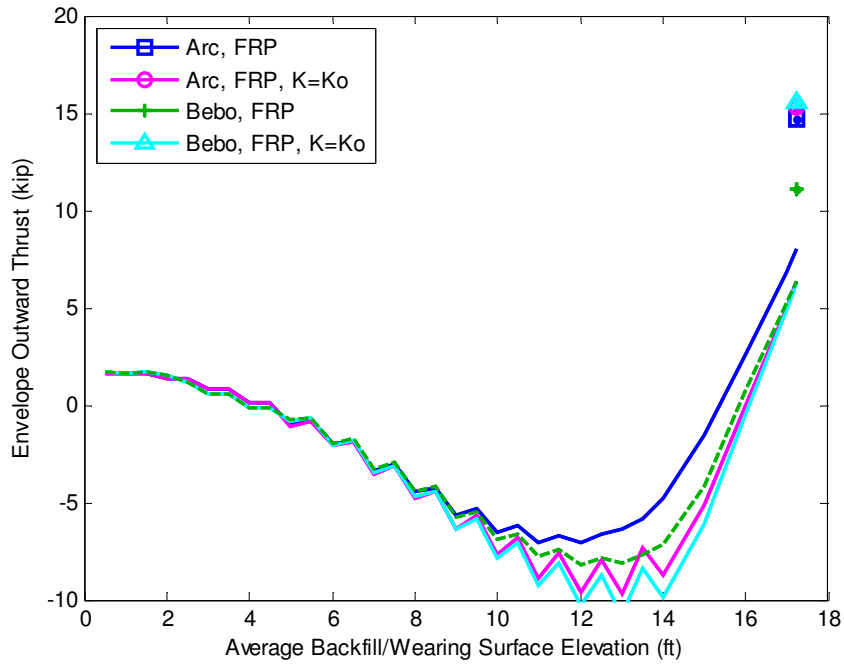

Figure 29 – Effect of Soil Springs on Backfilling and LL Thrust, FRP Deck, 3 ft of Backfill above the Crown

The outward thrust magnitude is reduced 29-36% when considering a nonlinear soil spring relationship for the Bebo arch, but it has practically no effect on the arc-shaped arch as shown in Table 7. The reason for the lack of significant benefit with respect to outward thrust with the arc-shaped arch is that many of the soil springs are actually still in the active state (i.e. K < Ko) at a backfill depth of the 3 ft. After the application of live loads, which causes K to increase, the response is similar to that for linear soil springs (K = Ko). As shown next, the soil-springs are more effective for larger crown burial depths.

Table 7 Peak Outward Thrust Magnitudes and Relative Differences Due to the Consideration of Nonlinear Soil Springs, 3 ft of Backfill above the Crown

		Arc			Bebo		
Deck	**Param**	**Nonlinear**	**K = Ko**	**Diff.**	**Nonlinear**	**K = Ko**	**Diff.**
Concr.	Outward Thrust	18.3	18.2	-1%	11.9	18.7	36%
FRP	Outward Thrust	14.7	15.3	4%	11.1	15.6	29%

This report shall not be reproduced, except in full, without the written approval of the AEWC Advanced Structures & Composites Center.

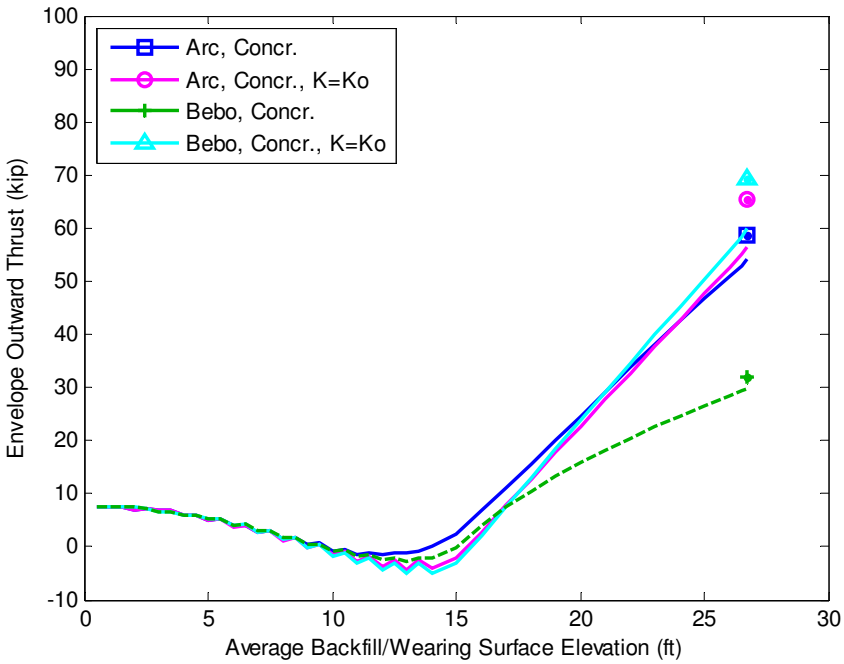

Figure 30 – Effect of Soil Springs on Backfilling and LL Thrust, Concrete Deck, 12.5 ft of Backfill above the Crown

This report shall not be reproduced, except in full, without the written approval of
the AEWC Advanced Structures & Composites Center.

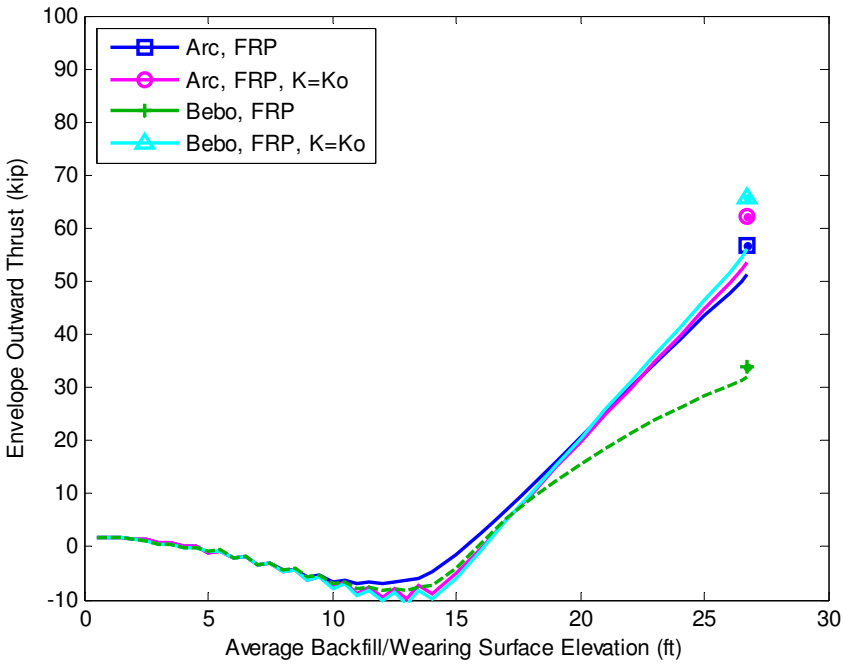

Figure 31 – Effect of Soil Springs on Backfilling and LL Thrust, FRP Deck, 12.5 ft of Backfill above the Crown

The outward thrust magnitude is reduced 48-54% when considering a nonlinear soil spring relationship for the Bebo arch, but only 8-10% for the arc-shaped arch as shown in Table 8 for a crown burial depth of 12.5 ft. This indicates that the use of nonlinear soil springs provides more benefit for the Bebo arch than the arc-shaped arch with respect to the improvement in foundation thrust. Additional improvement may be mobilized for both shapes when other types of foundations are considered (e.g. spread footings free to translate instead of the perfectly fixed foundations that are assumed in these analyses).

Table 8 Peak Outward Thrust Magnitudes and Relative Differences Due to the Consideration of Nonlinear Soil Springs, 12.5 ft of Backfill above the Crown

		Arc			Bebo		
Deck	**Param**	**Nonlinear**	**K = Ko**	**Diff.**	**Nonlinear**	**K = Ko**	**Diff.**
Concr.	Outward Thrust	58.8	65.4	10%	69.3	31.9	54%
FRP	Outward Thrust	56.9	62.3	8%	65.8	33.9	48%

III. Envelope Arch Axial Load

This report shall not be reproduced, except in full, without the written approval of the AEWC Advanced Structures & Composites Center.

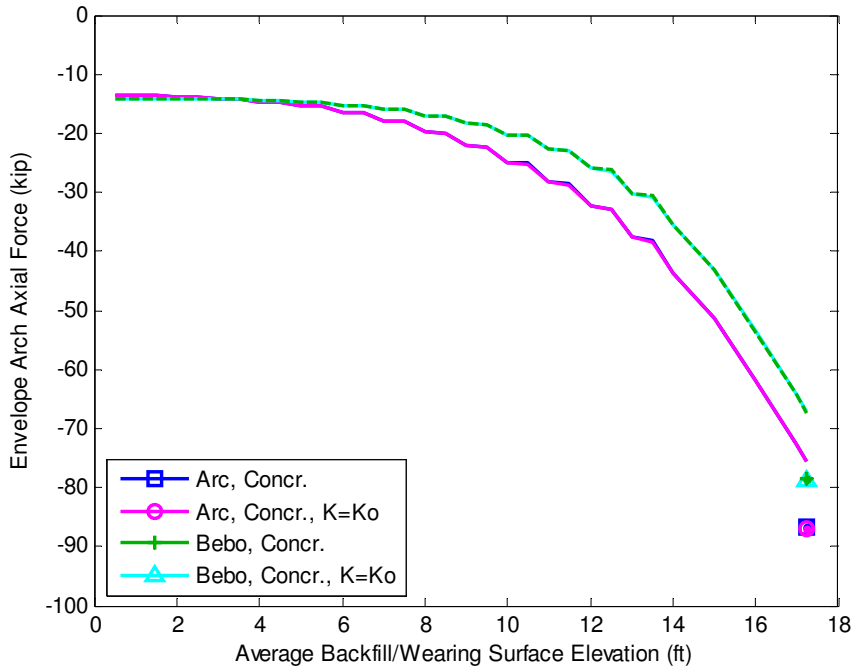

Figure 32 – Effect of Soil Springs on Backfilling and LL Arch Axial Loads, Concrete Deck, 3 ft of Backfill above the Crown

This report shall not be reproduced, except in full, without the written approval of
the AEWC Advanced Structures & Composites Center.

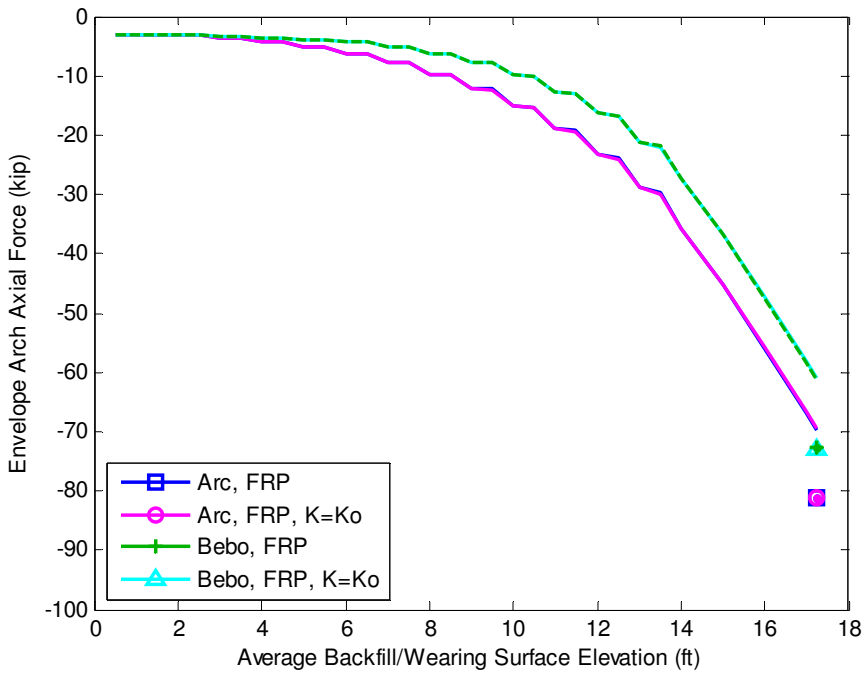

Figure 33 – Effect of Soil Springs on Backfilling and LL Arch Axial Loads, FRP Deck, 3 ft of Backfill above the Crown

The peak magnitude of arch axial force is practically unaffected by the soil spring relationship as shown in Figure 32, Figure 33, and Table 9. The difference in response is less than 1%.

Table 9 Peak Arch Axial Force Magnitudes and Relative Differences Due to the Consideration of Nonlinear Soil Springs, 3 ft of Backfill above the Crown

		Arc			Bebo		
Deck	**Param**	**Nonlinear**	**K = Ko**	**Diff.**	**Nonlinear**	**K = Ko**	**Diff.**
Concr.	Arch Axial Force (kip)	-78.6	-78.9	0.4%	-86.8	-87.1	0.3%
FRP	Arch Axial Force (kip)	-72.7	-72.9	0.3%	-81	-81.1	0.1%

X. SUMMARY AND CONCLUSIONS

MATLAB-based structural analysis code has been developed to capture the effects of nonlinear soil springs, staged construction, decking stiffness, and longitudinal benefit from concrete decking (see Appendix B for a collection of content specifically related to

This report shall not be reproduced, except in full, without the written approval of the AEWC Advanced Structures & Composites Center.

the programming aspect of the project). The code will be provided to AIT as a deliverable for this study. The effect of staged backfilling, arch geometry, and live loading was investigated by analyzing a variety of configurations that are representative of a proposed (or previously constructed) bridge project. Input parameters were based on values provided by AIT and were primarily based on the proposed Ellsworth Bridge project.

The following conclusions were drawn from results of analyses:

I. Staged Backfilling

1. Alternating soil lifts resulted in side-sway and non-symmetric response about midspan.
2. Staged backfilling allowed lateral earth pressure coefficients other than the at-rest coefficient to be rationally considered.
3. Staged backfilling allowed the structural response to be tracked throughout the construction period.
4. The bending moment response for the arch with the nonlinear bending stiffness relationship generally fell between those for the linear cracked arch and the linear uncracked arch.
5. The maximum moment during backfilling sometimes occurred at a point prior to the last construction load step depending on the total backfill level.
6. The type of arch bending stiffness considered did not have a large effect on the outward thrust.
7. The outward thrust was initially larger for the concrete-decked arches compared to the FRP-decked arches due to the increased self-weight.
8. The type of arch bending stiffness had practically no effect on the maximum axial load in the arch.

II. Arch Geometry

1. The shape of the arch had a large effect on the moment developed within the arch (total span and rise were held constant). Shapes that were steeper near supports and flatter near midspan (Bebo) resulted in much larger bending moments at large burial depths.
2. At shallow burial depths, the moments were largest in the arc-shaped arch and least for the Bebo arch, which may indicate that the optimal shape is dependent on crown burial depth.
3. The outward foundation thrust was greatest for the arc-shaped arch and least for the Bebo arch at all levels of backfilling.

This report shall not be reproduced, except in full, without the written approval of
the AEWC Advanced Structures & Composites Center.

4. The axial load in the arch was minimally affected by the arch shape, although the axial load in the Bebo arch was smaller for all levels of backfilling.

III. Live Loading

1. The magnitude of moment in the arc-shaped arch decreased as live loads were applied. This counter-intuitive result occurs when the crown burial depth is low (3 ft) and the arch is in such a position that it benefits from being "pushed back into place" by additional vertical loading (see Figure 7).
2. The magnitude of moment in the Bebo arch increased as live loads were applied, which may indicate that the arc-shaped arch is more effective for resisting moment due to live load at low crown burial depths.
3. The outward thrust due to live loading is greater for arc-shaped arches than the Bebo arch.
4. The change in axial load level due to live loading was similar for both arches. The total axial loads were larger in the arc-shaped arch compared to the Bebo arch.

IV. Relative Effect of Soil Springs

1. The use of nonlinear soil springs resulted in 26-59% lower arch bending moments.
2. Outward thrust was reduced by 29-54% for the Bebo arch. Less significant differences of around 0-10% were noted for the arc-shaped arch. It is expected that the relative effect of the soil-springs with respect to outward thrust will be reduced further for arches with other types of foundations that allow lateral movements (e.g. spread footings or pile-supported foundations).
3. The soil springs had practically no effect on the axial load level in the arches.

In summary, the consideration of nonlinear soil springs, the 3D effect of transverse decking stiffness, staged backfilling, and various arch geometries was shown to have a significant effect on the critical response values that would be used to design bridge structures. Many of the critical response values were reduced significantly by considering nonlinear soil springs. It was also shown that the arch geometry had a large effect on critical response values. The software developed as part of this project will provide a valuable tool to bridge designers in their efforts to optimize designs to achieve desired effects and ultimately improve the economic efficiency of these structures.

This report shall not be reproduced, except in full, without the written approval of
the AEWC Advanced Structures & Composites Center.

XI. REFERENCES

Faraji S, Ting JM, Crovo DS, Ernst H (2001). Nonlinear analysis of integral bridges: finite-element model. *Journal of Geotechnical and Geoenvironmental Engineering*, 127(5): 454-461.

MathWorks (2009). *Programming Fundamentals, MATLAB Version 7.9 (R2009b)*, The MathWorks, Inc. Natick, MA.

NCHRP (1991). *Manuals for the Design of Bridge Foundations*. National Cooperative Highway Research Program Report No. 343, Transportation Research Board, Washington, DC.

Ting JM and Faraji S (1998). *Force-Displacement Testing for Integral Abutment Bridges*. University of Massachusetts Transportation Center Report No. UMTC 97-13, University of Massachusetts, Amherst, MA.

USACoE (1994). *Design of Sheet Pile Walls*. CECW-ED Engineer Manual 1110-2-2504. Department of the Army, US Army Corps of Engineering, Washington, DC.

This report shall not be reproduced, except in full, without the written approval of the AEWC Advanced Structures & Composites Center.

XII. APPENDIX A – SCOPE OF WORK OF ORIGINAL PROPOSAL FROM UMAINE AEWC CENTER to AIT

Task 6: Simplified Modeling to Assess Soil-Structure Interaction Effects

This task will quantify the expected reduction in internal arch forces and foundation loads due to soil-structure interaction and staged backfilling. The results will guide AIT's decision-making when assessing how and whether to move forward with more sophisticated and costly studies on the potential benefits of soil-structure interaction, which may be analytical, laboratory-based, or field-based.

Staged backfill compaction causes incremental changes to the arch-soil system. Present AIT design methodology does not account for the stiffness of the backfill and the variation in horizontal soil pressure due to arch deflection. While both of these phenomena are difficult to simulate, there is a solid basis for assessing their effects through models that treat the soil as a series of uncoupled nonlinear springs. Precedents for this approach can be found in literature on integral abutment bridges (Faraji et al. 2001; Ting and Faraji 1998) and in design procedures for earth retaining structures (USACoE 1994). This task will be divided into four sub-tasks to systematically approach the problem.

Task 6.1: Develop FE Model of Arch Bridge to Simulate Staged Backfilling

We will develop a FE model for a single arch that incorporates beam elements for the arch, nonlinear springs for the soil, and additional transverse beam elements to simulate the decking. Unlike current AIT models, these models will be 3D, and the simulations will account for the effect of the variable structural stiffness of the arch-decking system on the soil reactions. Additionally, the models will allow the overlaying of a second set of arch elements to simulate arching action of the concrete decking. These additional beam elements will not be composite with the concrete-filled FRP arch, will have the same CG as the arch for simplicity of model generation, and will be assumed to have a constant stiffness, EI. The soil springs will be nonlinear, permitting the gradual transition from at-rest conditions to passive and active conditions to be simulated as the arch moves into and away from the backfill, respectively. The soil spring load-deflection relationships will be developed using the same methodology presented by Faraji et al. (2001) and Ting and Faraji (1998), which is based on soil stiffness information given in the NCHRP Report 343 (NCHRP 1991).

The model will simulate staged backfilling, where soil lifts are placed sequentially on alternating sides of the arch. As a soil lift is placed, its weight is applied, corresponding springs are added to the model, and all other soil springs in the model at or below the elevation of that soil lift will be updated to reflect any additional overburden pressure and incremental arch movements. The model will also be able to accommodate a nonlinear moment-curvature relationship for the filled arch. AIT will provide UMaine with

This report shall not be reproduced, except in full, without the written approval of the AEWC Advanced Structures & Composites Center.

appropriate arch nonlinear moment-curvature relationships, or MATLAB code to generate the arch nonlinear moment-curvature relationship.
Deliverable: A copy of the MATLAB FE code and a written description of the underlying assumptions.

Task 6.2: Simulate the Effect of Staged Backfilling

We will simulate the effect of staged backfilling for the same geometry and site conditions used in the design of the Ellsworth Bridge. AIT will provide geometry and design details. A medium-dense backfill material that is representative of the site backfill will be used for the simulations. The results of the analysis will be compared with the results of the analyses conducted by AIT in the design of the Ellsworth bridge arches to assess the significance of soil support. Quantities to be compared will include arch moments, arch axial loads, and foundation loads. A total of three basic models will be developed to assess the effect of arch stiffness: model (1) will use a nonlinear arch moment-curvature relationship; model (2) will use a linearly elastic arch with a constant cracked section; and model (3) will assume the arch is linearly elastic with a constant un-cracked section. For all three models, simulations will be run with and without the concrete deck. Additionally, three different heights of backfill above the arch crown (3 ft, 6 ft and 9 ft) will be simulated. This gives a total of 3x2x3 analyses.
Deliverable: Arch axial loads, arch moments, and foundation loads for all 18 analyses will be summarized in a report to AIT.

Task 6.3: Explore the Effect of Arch Geometry

We will develop additional FE models that will incorporate arch geometries having variable radii with more vertical legs and flatter tops. Such geometries are used by other manufacturers (i.e. ConSpan) to mobilize horizontal soil pressure and reduce foundation thrusts. AIT will provide UMaine with the geometry typical of a ConSpan arch for the same rise and span of the Ellsworth Bridge. UMaine will construct a model of an arch bridge with this geometry, as well as a second model with geometry intermediate between that of a ConSpan structure and the proposed Ellsworth Bridge. The effect of arch geometry will be assessed by comparing arch moments, thrusts, and foundation loads for these two models with the results from the proposed Ellsworth Bridge. Both models will assume a nonlinear arch moment-curvature relationship, and both models will be analyzed with and without a concrete deck with a fixed backfill height of 3 ft at the arch crown. These results can be used by AIT to assess potential reduction in foundation costs, as well as the effect on arch cross-sectional design and the feasibility of using variable radii arches.
Deliverable: Arch axial loads, arch moments, and foundation loads for all four analyses will be summarized in a report to AIT.

Task 6.4: Effect of Live Loading

In the final sub-task, live load effects will be examined. Two models will be run: (1) the Ellsworth Bridge; and (2) the flatter top arch geometry typical of a ConSpan structure as

This report shall not be reproduced, except in full, without the written approval of
the AEWC Advanced Structures & Composites Center.

specified by AIT for Task 2.3. Each model will be run with and without a concrete deck and 3 ft of backfill at the arch crown. Live load will be distributed to the arch using the methodology currently employed by AIT (AIT will provide UMaine with methodology and MATLAB code for live load distribution). To account for model nonlinearity, the live load effects will be determined by subtracting the results of DL + backfilling from the total DL + backfilling + LL. The arch will be modeled with a nonlinear moment-curvature relationship in all analyses.

Deliverable: Arch axial loads, arch moments, and foundation loads for all four analyses will be summarized in a report to AIT.

References

Faraji S, Ting JM, Crovo DS, Ernst H (2001). Nonlinear analysis of integral bridges: finite-element model. *Journal of Geotechnical and Geoenvironmental Engineering*, 127(5): 454-461.

NCHRP (1991). *Manuals for the Design of Bridge Foundations*. National Cooperative Highway Research Program Report No. 343, Transportation Research Board, Washington, DC.

Ting JM and Faraji S (1998). *Force-Displacement Testing for Integral Abutment Bridges*. University of Massachusetts Transportation Center Report No. UMTC 97-13, University of Massachusetts, Amherst, MA.

USACoE (1994). *Design of Sheet Pile Walls*. CECW-ED Engineer Manual 1110-2-2504. Department of the Army, US Army Corps of Engineering, Washington, DC.

This report shall not be reproduced, except in full, without the written approval of the AEWC Advanced Structures & Composites Center.

XIII. APPENDIX B – SOFTWARE PROGRAMMING SUMMARY

The discretization of the finite element mesh is performed automatically within the input files provided with this software. The basic strategy for node numbering is:

1. Node 1 is at X = +span/2, Y = 0, and Z = 0.
2. All arch nodes are defined sequentially from this point to the final arch node numbered numels+1 located at X = -span/2, Y = 0, and Z = 0.
3. Next, the decking/soil spring nodes are generated starting at the X,Y coordinates equal to those for Node 2 and Z = -spacing/2.
4. All nodes are generated along the length of the arch at Z = -span/2 (no nodes are generated at Y = 0).
5. This process is repeated moving in the +Z direction for all remaining nodes.

The basic strategy for element numbering is:

1. Element 1 connects Nodes 1 and 2, Element 2 connects Nodes 2 and 3, etc. until all of the arch elements are defined.
2. Next, decking elements are defined starting at the X,Y coordinates equal to those for Node 2 and Z = -spacing/2 and progressing towards +Z.
3. Once all of the decking elements are defined for a particular X,Y point, the sequence continues at the adjacent X,Y coordinate in the –X direction.
4. Finally, soil spring elements are numbered in the same order as the arch/decking nodes.

An example of node and element numbering for a model with 60 arch elements and 4 elements along the transverse length of the decking is shown in Figure B1.

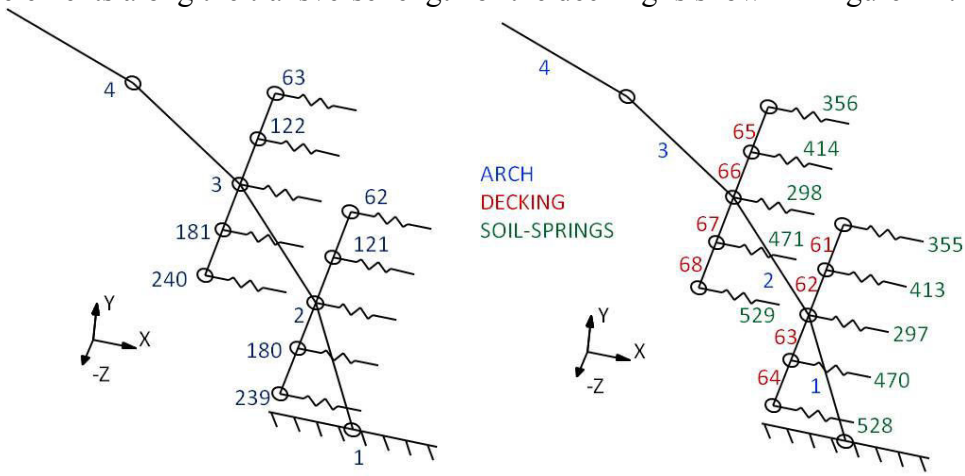

a) Nodes **b) Elements**

Figure B1 Example of Numbering Method, numels = 60, num_deck = 4 (Not to Scale)

This report shall not be reproduced, except in full, without the written approval of the AEWC Advanced Structures & Composites Center.

Table B1 – List of MATLAB Analysis Functions (Original AIT Functions Shown in Black Text, Underlined Functions have been Modified, and New Functions are Shown in Blue Text).

add_element_k	generate_T_beam
angles	generate_T_beam_3D
apply_3D_boundaries	get_cross_vector_for_decking
apply_boundaries	get_el_displ
apply_loads	get_envelope_results_for_current
arch_analysis	get_equivalent_arch_M_EI
assemble_stiff	get_K_given_deltaUx
beam_stiff_2D	get_M_and_EI_given_phi_axial
beam_stiff_3D	get_nodal_loads_for_soils
bousinnesq	get_self_weight_nodal_force_vector
Combine_envelopes	get_soil_spring_force
Combine_Fatigue_Env	Inputs_Ellsworth_3D
compute_live_load_force_vector	linear_arch
compute_LL_nodal_force	load_rate
compute_LL_nodal_force_3D	Multi_run
compute_member_forces	newton_solver_3D
compute_member_forces_3D	perform_3D_backfill_analysis
compute_residual_3D	perform_3D_LL_analysis
generate_results_table_for_3_elevations	plotting_loop
deck_stiff_3D	soilspring_stiff_3D
distribute_F_to_decking_elements	update_spring_props
DRAW_ALL	write_combined_envelopes
DRIVER_MAIN_3D	write_Fatigue_env
eliminate_horizontal_components	write_load_rate
generate_envelopes	write_multi
generate_F_soils	write_Single_Load_Case
generate_soil_lifts	writefile

This report shall not be reproduced, except in full, without the written approval of
the AEWC Advanced Structures & Composites Center.

Table B2 – Hierarchy of Functions used to Perform Backfilling and Live Load Analyses

DRIVER_MAIN_3D – main function for running a backfilling and live load analysis including all SSI and 3D aspects of this project (for the proposed Ellsworth Bridge).

1. *perform_3D_backfill_analysis* - main function for running a backfilling analysis.
    a. *Inputs_Ellsworth_3D*, *Inputs_ConSpan_3D*, etc. – expanded version of existing AIT input files to incorporate the necessary additional information to define the model beyond existing 2D models.
    b. *apply_3D_boundaries* –applies applicable boundary conditions to 2D or 3D models based on the type of boundary chosen in the input file.
    c. *get_self_weight_nodal_force_vector* –generates the loads corresponding to the self weight of the arch and decking. It will distribute the weight of the decking elements to the decking elements if applicable. Otherwise the weight of the decking elements is applied directly to the arch.
        i. apply_loads – slightly modified version of existing AIT function for generating loads. The only modification is to adjust the indices to account for 3D models (e.g. M_{zz} is entry 6 instead of entry 3). Here, <u>INCLUDED_FORCES</u> is set to 5 so that loads corresponding to self-wt. of the arch and decking are generated. The components of self-wt. due to arch and decking are separated so that the decking self-wt can be distributed among the decking elements while the arch self-wt is only applied to the arch nodes.
        ii. *distribute_F_to_decking_elements* –uses the global variable F, which should be set so that it contains only the forces corresponding to the self-wt of the decking. When input, the forces are all lumped on the arch nodes. The output for the function is a force vector where self-wt of decking has been distributed proportionately among decking nodes.
    d. *generate_soil_lifts* –returns a vector of lift elevations based on total lift height specified. Lifts are applied on alternating sides of the arch in 12” increments until reaching the height of the arch. After which, lifts are applied in 12” increments over the entire structure until the elevation is within 12” of the specified maximum height. The remaining fractional lift, if applicable, is applied as a final lift.
    e. *generate_F_soils* –generates the vector of forces corresponding to soil loading. <u>cur_grade</u> and <u>last_grade</u> are the only input parameters and each of these contains an elevation for the right and left sides of the arch, respectively. Vertical forces are computed at all nodes below grade. Horizontal forces based on Ko are only computed for nodes that are located between the last grade and the current grade since the horizontal component

This report shall not be reproduced, except in full, without the written approval of the AEWC Advanced Structures & Composites Center.

of force below the last grade is handled by the soil springs that are now activated.

i. *get_nodal_loads_for_soils* –takes as input the connectivity of an element, the vertical and horizontal stresses at the top and bottom of the element, and the applicable current grade level. Three cases are considered: 1) element above grade, forces = 0, 2) element partially below grade, and 3) element completely below grade. For cases (2) & (3), shape functions are used to distribute the linearly varying soil pressure to the end nodes, resulting in statically equivalent nodal forces. This function considers the full tributary width of the arch, so the forces must be distributed to the decking elements, if applicable, which is done in *generate_F_soils*.

1. *generate_T_beam_3D* –transforms the calculated statically equivalent nodal loads to the orientation of the element.

f. *newton_solver_3D* –main routine for solving a single nonlinear 3D load step.

i. *compute_residual_3D* –computes a vector of residual forces, which is the difference between the member forces and the applied forces per node and dof.

1. *get_cross_vector_for_decking* –returns a vector with x, y, and z components of a vector that is perpendicular to the surface of the decking in the strong axis direction. The purpose is to properly orient the weak and strong axes when computing the transformation vector.

2. *assemble_stiff* – main function for generating the global stiffness matrix.

a. *beam_stiff_2D* – same as previous AIT code.

b. *beam_stiff_3D* – computes an element stiffness matrix for a 3D element, which can either be an arch element, decking element, or soil spring element.

i. *get_equivalent_arch_M_EI* – this function returns the moment and curvature values for the arch elements. It also adds in the components for the concrete deck, if applicable.

1. *get_M_and_EI_given_phi_axial*– returns interpolated M and EI values based on a moment-curvature relationship provided by AIT for a 12” arch. The method used by this function

This report shall not be reproduced, except in full, without the written approval of the AEWC Advanced Structures & Composites Center.

was somewhat optimized for efficiency since it is called so many times during a nonlinear analysis.

ii. *soilspring_stiff_3D* –returns the element stiffness matrix for a soilspring element based on the element's properties (one of which is the 'zero' position of the spring), the current grade, and the incl_force (tells whether additional loads should be applied beyond backfilling loads).

1. *get_soil_spring_force* – this function returns the force in a soilspring based on its depth, zero value, and which forces are applied

a. *get_K_given_deltaUx* – returns lateral pressure coefficient K_{soil} based on relative displacement and the user-defined soil spring relationship

iii. *deck_stiff_3D* – returns the element stiffness matrix for a decking element. Elements at the ends of the decking (planes of symmetry) are recognized and applicable stiffness matrices are applied to address the boundary conditions at the planes of symmetry (rotation about applicable axis = 0).

iv. *get_cross_vector_for_decking*

v. *generate_T_beam_3D*

vi. *add_element_k* – adds element stiffness matrix to global stiffness matrix.

3. *apply_boundaries* – zeros applicable values of F, U, R, and K to account for boundary conditions.
4. *compute_member_forces_3D* – returns a vector of <u>member_forces</u> for each element

a. *get_el_displ* – returns a vector of displacements for a particular element.

b. *generate_T_beam_3D*

c. *get_cross_vector_for_decking*

d. *beam_stiff_3D*

This report shall not be reproduced, except in full, without the written approval of the AEWC Advanced Structures & Composites Center.

e. *deck_stiff_3D*
f. *get_equivalent_arch_M_EI*
i. *get_M_and_EI_given_phi_axial*
g. *get_soil_spring_force*
5. *compute_residual_3D*

ii. *get_envelope_results_for_current* – returns results envelope for the current load step.
iii. *update_spring_props* – modifies PROPS by setting a flag for elements that are now activated due to last_grade < z < cur_grade and also saves the applicable 'zero' displacement value for newly activated springs.

2. *perform_3D_LL_analysis* - main function for running a live load analysis. This function is designed to resume an analysis from a previously solved backfilling analysis. The user must specify which load step to resume from. Files that were saved from the previous analysis are loaded to initialize element properties, etc. The previous analysis should always end with a backfill level above the arch (i.e. all springs activated).
   a. *apply_loads*
   b. *distribute_F_to_decking_elements*
   c. *eliminate_horizontal_components* – takes as input a vector of nodal forces containing both x and y force components (e.g. one that was generated using AIT's apply_loads function) and removes horizontal components since the horizontal components are handled by the soil springs.
   d. *compute_live_load_force_vector* – utilizes existing code written by AIT to generate the nodal force vector corresponding to vehicular live loads. Both vertical forces and stresses are generated since the forces will be applied and the stresses will be used to generate spring forces.
      i. *compute_LL_nodal_force_3D* –returns a force that is generated using the integral solution for the Boussinesq equation provided by AIT. The only change made to the code was to replace B(1) = -TW/2 and B(2) = TW/2 with B(1) = B1 and B(2) = B2, respectively, where B1 and B2 are input to the function.
   e. Remainder of analysis is the same as for step 1 above.

This report shall not be reproduced, except in full, without the written approval of the AEWC Advanced Structures & Composites Center.

Table B3 – Summary of hard-wired parameters in new functions

Parameter	Function Containing Definition
Arch geometric parameters (**span**, **rise**, **spacing**, etc.)	*Inputs_X*, where *X* = '*Ellsworth_3D*' for example
Site parameters (**rho**, **depth_crown**, etc.)	*Inputs_X*, where *X* = '*Ellsworth_3D*' for example
Some live load parameters (**vehicle**, **axle_space**, etc.)	*Inputs_X*, where *X* = '*Ellsworth_3D*' for example
Analysis parameters (**numels**, **num_deck**, etc.)	*Inputs_X*, where *X* = '*Ellsworth_3D*' for example
Transverse decking properties (**E_deck**, **A_deck**, **I_deck**)	*Inputs_X*, where *X* = '*Ellsworth_3D*' for example
Longitudinal decking properties (**E_deck**, **A_deck**, **I_pos**, **I_neg**)	*Inputs_X*, where *X* = '*Ellsworth_3D*' for example
Distance from centerline of arch to soil -- used to calculate effective soil depth (**t_deck**)	*Inputs_X*, where *X* = '*Ellsworth_3D*' for example
Effective height for soil springs (**H_effective**)	*Inputs_X*, where *X* = '*Ellsworth_3D*' for example
Soil spring parameters (**Ka**, **Ko**, **Kp**, **delta_Ka**, **delta_Kp**)	*get_K_given_deltaUx*
AASHTO lane load of 640 plf (over 10 ft width) **lane_AASHTO**	*get_soil_spring_force*
AASHTO vehicular live load parameter (**num_axles**, **axle**, **axle_spacing**)	*compute_live_load_nodal_force_vector*
Arch M-κ relationship	*get_M_and_EI_given_phi_axial* and files saved to the working directory
Nonlinear solution tolerance	*newton_solver_3D*

This report shall not be reproduced, except in full, without the written approval of the AEWC Advanced Structures & Composites Center.

Table B4 – Things to be aware of

1. It is not recommended to use completely vertical elements (i.e. adjacent arch nodes have exactly the same x-value) since this may cause errors. The orientation of the element from horizontal may be taken as 270 degrees when it should be 90 degrees. The implementation of atan2 or another method may alleviate this issue.
2. Vehicular live loading, when non-symmetric, causes torsion and bending about the Y-Y axis of the arch elements. On the other hand, all other loads are symmetric and there is no torsion or Y-Y bending. Currently these forces are neglected (set equal to zero) since torsional properties are unknown, which appears to have negligible effect on the solution.
3. It is not necessary to apply backfilling loads incrementally once the elevation of the backfill is above the arch because all soil springs are activated at this point. However, the risk of neglecting to do this is that the critical construction response may be missed.
4. Similarly, the wearing surface, lane load, and vehicular live load could all be applied at the same time if desired.
5. The transverse bending stiffness of the concrete deck for this particular bridge happens to be almost equal for positive or negative cracked-section bending. This may not be the case for other structures and additional work may be required to address this if it is important.

AEWC Advanced Structures & Composites Center
5793 AEWC Bldg
University of Maine
Orono, ME 04469-5793

Telephone: 207-581-2123
FAX: 207-581-2074
contactaewc@umit.maine.edu
www.aewc.umaine.edu

This report shall not be reproduced, except in full, without the written approval of
the AEWC Advanced Structures & Composites Center.

Table B5 –Ideas to improve run-time efficiency

1. Reduce the number of decking elements.
    a. Every additional decking element means ≈N*2 more total elements, where N is the number of arch elements.
    b. Perform convergence study to examine the effect. The effect of the decking elements may be negligible if the decking stresses are not important.
2. Increase the tolerance in 'newton_solver_3D'
    a. Again a convergence study should be performed. It is suspected that the tolerance can be increased a lot without sacrificing much accuracy in the key results.
3. Perform backfill analysis, then add DW, then add lane load and use this as the starting point for all subsequent analyses (live load vehicle in various positions). Thus, the time to run an envelope analysis is approximately equal to the time required for one full nonlinear Newton iteration multiplied by the number of envelope configurations.
    a. May need to look at several combinations when load factors come into play.
4. Eliminate or reduce screen prints ('sprintf' commands).
5. Develop code in another programming language.
6. Verify that the user's processor is being fully utilized, particularly for multi-core processors.

This report shall not be reproduced, except in full, without the written approval of
the AEWC Advanced Structures & Composites Center.

XIV. APPENDIX C – SUPPORTING CALCULATIONS

Page: 1
By: JDC Date: 5/2/2011
Checked by: ____ Date: 5/2/2011

AEWC Center

5793 AEWC Building
Orono, Maine 04669
Telephone: (207) 581-2123
Fax: (207) 581-2074
www.aewc.umaine.edu

Designed By: JDC
Date: 01/20/11
Checked By:
Date:
Job Number: 906F

Project: AIT Soil-Structure Interaction
Task: Calculate Analysis Properties

References
1. Proposed decking design drawing provided by Matthew Pellerin of AIT.

Uncracked decking properties in the transverse direction (spanning arches)

AASHTO 2007 allows either uncracked or cracked sections to be considered depending on the expected situation, assume cracked

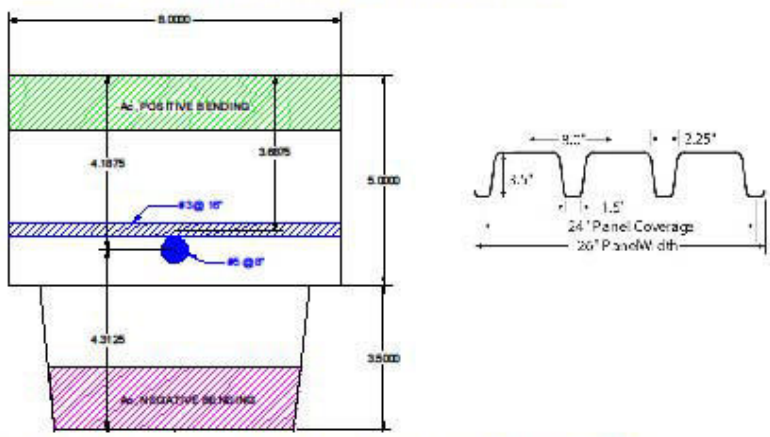

Concrete section - perpendicular to arch span (some properties from AutoCAD)

TRANSVERSE

$$Ag := \frac{21.44in^2 + 8in \cdot 5in}{8in} = 7.68 \cdot \frac{in^2}{in}$$

Concr. strength $f_c := 4350psi$ (MDOT spec.)

Concr. stiffness $E_c := 57000 \cdot \sqrt{f_c \cdot psi}$ $\boxed{E_c = 3759 \cdot ksi}$

Modular ratio $n_s := \frac{29000ksi}{E_c}$ $n_s = 7.71$

UNCRACKED

Ybar (top)

$$y_t := \frac{8in \cdot 5in \cdot 2.5in + 21.44in^2 \cdot 6.71in + \frac{\pi}{4} \cdot \left(\frac{5}{8}in\right)^2 \cdot (n_s - 1) \cdot 4.18in}{8in \cdot 5in + 21.44in^2 + \frac{\pi}{4} \cdot \left(\frac{5}{8}in\right)^2 \cdot n_s}$$ $y_t = 3.96 \cdot in$

C:\Documents and Settings\joshua.clapp\Desktop\Arch Decking Calcs.xmcd

This report shall not be reproduced, except in full, without the written approval of the AEWC Advanced Structures & Composites Center.

Page: 2
By: JDC Date: 5/2/2011
Checked by: ___ Date: 5/2/2011

TRANSVERSE (continued)

Moment of inertia

$$I := \frac{\frac{8in\cdot(5in)^3}{12} + 8in\cdot 5in\cdot(y_t - 2.5in)^2 + 21.86in^4 + 21.44in^2\cdot(6.71in - y_t)^2 + \frac{\pi}{4}\cdot\left(\frac{5}{8}in\right)^2\cdot(n_s - 1)\cdot(4.18in - y_t)^2}{8in} \qquad I = 44.09\cdot\frac{in^4}{in}$$

Equivalent thickness for self-weight

$$t := \frac{\left(8in\cdot 5in + 21.44in^2 + 0.125in\cdot 8in\right)}{8in} \qquad t = 7.81\cdot in$$

POSITIVE BENDING CRACKED

Solve for ybar and I

Given $\quad y_{bar} := 0.5in \quad A_s := 0.31in^2 \quad d := 4.1875in$

$$8in\, y_{bar}\cdot\frac{y_{bar}}{2} - n_s\cdot A_s\cdot(d - y_{bar}) = 0$$

$$y_{bar} := Find(y_{bar}) \qquad y_{bar} = 1.31\cdot in$$

$$I := \frac{y_{bar}^3}{12} + y_{bar}\cdot\left(\frac{y_{bar}}{2}\right)^2 + n_s\cdot\frac{A_s}{8in}\cdot(d - y_{bar})^2 \qquad I = 3.224\cdot\frac{in^4}{in}$$

NEGATIVE BENDING CRACKED

Given $\quad y_{bar} := 0.5in \quad A_s := 0.31in^2 \quad d := 4.31in$

$$5.75in\, y_{bar}\cdot\frac{y_{bar}}{2} + \frac{6.5in - 5.75in}{3.5in}\cdot y_{bar}\cdot\frac{y_{bar}}{2}\cdot y_{bar}\cdot\frac{1}{3} - n_s\cdot A_s\cdot(d - y_{bar}) = 0$$

$$y_{bar} := Find(y_{bar}) \qquad y_{bar} = 1.51\cdot in$$

$$I := \frac{6.7179in^4}{8in} + n_s\cdot\frac{A_s}{8in}\cdot(d - y_{bar})^2 \qquad I = 3.181\cdot\frac{in^4}{in}$$

Say I = 3.2 in^4/in both ways

LONGITUDINAL

UNCRACKED

$$I_{long} := \frac{(5in)^3}{12} = 10.42\cdot\frac{in^4}{in} \qquad A_{long} := 5in = 5.00\cdot\frac{in^2}{in}$$

Given $\quad y_{bar} := 0.5in \quad A_s := 0.11in^2 \quad d := 3.6875in$

$$16in\, y_{bar}\cdot y_{bar} - n_s\cdot A_s\cdot(d - y_{bar}) = 0$$

$$y_{bar} := Find(y_{bar}) \qquad y_{bar} = 0.42\cdot in$$

C:\Documents and Settings\joshua.clapp\Desktop\Arch Decking Calcs.xmcd

This report shall not be reproduced, except in full, without the written approval of the AEWC Advanced Structures & Composites Center.

Page: 3
By: JDC Date: 5/2/2011
Checked by: ___ Date: 5/2/2011

LONGITUDINAL (continued)

POSITIVE BENDING CRACKED

$$I_{pos} := \frac{y_{bar}^3}{12} + y_{bar}\left(\frac{y_{bar}}{2}\right)^2 + n_s \cdot \frac{A_s}{16in}\cdot(d - y_{bar})^2 \qquad I_{pos} = 0.592\cdot\frac{in^4}{in}$$

Given $y_{bar} := 0.5in$ $\quad A_s := 0.11in^2$ $\quad d := 1.3125in$

$$16in\, y_{bar}\cdot y_{bar} - n_s\cdot A_s\cdot(d - y_{bar}) = 0$$

$$y_{bar} := \mathrm{Find}(y_{bar}) \qquad y_{bar} = 0.24\cdot in$$

NEGATIVE BENDING CRACKED

$$I_{neg} := \frac{y_{bar}^3}{12} + y_{bar}\left(\frac{y_{bar}}{2}\right)^2 + n_s \cdot \frac{A_s}{16in}\cdot(d - y_{bar})^2 \qquad I_{neg} = 0.066\cdot\frac{in^4}{in}$$

FRP decking - CP155

$$n_{FRP} := \frac{4200ksi}{E_c} \qquad n_{FRP} = 1.12$$

$$I_{FRP} := \frac{11.16in^4}{ft} \qquad I_{FRP} = 0.93\cdot\frac{in^4}{in}$$

$$A_{FRP} := \frac{3.64in^2}{ft} \qquad A_{FRP} = 0.30\cdot\frac{in^2}{in}$$

$$wt_{FRP} := 3.75psf \qquad t_{eq} := \frac{3.75psf}{145pcf} \qquad t_{eq} = 0.31\cdot in$$

Arch Moment of Inertia

Effective diameter for EI calculation $\quad d := 11.8in$

Uncracked $\quad I_{uncracked} := \frac{\pi\cdot d^4}{64} = 951.70\cdot in^4$

$$EI_{uncracked} := E_c\cdot I_{uncracked} = 3.58\times 10^6\cdot kip\cdot in^2$$

Cracked $\quad EI_{cracked} := \frac{669.21kip\cdot in}{\frac{0.000911}{in}} = 7.35\times 10^5\cdot kip\cdot in^2$

Ratio uncracked to cracked $\quad \frac{EI_{uncracked}}{EI_{cracked}} = 4.87$

Ratio arch to concr. deck M+ $\quad \frac{EI_{cracked}}{I_{pos}\cdot E_c\cdot 60in} = 5.51$

Ratio arch to concr. deck M- $\quad \frac{EI_{cracked}}{I_{neg}\cdot E_c\cdot 60in} = 49.58$

C:\Documents and Settings\joshua.clapp\Desktop\Arch Decking Calcs.xmcd

This report shall not be reproduced, except in full, without the written approval of
the AEWC Advanced Structures & Composites Center.